TECHNISCHE UNIVERSITÄT DRESDEN

FACULTY OF MECHANICAL SCIENCE AND ENGINEERING

Institute of Natural Materials Technology

ANALYSIS OF RATE-DEPENDENT DEFORMATION AND FRACTURE PHENOMENA DURING CUTTING OF VISCOELASTIC MATERIALS

DISSERTATION

submitted for the award of the academic grade

Doktor-Ingenieur
(Dr.-Ing.)

submitted by

Dipl.-Ing. Stefan Schuldt

born 23.10.1982
Wismar, Germany

Date submitted 3. November 2017

Referees:

Prof. Dr. Harald Rohm	Technische Universität Dresden
Prof. Dr. Jens-Peter Majschak	Technische Universität Dresden

Analysis of rate-dependent deformation and fracture phenomena during cutting of viscoelastic materials

Schuldt, S. – Dresden: Technische Universität Dresden, Faculty Mechanical Engineering, doctoral thesis, 2017, 109 pages, 59 figures, 9 tables

The cutting of foods is characterized by deformation, fracture and friction processes, and the viscoelastic properties of the cutting materials determine their rate-dependent cutting behavior. This is responsible for uncontrolled fracture and deformation events with increasing cutting velocity. There is a significant information deficit regarding the assignment of material properties and cutting parameters, as well as regarding a process description for industrial high-speed cutting.

The aim of the work is the analysis of the velocity-dependent cutting behavior of foods up to the high-speed range. The focus is on the deformation and fracture phenomena, analysed by methods of classical material analysis but also associated cutting experiments performed in the range from low to high cutting velocities. For high-speed analyses, a test station enabling cutting velocities of up to 10 m/s was designed. To identify relevant material and cutting parameters and to establish a systematic experimental program, elastomer-based model systems with controllable viscoelastic profiles were developed. The results of the respective investigations were further verified for foods. The velocity-dependent deformation behavior during cutting could be described by dynamic-mechanical material analyses in the frequency range. Cutting force slopes at the beginning of the cutting process correlated with the complex moduli and were furthermore dependent on the cutting velocity; this dependency corresponded to the frequency behavior from material analysis. The fracture properties could be attributed to ductile (polymeric systems) or brittle behavior (cellular plant systems). Confectionary products had a strong temperature- and time-dependent behavior with ductile-brittle transition within the experimental conditions.

The results obtained demonstrate that there is a significant relationship between viscoelasticity and velocity-dependent cutting behavior. They allow a phenomenological process description of high-speed cutting and can be used as a basis for the balancing of cutting forces and as input parameters for numerical analyses of the cutting process.

Analyse von geschwindigkeitsabhängigen Deformations- und Bruchphänomenen beim Schneiden von viskoelastischen Stoffen

Schuldt, S. – Dresden: Technische Universität Dresden, Fakultät Maschinenwesen, Dissertation, 2017, 109 Seiten, 59 Abbildungen, 9 Tabellen

Das Schneiden von Lebensmitteln ist geprägt durch Deformations-, Bruch- und Reibvorgänge. Dabei bestimmen die viskoelastischen Eigenschaften der Schneidgüter deren geschwindigkeitsabhängiges Schneidverhalten. Dies führt mit zunehmender Schneidgeschwindigkeit zu unkontrollierten Bruch- und Deformationsereignissen. Dabei besteht ein Informationsdefizit bei der konkreten Zuweisung von Materialeigenschaften und Schneidparametern sowie einer Verfahrensbeschreibung für das industrielle Hochgeschwindigkeitsschneiden.

Ziel der Arbeit ist die Analyse des geschwindigkeitsabhängigen Schneidverhaltens von Lebensmitteln bis in den Hochgeschwindigkeitsbereich. Der Fokus richtet sich auf die Untersuchung der Teilphänomene Deformation und Bruch durch Methoden der klassischen Materialanalyse sowie zugeordnete Schneidexperimente im Bereich von niedrigen bis hohen Schneidgeschwindigkeiten. Für entsprechende Hochgeschwindigkeitsanalysen wurde ein Versuchsstand mit Schneidgeschwindigkeiten von bis zu 10 m/s konzipiert. Zur Identifikation relevanter Material- und Schneidparameter und zur Aufstellung des systematischen Versuchsprogramms wurden Modellsysteme auf Elastomerbasis mit steuerbarem viskoelastischen Profil entwickelt. Die Ergebnisse wurden für Lebensmittel verifiziert. Das geschwindigkeitsabhängige Deformationsverhalten beim Schneiden konnte durch dynamisch-mechanische Materialanalysen im Frequenzbereich beschrieben werden. Dabei korrelierten Kraftanstiege zu Beginn des Schneidvorganges mit den Komplexmoduln. Die Anstiege zeigten eine Abhängigkeit von der Geschwindigkeit; diese entsprach dem Frequenzverhalten aus der Materialanalyse. Die Brucheigenschaften konnten produktspezifisch duktilem (polymere Systeme) oder sprödem Verhalten (zelluläre, pflanzliche Systeme) zugeordnet werden. Zuckerwaren zeigten ein stark temperatur- und zeitabhängiges Verhalten mit duktil-sprödem Übergang innerhalb der Versuchsbedingungen.

Die gewonnenen Erkenntnisse demonstrieren den Zusammenhang von Viskoelastizität und geschwindigkeitsabhängigem Schneidverhalten. Sie erlauben eine phänomenologische Verfahrensbeschreibung des Hochgeschwindigkeitsschneidens und können als Basis für die Bilanzierung von Schneidkräften und als Eingangsparameter für numerische Analysen des Schneidvorganges dienen.

Vorwort

Die vorliegende Arbeit reiht sich in eine lange Tradition des Instituts ein, in welcher seit mindestens den 80er Jahren (in enger Kooperation mit dem Kombinat NAGEMA, Dresden) Fragestellungen zur Optimierung industrieller Schneidverfahren an Lebensmitteln bearbeitet wurden. Dabei entstandene Pendel- und Rotationsversuchsstände erlaubten bereits damals schon die Durchführung von umfangreichen Schneidexperimenten mit Schneidkraftaufnahme bis in den Hochgeschwindigkeitsbereich, in Abhängigkeit einer breiten Schneidgutauswahl und der technischen Eingangsparameter Keilwinkel, Schärfe und Zügigkeit. In den Umwälzungen nach der Wende wurden die Versuchsstände abgebaut und die Ergebnisse der Untersuchungen nur fragmentarisch publiziert; viel Wissen ging verloren. Weitergeführt wurde die Schneidforschung durch ein DFG-Projekt zum Ultraschallschneiden, initiiert durch Prof. Lothar Linke und Yvonne Schneider. Dies führte, begleitet und befördert durch Prof Harald Rohm, zu zwei Doktorarbeiten und zahlreichen Veröffentlichungen. Auf dieser wissenschaftlichen Basis machte ich im Januar 2011 innerhalb eines IGF-Projektes[1] zur Oberflächen-, Schärfe- und Verschleißcharackterisierung von Messerklingen meine ersten Schritte in der Schneidforschung. In einer anschließenden DFG-support-the-best-Förderung[2] über die Deutsche Exzellenzinitiative, in Zusammenarbeit mit der Arbeitsgruppe von Professor Kästner (Festkörpermechanik), konnten Grundlagen zum Schneidverhalten und dem Einfluss der Viskoelastizität auf die geschwindigkeitsabhängigen mechanischen Eigenschaften gelegt und ausgebaut werden. Außerdem wurden wesentliche messtechnische Bestandteile für Hochgeschwindigkeitsversuche finanziert. Parallel dazu bot sich in einem ZIM-Verbund[3] in Zusammenarbeit mit der Professur für Verarbeitungsmaschinen und Verarbeitungstechnik und der Firma Theegarten-Pactec die Möglichkeit einen Hochgeschwindigkeitsversuchstand aufzubauen. Die daraus resultierenden Forschungsergebnisse bilden einen Hauptteil dieser Arbeit. Durch ein abschließendes Stipendium der Graduiertenakademie der TU Dresden konnte ich die umfassenden Ergebnisse in der nun vorliegenden Promotionsschrift konzentrieren. Diese ist somit, neben einer gewissen Portion Fleiß und Hingebung, auch das Ergebnis günstiger Fügung und forschungsfördernder Umstände. Deshalb schließt mein Dank auch die Mittelgeber aus öffentlicher und privater Hand mit ein.

[1]IGF – Industrielle Gemeinschaftsforschung; [2]DFG – Deutsche Forschungsgemeinschaft; [3]ZIM – Zentrales Innovationsprogramm Mittelstand

Mein besonderer Dank gilt Prof. Dr. Harald Rohm für die Übernahme der Betreuung der vorliegenden Arbeit und für die offene, vertrauensvolle und promotionsfördernde Atmosphäre am Lehrstuhl. Großer Dank geht an Prof. Dr. Jens-Peter Majschak für das Interesse am Forschungsthema und die Übernahme der Gutachtertätigkeit.

Herzlich möchte ich Dr.-Ing. Yvonne Schneider danken für ihre Geduld mit mir, ihre Beharrlichkeit und ihr stets offenes Ohr. Weiterhin danke ich Dipl.-Ing. Tilman Witt für seine Fähigkeiten einen Versuchsstand aufzubauen, sein interdisziplläres Forschungsinteresse, unseren Arbeitseinsatz nach Wernigerode und seine Hilfsbereitschaft. Ohne ihn hätte die vorliegende Arbeit anders ausgesehen.

Danken möchte ich meinen Büropartnern Dr.-Ing. Gunther Arnold und Dr.-Ing. Nazir Kizzie-Hayford für die entspannte, humorvolle und freigeistige Büroatmosphäre sowie meiner temporären Büropartnerin Dipl.-Ing. Susanne Struck für die solidarische Unterstützung während der Endphase der Promotion und die vielen lustigen gemeinsamen Momente. Mein Dank gilt auch den Studenten (v. A. Johannes, Michael, Jens, Lorenz, Lukas, Louis, Anton), die ich in insgesamt 16 wissenschaftlichen Arbeiten betreuen durfte und die mich thematisch und zwischenmenschlich vorangebracht haben. Dann danke ich natürlich dem Mensateam, welches über die Jahre einige Fluktuation erfahren hat und allen Mitarbeitern des Institutes für die freundliche und angenehme Arbeitsatmosphäre.

Meinen lieben Eltern, die mir die Freiheit zur eigenen Entfaltung und Auslebung meiner Eigenarten geschenkt haben, möchte ich danken für das Vertrauen in mich; meinen Schwiegereltern danke ich für die familiäre Unterstützung und unendliche Geduld mit den Kindern und mir. Meiner tollen Frau Andrea danke ich für ihr Vertrauen, ihre Unterstützung, ihr Verständnis für mich und meine Marotten, ihre ausgeglichene und besonnene Art und das Ertragen meiner Launen. Abschließend danke ich unseren lieben, wunderbaren, einzigartigen, nervtötenden Kindern Lotta, Hanne und Otto, die mich die für eine Promotion erforderliche Belastbarkeit gelehrt haben und mir den nötigen Arbeitsausgleich sowie unzählige Vorabendschläfe beschert haben.

Table of contents

Symbols and abbreviations

a	constant of **Eq. 4.4**	[kg/(s·mm)]
a_M	constant of the model approach of **Eq. 5.5**	[kg/(s·mm)]
Al_2O_3	corundum	
β	wedge angle of a blade	[°]
b	exponent of **Eq. 4.4** reflecting the velocity dependence of s_0	[-]
BSI	blade sharpness index [-]	
CI	(blade displacement at) cut initiation depth	[mm]
δ	phase shift	[°]/[rad]
d	cutting stiffness	[N/mm]
d_0	initial cutting stiffness	[N/mm]
DMA	dynamic mechanical analysis	
ε	strain	[-]
ε_f	fracture strain	[-]
E^*	complex modulus	[Pa]
E'	storage modulus	[Pa]
E''	loss modulus	[Pa]
EPDMs	ethylene propylene diene monomer rubber (soft)	
EPDMh	ethylene propylene diene monomer rubber (hard)	
f17	food model with 17 % (w/w) filler	
f20	food model with 20 % (w/w) filler	
f31	food model with 31 % (w/w) filler	
f35	food model with 35 % (w/w) filler	
f40	food model with 40 % (w/w) filler	
f45	food model with 45 % (w/w) filler	
f20s20	food model with 20 % (w/w) filler and 20 % (w/w) softener	
f35s20	food model with 35 % (w/w) filler and 20 % (w/w) softener	
FPZ	fracture process zone	
F	force	[N]
F_{adh}	adhesion force involved into friction processes	[N]
F_C	cutting force	[N]
F_{CI}	cutting force at cut initiation	[N]
F_{def}	deformation force involved into cutting	[N]
F'_{def}	elastic deformation force involved into cutting	[N]
F'_{def}	viscous deformation force involved into cutting	[N]
F_F	friction force	[N]
F_{F1}	friction force at the blade wedge	[N]
F_{F2}	friction force at the blade flanks	[N]
F_{fract}	fracture force involved into cutting	[N]
F_N	normalized cutting force	[N]
F_{norm}	normalized cutting force	[N]
$F_{N,CI}$	normalized cutting force at cut initiation depth	[N]
$F_{N,max}$	normalized maximum cutting force	[N]
F_{SD}	deformation forces acting orthogonal to the surface of the blade	[N]
F_{SD1}	deformation forces acting orthogonal to the surface of the blade wedge	[N]
F_{SD1}	deformation forces acting orthogonal to the surface of the blade flanks	[N]
F_{tribo}	friction force involved into cutting	[N]
F_{VE}	viscoelastic deformation force involved into friction processes	[N]
G^*	complex shear modulus	[P]
G'	storage shear modulus	[Pa]
G''	loss shear modulus	[Pa]
h	sample height	[mm]
HSTS	high-speed testing station	
J	fracture toughness	[J/m²]

l	blade displacement	[m]
$l_{FN,max}$	blade displacement at normalized maximum cutting force	[mm]
k	constant of **Eq. 4.1**	[(Pa·s)/rad]
μ	coefficient of friction	[-]
m_i	operation parameter similar to b, see section 5.1.2	[-]
n	exponent of **Eq. 4.1** reflecting the frequency dependence of E^*	[-]
n	number of replications	[-]
NBR	nitrile butadiene rubber	
ω	angular frequency	[rad/s]
π	Pi	[-]
p	probability value	[-]
P	free pass	[N]
σ	stress	[Pa]
σ_f	fracture stress	[Pa]
r	regression coefficient	[-]
SiO_2	seasand	
s_0	initial slope of normalized cutting force	[N/mm]
$s_{0,M}$	initial slope of the model approach	[N/mm]
$s_{0@10^{-3}m/s}$	initial slope of F_N at a cutting velocity of 10^{-3} m/s	[N/mm]
SSC	steady state cutting	
$tan\ \delta$	loss factor	[-]
tts	temperature time superposition	
u	cutting length	[mm]
UTM	universal testing machine	
v	cutting velocity	[m/s]
w	cutting width	[mm]
W	cutting work/energy	[Nm]
W'	elastically stored work/energy	[Nm]
W''	dissipated work/energy	[Nm]
W''_{visc}	dissipated work/energy because of viscous flow	[Nm]
W''_{frict}	dissipated work/energy due to inner friction after van Vliet et al. (1993)	[Nm]
W''_{fract}	fracture work/energy	[Nm]
W_C	cutting work/energy	[Nm]
W_{CI}	work/energy required for cut initiation	[Nm]
W_{def}	deformation work/energy involved into cutting	[N]
W'_{def}	elastic deformation work/energy involved into cutting	[N]
W'_{def}	viscous deformation work/energy involved into cutting	[N]
W_{fract}	fracture work/energy involved into cutting	[N]
W_{tribo}	friction work/energy involved into cutting	[N]
X	cutting pass	[N]

1 Introduction to cutting of foods

Cutting with a blade is the most prominent method in food processing to separate products into pieces with defined macroscopic dimensions. Segment size and shape accuracy, accurate product positioning before packaging and clean manufacturing demand high precision in processing. These factors depend on technical parameters such as cutting velocity, blade geometry and blade sharpness, and on the material properties of the food, e.g., mechanical properties, homogeneity, thermo-physical state (**Figure 1.1**).

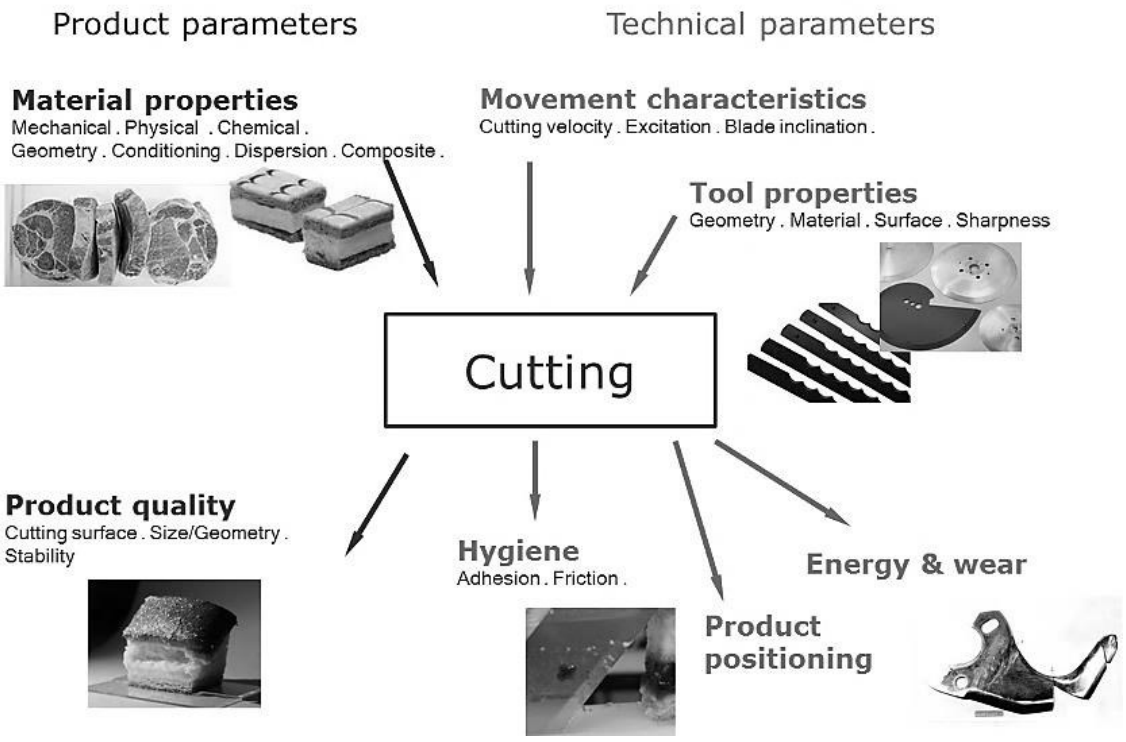

Figure 1.1: Schematic process characteristics of industrial food cutting showing important input parameters (top) and output parameters (bottom).

During the cutting process the motion of the cutting tool through the material leads to a complex interplay of deformation and fracture including a certain amount of friction between the moving device and the substrate (Dowgiallo, 2005; Schneider et al., 2009). This interaction of deformation, fracture and friction processes manifests itself in the cutting force profile which results from the resistance of the material against penetration of the cutting tool and it essentially determines the final quality attributes of the material to be cut. In general, a high cutting quality can be achieved if product deformation and cut-

ting forces are minimized. Depending on the specific mechanical and physicochemical properties of a particular food, another important issue that may contribute to cutting quality is the reduction of friction between blade and product (Atkins, 2009; Schneider et al., 2010). The relationship between deformation, fracture and friction forces and the resulting cutting quality can be referred to as cutting behavior.

The food industry usually processes agricultural materials into more or less complex products with liquid, semi-solid or hard and tough texture. In practice, foods can assume any condition between pure elastic and pure viscous behavior and, in most cases, a time and deformation dependent combination, denoted as viscoelasticity, is observed. The time dependency of viscoelastic materials is responsible for phenomena such as stress relaxation and creep (Metzger, 2014; Miri, 2011). Fracture occurs when the deformation caused by the blade leads to local stresses that exceed the strength of the material. If the kinetics of relaxation and creep processes in front of the cutting edge is faster than the chosen cutting velocity, no fracture occurs. This results in extensive deformation and irreversible structural damage. To prevent these effects, the apparent stiffness of the material has to be increased by applying a higher cutting velocity to limit the viscoelastic energy dissipation, or by cutting at lower material temperature to reduce structural mobility and flexibility (Steffe, 1996; Schneider et al., 2010). To achieve the highest possible cutting quality it is essential to identify and to describe these material properties in context of the relevant cutting process parameters.

In the industrial cutting of foods cutting velocities (relative motion between blade and product) of more than 1 m/s are state of the art. To increase the production flow-rate there is a general trend to faster processing; but, depending on the specific mechanical behavior of the viscoelastic products, this may lead to uncontrolled fracture phenomena such as product splintering, and undesired deformation effects such as irregular cutting surfaces, product deformation and insufficient cut accuracy. This is, in line with production interferences, a major limitation for a further increase of the throughput of industrial cutting machines. Since cause and effects are often unknown, the development and optimization of such machines is mainly based on an empirical adaptation of technical parameters, whereas an analytical correlation of product characteristics with damage events is frequently lacking. Hence, on the one hand, there is a need to understand the

relation between the mechanical properties and the cutting behavior of the products. On the other hand, there are obstacles in the process monitoring of high-speed cutting since testing devices for material characterization of foods normally operate in the dimension of mm/min or a few cm/min (Chen & Opara, 2013), and there is no standard testing machine available on the market that allows material characterization of solid foods and the corresponding process analysis at a testing velocity > 1 m/s; tailor-made solutions for test stations place high demands on design and measurement technology.

In summary there is a need to describe the cutting characteristics over a wide cutting velocity range up to high-speed on the basis of the material properties of viscoelastic foods. For this, methods have to be evaluated which relate parameters from material characterization and cutting force sequences, and cutting tests have to be carried out in the high speed range. The aim of the literature review is to describe the cutting process on phenomenological and energetic basis focusing on the involved mechanisms of deformation, fracture and friction. Furthermore, the influence of the viscoelasticity and rate dependency with regard to cutting mechanisms will be summarized. Finally, a brief overview of possibilities for the detection of high-speed cutting operations is given.

2 Literature review

2.1 Cutting forces and phenomena in orthogonal cutting

When cutting into a soft material with a straight edge blade, a deformation zone is formed in front of the cutting tool with increasing stress intensity in the vicinity of the blade tip (**Figure 2.1**). If exceeding the strength of the material a crack or cut is initiated that is growing with ongoing blade displacement l [m] (in the case of stable crack growth). Hence the material in front of the blade tip is deformed to a certain amount until fracture occurs.

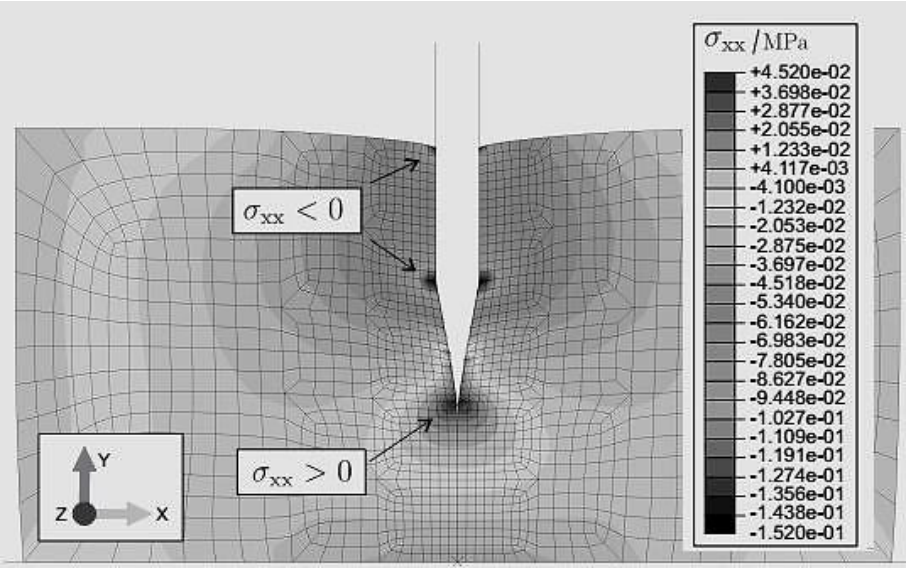

Figure 2.1: Stress distribution and deformation in orthogonal cutting with a straight edge blade. (from Boisly et al., 2016)

For isotropic materials and with constant boundary conditions the deformation (and crack initiation) zone in front of the blade tip will be shifted by the amount the blade penetrates into the material (McCarthy et al., 2007). In addition to deformation forces in front of the cutting edge, friction forces will arise from the relative motion between blade flanks and the material after cut initiation since restoring forces act vertically to the direction of movement and on the newly formed separating surfaces (Dowgiallo, 2005; McCarthy et al., 2007).

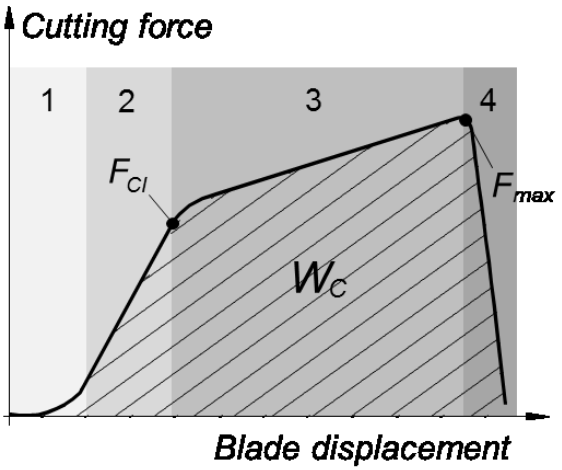

Figure 2.2: Cutting force course example for a large blade that stops after cutting the smaller sample, with a (1) start-up phase, (2) deformation phase, (3) separation phase and a (4) detaching phase. F_{Cl} depicts the force at cut initiation, F_{max} depicts the maximum cutting force and the area under the force course equals the cutting work W_C. The figure is based on table 1 in Schneider et al. (2002).

According to Schneider et al. (2002), four phases can be distinguished in a cutting process (**Figure 2.2**): The start-up phase (1) in which full contact between cutting edge and product is achieved, is followed by a deformation phase (2) in which the cutting force F_C [N] increases linearly. The separation phase (3) starts when a cut is initiated (F_{Cl} in **Figure 2.2**) which leads to an alteration of the F_C-slope. Phase (3) is determined by deformation and fracture in front of the blade as well as by friction between blade and product. In the detaching phase (4) the product is completely separated, and F_C drops to zero with decrease of the blade-product contact area. As a consequence, the contributions to F_C come only from deformation in phase (1) and (2), from deformation, fracture and friction in phase (3), and only from friction in phase (4) (Brown et al., 2005; Dowgiallo et al., 2005; Schneider et al., 2002).

For the separation phase (3) Tscheuschner (2004) established a cutting force balance as a function of the wedge angle β [°] of the blade (**Figure 2.3**):

$$F_C = F_R + 2 \cdot F_{SD\,1} \cdot \sin\frac{\beta}{2} + 2 \cdot F_{F\,1} \cdot \cos\frac{\beta}{2} + 2 \cdot F_{F\,2} \qquad \text{Eq. 2.1}$$

with a resistance force F_R [N] at the blade tip, friction forces from relative motion between blade and product at both sides of the blade wedge $F_{F\,1}$ [N] and both blade flanks

$F_{F\,2}$ [N] and with deformation forces at both sides of the blade wedge $F_{SD\,1}$ [N]. All side deformation forces F_{SD} [N] are acting orthogonal to the direction of the respective friction forces. As a friction force can be written as the product of the normal force and the friction coefficient μ [-], F_{SD} can be written as:

$$F_{SD} = F_F/\mu \qquad \text{Eq. 2.2}$$

so that **Eq. 2.1** can be summarized to:

$$F_C = F_R + 2 \cdot F_{F\,1}(\sin\frac{\beta}{2}/\mu + \cos\frac{\beta}{2}) + 2 \cdot F_{F\,2} \qquad \text{Eq. 2.3}$$

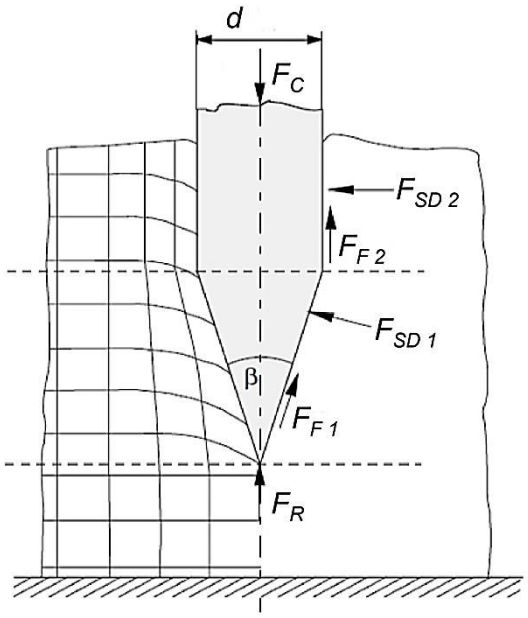

Figure 2.3: Outline of orthogonal cutting with a blade of thickness *d* with wedge angle *β* and forces involved: cutting force F_C, resistance force F_R, friction forces $F_{F\,1}$ and $F_{F\,2}$ and side deformation forces $F_{SD\,1}$ and $F_{SD\,2}$, (modified after Tscheuschner (2004) and Zahn (2009)).

As the second and the third summand of the equation can be described by tribological parameters both can be simplified to one friction force F_{tribo} [N]:

$$2 \cdot F_{F\,1}(\sin\frac{\beta}{2}/\mu + \cos\frac{\beta}{2}) + 2 \cdot F_{F\,2} = F_{tribo} \qquad \text{Eq. 2.4}$$

which leads to

$$F_C = F_R + F_{tribo} \qquad \text{Eq. 2.5}$$

F_{tribo} depends on $F_{SD\,1}$, $F_{SD\,2}$ [N] and on the surface properties of both friction partners and can decisively influence the cutting force. F_R is the force required to disintegrate the material cohesion and separate the product. This happens after the material has been deformed so far that the stress typically occurring in front of the blade tip exceeds the fracture tension of the material (at the end of cutting phase (2)). According to McCarthy et al. (2007, 2010) and own observations the deformation may remain in front of the blade, even after a cut has been initiated, i. e., the deformation zone in front of the blade tip travels with progressive advancement of the blade and corresponds to the blade displacement at cut initiation depth (*CI*, [mm]). The crack length therefore corresponds to the blade displacement minus *CI*. As a result, F_R can be divided into a deformation and a fracture force F_{def} [N] and F_{fract} [N]. This leads to the equation introduced by Dowgiallo (2005):

$$F_C = F_{def} + F_{fract} + F_{tribo} \qquad \text{Eq. 2.6}$$

Cutting experiments for fracture parameter determination with wires have shown that the fracture force depends decisively on the radius of the cutting tool (Gamonpilas et al., 2009; Goh et al., 2005; Kamyab et al., 1998). Therefore, the sharpness of the blade has a significant influence on the measured total cutting force F_C (Schuldt et al., 2013). According to literature (see e. g. Dowgiallo (2005) and Lyuten et al. (1991)) F_{def} is dedicated to elastic (F'_{def} [N]) and viscous deformation (F''_{def} [N]) so that **Eq. 2.6** can also be written as:

$$F_C = F'_{def} + F''_{def} + F_{fract} + F_{tribo} \qquad \text{Eq. 2.7}$$

Hence, depending on the mechanical properties of the product and the geometrical properties of the blade, the fracture and deformation forces can make up a large part of the cutting force.

Due to the movement of the blade through the product, the cutting work W_C [Nm] can be determined as the area under the F_C/l-course (see **Figure 2.2**):

$$W_C = \int_{l=0}^{l_{max}} F_C(l)\,dl \qquad \text{Eq. 2.8}$$

which leads to:

$$W_C = W'_{def} + W''_{def} + W_{fract} + W_{tribo}$$ Eq. 2.9

In summary, the force applied during cutting is distinctively influenced by the mechanical properties, i. e. the deformation and fracture properties, of the viscoelastic cutting materials, as well as their frictional properties. According to Luyten et al. (1992) the rate of cutting is directly related to the rate of fracturing. Therefore, for examining the influence of the cutting velocity on the cutting behavior, it is obvious to characterize the rate-dependent deformation, fracture and friction properties of these materials.

2.2 Rate dependency of deformation and fracture of viscoelastic materials

In theory there exist solids that show a pure elastic (or Hookean) behavior if exposed to a stress σ [Pa] or strain ε [-] (Hookean spring). In these materials all mechanical energy is reversibly stored. On the other side there exist materials that dissipate all exposed mechanical energy which is referred to linear viscous (or Newtonian) behavior (Newtonian dashpot). In practice solids often show viscoelastic material behavior. It means that the reaction of the material to an applied stress or strain comprises partly of a viscous and partly of an elastic component (Steffe, 1996; Vincent, 2012). That is a typical behavior of (solid) foods.

Methods to determine deformation properties usually focus on the ratio of stress (or force) to strain. Theoretically there exist three simple deformation modes: all-sided compression, simple shear and uniaxial tension/compression. The stress or deformation can be applied constantly or monotonically changing (static experiments) or fluctuating with a certain frequency (dynamic experiments) (Luyten, 1988; Luyten et al., 1992).

If a viscoelastic material is exposed to (small) deformation that does not irreversibly alter its structure, the ratio between stress and strain is constant. That means the stress proportionally increases with strain. This deformation range is called linear viscoelastic region. The σ/ε ratio in the linear viscoelastic region is called “modulus” and is a measure of material stiffness (Lakes, 2004; Metzger, 2014; Steffe, 1996, van Vliet et al., 1993). The Young‘s modulus is e.g. determined from uniaxial tension experiments (**Figure 2.4**).

The ratio between the viscous and the elastic component depends on the time scale of the experiment. At long time scales more energy can be dissipated by viscous flow or relaxation, because these are processes that take time. At short time scales the reaction of the material is more elastic, hence more energy is reversibly stored or less energy can be drained off (Lyuten, 1988).

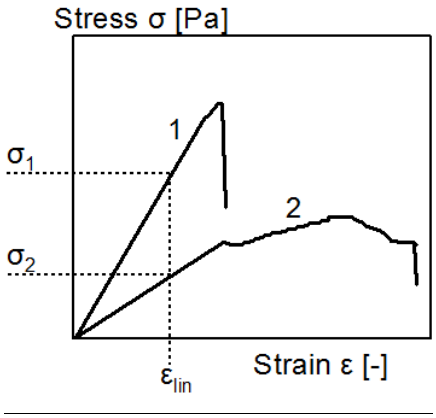

Figure 2.4: Scheme for determination of Young's modulus (ratio of stress σ to strain ε in the linear region ε_{lin}) out of uniaxial tension experiments (until fracture) for two materials (1, 2).

If the stress or strain is applied by sinusoidal oscillation on a viscoelastic material the resulting (or measured) strain or stress is delayed. That means a phase shift δ [°] can be measured between input and output signal (**Figure 2.5**, left). This phase shift has a value between 0° (pure elastic) and 90° (pure viscous). From dynamic mechanical analyses (DMA) a complex modulus E^* [Pa] (from uniaxial experiments; G^* [Pa] from shear experiments) is derived from the ratio of σ and ε amplitude. The complex modulus can be plotted on a complex plane (**Figure 2.5**, right). From that E^* equals the square root of sum of squares of loss modulus E'' [Pa] (G'' [Pa] from shear experiments) and storage modulus E' (Pa) (G' [Pa] from shear experiments). E'' is the imaginary part of E^* and a measure of the dissipated energy in a material (viscous component). E' is the real part of E^* and a measure of elastically stored energy (elastic component). The ratio E''/E' is designated as loss factor $tan\ \delta$ [-] and is like that a measure of the viscoelastic contribution of a system (Lakes, 2004; Metzger, 2014; Vincent, 2012). The time scale of an experiment is the time during which a certain stress is exerted on a material. It can be varied by changing the deformation or stress rate in a static experiment or by changing the frequency in dynamic tests (Luyten, 1988).

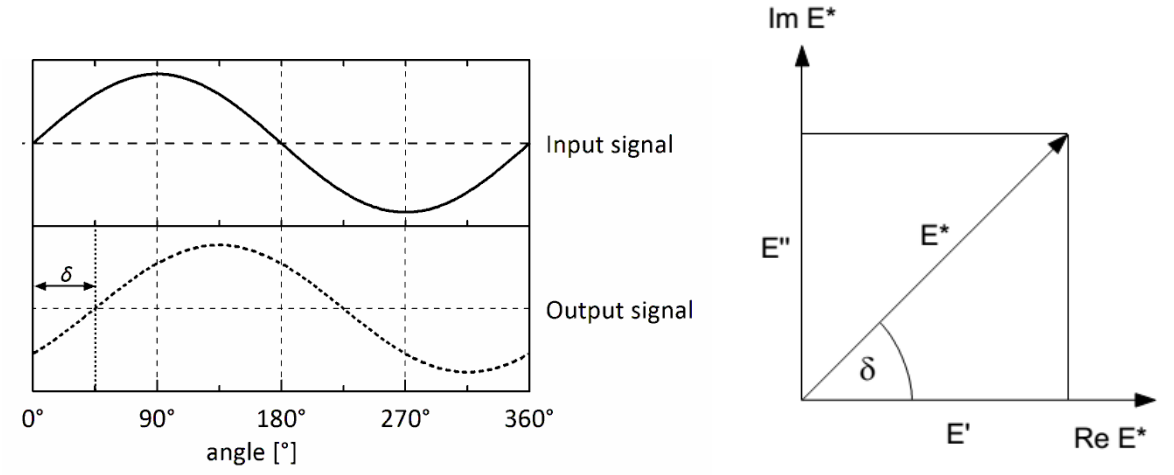

Figure 2.5: Phase shift δ of 45° between input signal (full line) and output signal (dotted line) from a dynamic mechanical measurement (left). Vector diagram with loss modulus *E''*, storage modulus *E'* and the resulting complex modulus *E** (after Metzger, 2014) (right).

If the rate at which the stress or strain is applied to a viscoelastic material is increased (decrease of time scale) the ratio between stress and strain increases in static and dynamic experiments, as less energy can be dissipated. That means that moduli increase with higher frequency or higher testing velocity (**Figure 2.6**).

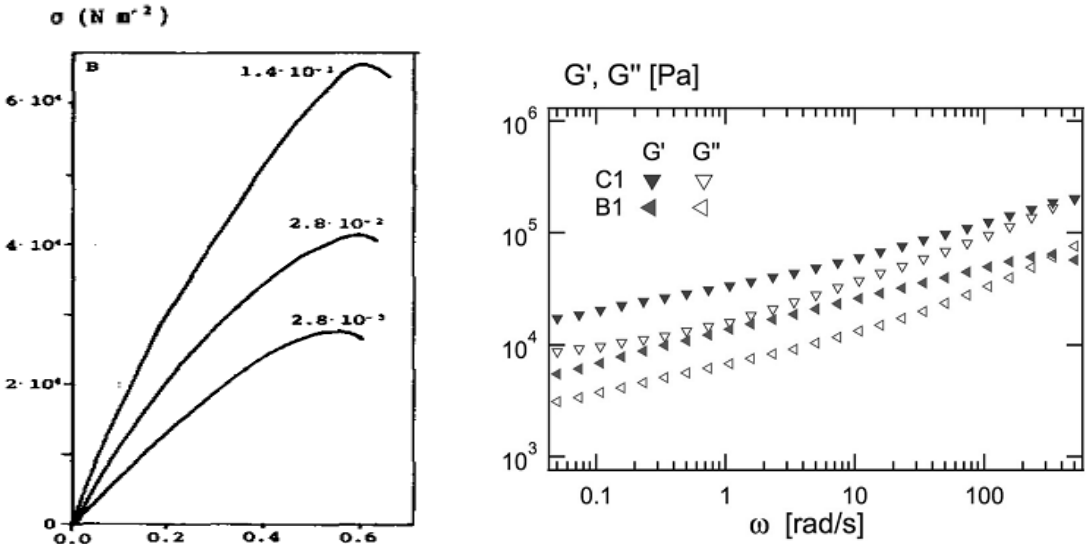

Figure 2.6: Compression curves for cheese at a strain rate of $2.8 \cdot 10^{-3}$, $2.8 \cdot 10^{-2}$, $1.4 \cdot 10^{-1}$ (reproduced from Lyuten, 1988) (left); Frequency dependence of storage modulus G' and loss modulus G'' of different chewing gums (C1, B1) (reproduced from Martinetti et al., 2014) (right).

To impose stress or deformation to a material a work or energy *W* [Nm] is needed. Considering σ as the applied force related to the initial cross sectional area of the specimen (engineering stress) and ε as the length change referred to the initial length (Cauchy

strain) the area under the σ/ε-course linearly correlates to W as it is the area under the F/l-course (**Eq. 2.8**). According to the above given considerations this imposed energy is partly elastically stored (W' [Nm]) and partly dissipated (W'' [Nm]):

$$W = W' + W'' \qquad \text{Eq. 2.10}$$

This equation applies for small deformations where no irreversible damage appears in the material but also for further deformation that exceeds the linear viscoelastic region. In this case the ratio between stress and deformation changes and irreversible damage of the material can occur (Luyten, 1988). According to van Vliet et al. (1993) friction between the structural elements of composite foods (gel systems with filler, dispersions) can contribute to the energy dissipation, especially at large deformations. From that W'' can be written as sum of energy of viscous flow W''_{visc} [Nm] and inner friction W''_{frict} [Nm] which gives:

$$W = W' + W''_{visc} + W''_{frict} \qquad \text{Eq. 2.11}$$

If the deformation is increased in a way that the imposed stress exceeds material cohesion fracture can appear so that additional fracture energy W''_{fract} [Nm] has to be considered:

$$W = W' + W''_{visc} + W''_{frict} + W''_{fract} \qquad \text{Eq. 2.12}$$

As a part of the elastically stored energy in the fracture process zone is released to W''_{fract}, the fracture energy comes from W' (van Vliet et al., 1993; van Vliet, 1996). Hence W is the sum of an elastic energy, a dissipative energy due to deformation, and a dissipative energy due to fracture which coincides with the first three summands of **Eq. 2.9** which additionally includes W_{tribo} due to friction between blade and the material. This leads to the cutting energy (W_C) equation that was proposed by Schuldt et al. (2016a):

$$W_C = W' + W''_{visc} + W''_{frict} + W''_{fract} + W_{tribo} \qquad \text{Eq. 2.13}$$

Fracture can be defined as the break of all bonds between structural elements in a certain macroscopic plane which leads to a structural breakdown of the material over length scales much larger than the structural elements (van Vliet et al., 1993). There are

certain parameters describing fracture properties of foods. Some of the most prominent are the fracture stress σ_f [Pa], fracture strain ε_f [-] and fracture toughness [J/m²].

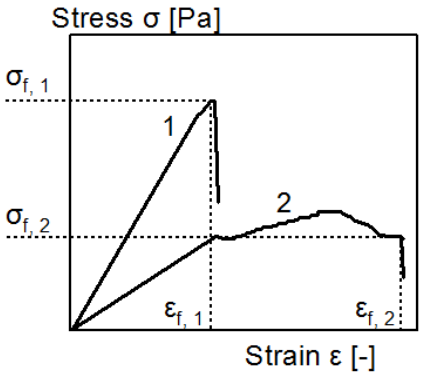

Figure 2.7: Scheme for determination of fracture stress σ_f and fracture strain ε_f out of uniaxial tension experiments for two materials (1, 2), with material 1, shortly fracturing after linear deformation and material 2, extensively yielding before failure (after ISO 527-1: 2012).

Fracture stress is the stress that is needed for total fracture of a specimen at a certain strain (ε_f) (**Figure 2.7**). Therefore W to gain σ_f can include amounts of elastically stored energy, fracture energy and energy that is dissipated due to viscous flow and inner friction (**Eq. 2.12**). In the example in **Figure 2.7**, a material 1 is shown which totally fractures shortly after exceeding the linear deformation range. Material 2, on the other hand, passes through a pronounced non-linear deformation until total fracture occurs. Although the total energy for material failure (area under σ/ε-curve) is slightly larger for material 2, its σ_f is only about half as big as that of material 1. The single evaluation of σ_f can therefore lead to misinterpretations in comparing the fracture resistance of different materials. However, since it is easy to determine, the fracture stress is an often used measure for the evaluation of the fracture properties of foods (Luyten et al., 1992) and polymers (ISO 527-1: 2012).

Fracture toughness can be described by the fracture energy W_{fract} which comes from W' (van Vliet, 1996). It is the work that is needed for exceeding material cohesion and creating new surfaces. Depending on the area of research different terms for explaining fracture toughness are used: Williams (2009) stated that fracture toughness can be described by the surface energy of a material. If this material does not fracture in a brittle but a “tough” (or ductile) manner an amount of plastic/viscous work has to be added to describe fracture toughness. Van Vliet et al. (1991) described that two mechanisms are

involved into macroscopic fracture of gel-like foods: (real) fracture and yielding. Both mechanisms have to be explained on a microscopic level: (real) fracture leads to "simultaneous breaking of bonds between the structural elements of the network" and the formation of a crack. Yielding is referred to as viscous flow and located around the crack tip; it can lead to an increase of fracture strain (van Vliet et al., 1991). In polymer science the mechanism (real) fracture is referred to as "work of separation". Mechanisms that substantially contribute to this work of separation are "crazing" and "cavitation" which are described as „void growth in the fracture process zone (FPZ)" which precedes crack growth (**Figure 2.8**). The starting points are defects (voids, also described as holes) in the material. Void growth is thereby caused by tensile stresses in front of the crack tip, which leads to crack growth which overturns material cohesion. The term "yielding" that was used by van Vliet et al. (1991) is described as "viscoelastic dissipation" in the FPZ. Both micromechanical mechanisms, void growth and viscoelastic dissipation, contribute to fracture toughness (Tang et al., 2008).

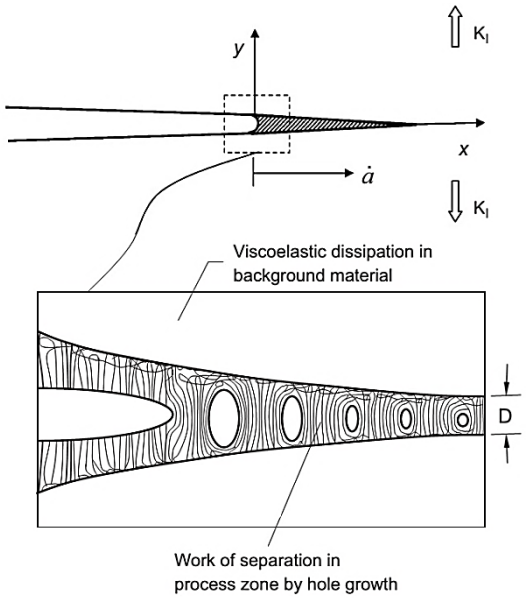

Figure 2.8: Schematic of craze-like microporous zone surrounding a crack growing steadily under small-scale yielding conditions (Tang et al., 2008).

Even though fracture stress is macroscopically derived from the force response of a specimen and the energy needed for fracture includes different mechanisms (**Eq. 2.12**), fracture toughness being one of those, fracture stress and fracture toughness are often considered as equivalent (Lillford, 2001). This clearly can only hold for dominant elastic

materials, ideally with small fracture strain, which can be the case for biscuits or food gels (Lillford, 2001; Gamonpilas et al., 2009) or for materials that fracture in a brittle manner. If viscous flow (W''_{visc}) and/or inner friction (W''_{frict}) highly contribute to the overall energy W, fracture stress and fracture toughness could somehow deviate from each other.

In viscoelastic systems σ_f can be velocity-dependent as it comes from rate-dependent deformation parameters (see **Figure 2.6**). It normally increases with increasing deformation speed because more energy is required to deform the material to a certain extent and fracture energy (i.e. fracture toughness) is often increasing (van Vliet et al., 1993). It is known that fracture strains from compression or tensile experiments of polymeric food systems can increase, fall or stay constant with rate increase (van Vliet et al., 1993; van Vliet & Walstra, 1995). After van Vliet et al. (1993) the trends for σ_f and ε_f arise from two energy dissipation mechanisms referring to:

1. viscoelasticity and
2. friction between the different structural elements of composite systems.

The first mechanism means that energy dissipation because of viscous flow is higher for lower strain rates. Thus the viscous contribution tends to be stronger and the decrease of storage modulus is steeper than the decrease of loss modulus at decreasing strain rate. It follows that transport of elastically stored energy to the crack tip can be inhibited because of stress relaxation during crack growth (Luyten et al., 1991). Hence the material has to be deformed further to reach an amount of energy (W) to induce or propagate fracture. This means that ε_f increases with decreasing strain rate (Luyten & van Vliet, 1995; van Vliet et al., 1993). For small velocities σ_f can also decrease with increasing deformation rate if W''_{visc} is the dominating part of W (Luyten & van Vliet, 1995; van Vliet et al., 1993; van Vliet & Walstra, 1995).

The second mechanism comes from the composite nature of foods. Thus different structural elements with different mechanical properties in one material have the effect that deformation of such a material can be inhomogeneous especially at larger deformations where fracture occurs. This will cause friction between the structural elements of the food (van Vliet et al., 1993; van Vliet & Walstra, 1995). From considerations of local rate of deformation and crack speed van Vliet et al. (1993) derived that this energy dissipation tends to increase with deformation speed. This could have the effect that the

stored energy stays low and the energy transport to the crack tip "proceeds inefficiently" which can also contribute to the increase of σ_f and lead to fracture strain increase with increasing deformation rate (van Vliet et al., 1993). However this theory for σ_f increase is not generally accepted (Gamonpilas et al., 2009). Another reason for rate-increasing ε_f is that at small deformation rates, more time is available for crack propagation. A small stress that acts for long time (referred to the time scale of the experiment) can induce fracture at small deformations when the induced stress is sufficiently large to ensure slow crack propagation. This can lead to an increase of fracture strain at higher velocities (Luyten & van Vliet, 1995; Boisly et al., 2016; Rohm & Lederer, 1992).

Another factor influencing the rate dependence of σ_f is fracture toughness which can decrease or increase with strain rate or velocity (Abadyan et al., 2012; Landis et al., 2000; Luyten & van Vliet, 1995; Tang et al., 2008). According to van Vliet et al. (1993) in viscoelastic materials the fracture energy is associated to the storage modulus which represents the number of effective elastic interlinks per unit cross-sectional area. Thus the rate-dependent increase of storage modulus causes an increase of fracture toughness with increasing velocity (van Vliet et al., 1993). Work of separation and viscoelastic dissipation, both contributing to fracture toughness, can act simultaneously (see e.g. Cessna, 1974; Dijkstra et al., 2002, Tang et al., 2008) (**Figure 2.9**).

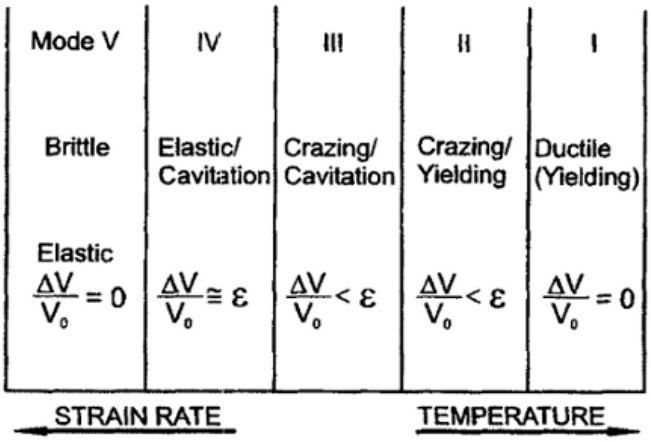

Figure 2.9: Deformation map according to Cessna (1974) giving deformation mechanisms as a function of strain rate or, equivalently, temperature (from Dijkstra et al., 2002).

After Tang et al. (2008) for tough fracture (with stable crack growth) of polymeric systems two regimes can exist in one material: (1) the regime where the work of separation is dominating and (2) the regime where viscoelastic dissipation is the dominating

contribution to fracture toughness. If crack or fracture velocity is enhanced (which is associated with higher deformation speed) an increase of void growth (which can be regarded as defects) in the FPZ is enhancing work of separation (Luyten & van Vliet, 1995; Tang et al., 2008). Simultaneously viscous energy dissipation decreases because of shorter time scales. Hence with increasing crack velocity fracture toughness is increasing in regime (1) and decreasing in regime (2). Both regimes can appear in one material from slow to high velocity (**Figure 2.10**). The regimes are influenced by the initial void or defect size and the rate dependence of the void growth mechanism and the rate dependence of the bulk material (Tang et al., 2008).

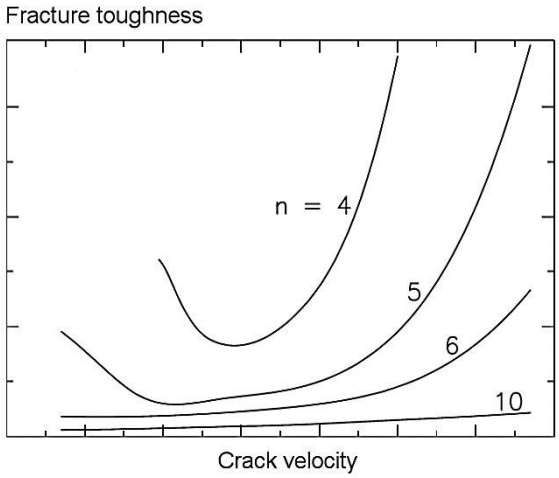

Figure 2.10: Calculated values of fracture toughness for a viscoelastic solid in the regime of stable crack growth (tough fracture) over the crack velocity for different boundary conditions (indicated by n) (modified after Tang et al., 2008).

As stated above the time scale is important for the viscoelastic characteristics. Generally increasing the rate or velocity of deformation reduces the time scale for viscous dissipation and simultaneously increases the stress in the material. If this stress exceeds the amount of stress that is needed for fracture and if the time scale is too short for sufficient energy dissipation fracture progressively shifts from tough to brittle (van Vliet et al., 1993). That means the material fractures without plastic deformation (Bryan & Ahuja, 1993; Gdoutos, 2005) and unstable crack growth with high crack speed can appear (Bryan & Ahuja, 1993; Farahmand, 2001). As brittle fracture equals tough fracture but without plastic work, brittle fracture only refers to the surface energy which is consequently smaller than the energy needed for tough fracture (Williams, 2009) (**Figure 2.11**).

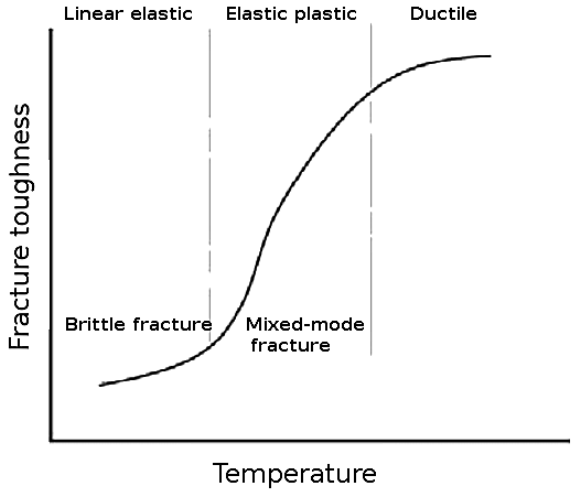

Figure 2.11: Schematic of fracture toughness dependence on temperature with transition from full ductile to brittle (linear elastic) behavior (modified after Aderinola et al., 2014)

Increasing the temperature of a material increases the molecular mobility and like that enhances relaxation processes. On molecular level this can be referred to an increase of possible transposition processes of molecules in a polymeric network (Wrana, 2014). In opposite this leads to a decrease of viscous dissipation with temperature decrease which is in principle the same effect as decreasing the time scale or increasing the strain rate. Hence for many polymeric single-phase systems and blends time and temperature can be considered as equivalent impacts (Cho & Lee, 1998; van Gurp & Palmen, 1998; Wrana, 2014). Therefore, under certain circumstances shift of the deformation parameters on the time scale is possible (Dealy & Plazek, 2009; van Gurp & Palmen, 1998) (**Figure 2.12**). This method of temperature-time superposition (tts) is used to open up areas which are difficult to measure (e.g. to display very long and short time scales). Although tts is derived from deformation processes (Wrana, 2014), it was also possible to verify a validity for fracture parameters (Cho & Lee, 1998; Pohlit et al., 2008), since these are also dependent on the deformation behavior. As a lower temperature has the same effect as a shorter time scale, decreasing the temperature promotes brittle fracture (Cessna, 1974; Olwig, 2006) (**Figure 2.11**). The Cessna deformation map effectively illustrates this relation of strain rate, temperature and deformation mechanisms from ductile to brittle (**Figure 2.9**).

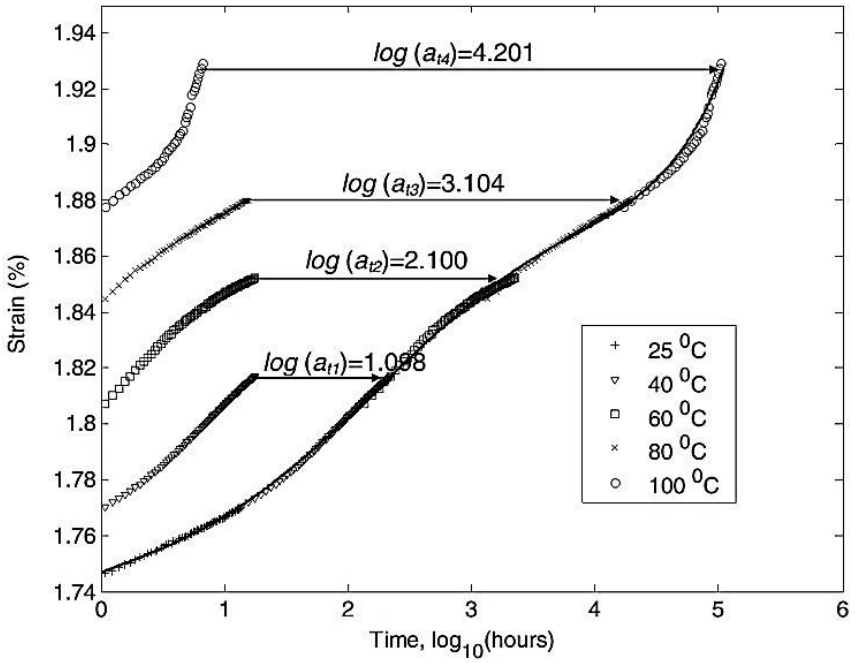

Figure 2.12: Explanation of the shift principle of temperature time superposition by means of creep data on aramid fibers at different temperatures (reference temperature equals 25 °C; a, shift factor) (Alwis & Burgoyne, 2006).

2.3 Rate dependent friction properties of viscoelastic materials

Tribology deals with friction, lubrication and wear of surfaces, which are in a relative movement to one another. The interfacial effects between solid bodies as well as between solids and liquids or gases are considered (Dresselhuis et al., 2007; Moore & Geyer, 1972). An important tribological quantity is the friction force F_F [N]. It reflects the mechanical resistance of the friction bodies against a relative movement. From this the coefficient of friction $\mu = F_F/F_{norm}$ [-] is calculated, with the normal force F_{norm} [N] acting orthogonal to the plane of movement. A distinction is made between static friction and sliding friction. If the attacking forces are not sufficient to allow a movement, this is referred to as static friction. The sliding friction is defined as resistance to an existing relative movement of the friction partners (Czichos & Habig, 2010). Stick-slip is an alternation of static and sliding friction and is favored by low relative speed or high surface pressure and deformable friction bodies (Czichos & Habig, 2010; Schneider et al., 2009). Depending on whether a lubricant is present, dry and lubricated friction can be distinguished (Czichos & Habig, 2010). The following sections describe the phenomena associated with friction

between hard (metal) and soft friction bodies, as it is the case when cutting food with a blade.

Friction can be attributed to different interaction mechanisms. These can be distinguished in atomic or molecular (adhesion) interactions in the contact area and mechanical interactions in the bulk of the material (elastic and plastic deformations) (Atkinson, 1975; Czichos & Habig, 2010; Moore & Geyer, 1972). Hence the friction force can be expressed as the sum of a viscoelastic deformation force F_{VE} [N] from the material bulk and the adhesion force F_{adh} [N] (Lorenz et al., 2013a; Moore & Geyer, 1972):

$$F_F = F_{VE} + F_{adh} \qquad \text{Eq. 2.14}$$

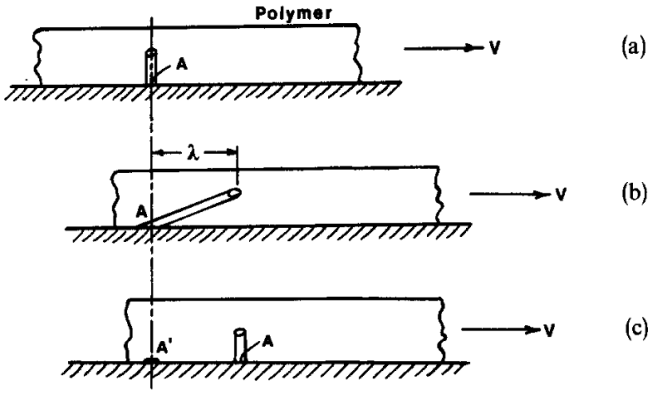

Figure 2.13: Simplified stick-slip model of adhesion: (a) "adhesion" takes place at points A; (b) elastomer sample moves a distance λ at velocity V, and frictional drag is developed. Elastic energy is stored in element; (c) adhesion at A' fails. Energy stored in element is returned in part to system. New point of attachment at A (Moore & Geyer, 1972).

Adhesion in combination with relative movement of the friction bodies leads to the formation, growth and breaking of bonds in the real contact area. Mainly responsible for these adhesion phenomena are hydrogen bonds and van der Waals forces. The real contact area is composed of the sum of the micro contact areas and depends on temperature, F_{norm} and the sliding velocity as well as the surface roughness and the mechanical properties of the friction bodies (Czichos & Habig, 2010; Moore & Geyer, 1972). F_{adh} can be expressed as the product of a "frictional shear stress" and the local area of contact; both depend on sliding velocity and temperature (especially the frictional shear stress) (Lorenz et al., 2013a; Moore & Geyer, 1972).

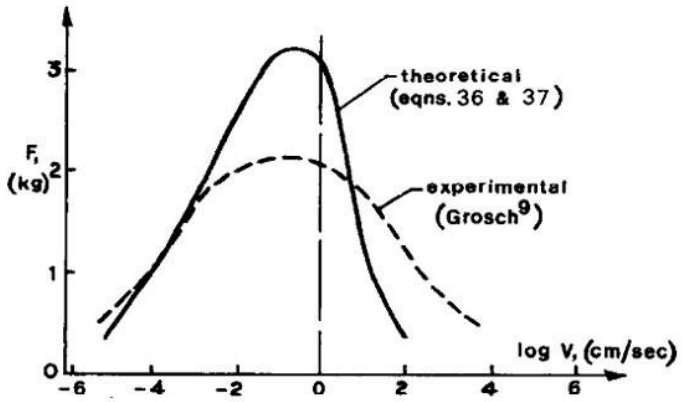

Figure 2.14: Experimentally and theoretically derived friction force due to adhesion versus sliding velocity (Moore & Geyer, 1972).

Adhesion in sliding friction is often described as a thermally activated molecular stick-slip process and can lead to a deformation of the soft friction surface (**Figure 2.13**). Due to the temporally dependence on the formation and breaking of bonds, the adhesion process is rate-dependent (**Figure 2.14**) (Moore & Geyer, 1972). At low velocity, an increase in velocity initially leads to an increase in bond development and breaking, which leads to an increase of F_{adh} (more bonds will be formed and ruptured per time). Above a specific velocity, the adhesion force decreases again as the contact time between the friction bodies is limiting the development and breaking of bonds at the friction interface. This behavior results in a maximum of the friction force due to pure adhesion at a specific sliding velocity (Grosch, 1963; Moore & Geyer, 1972). Thus adhesion plays a subordinate role at very high velocities (Grosch, 1963), but it can certainly play a dominant role in friction at lower velocities (Grosch, 1963; Schell, 2005).

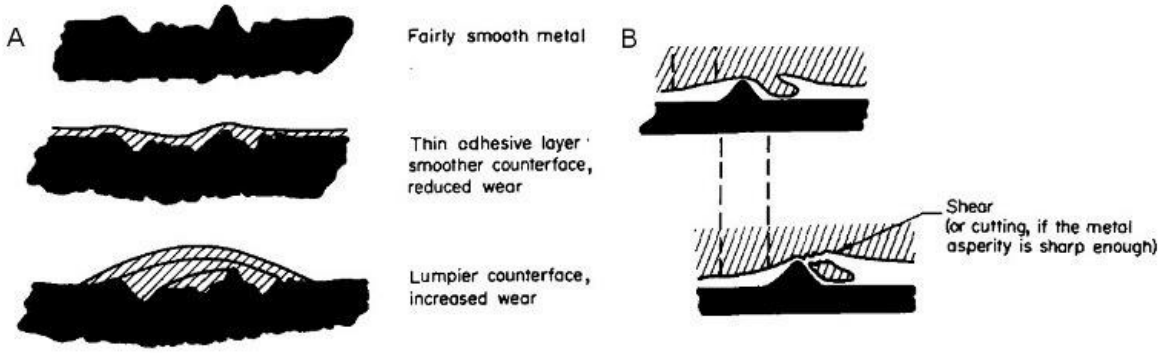

Figure 2.15: A schematic representation of the effects of different transfer films in adhesive wear (A); a schematic representation of abrasive wear: the metal asperity shears or cuts parts from the soft friction body (B) (from Atkinson, 1975).

As a result of friction a transfer film of the softer material can be formed on the hard friction partner, which can change the adhesion conditions in the area of contact and can lead to adhesive wear. This can increase or decrease the wear rate (**Figure 2.15, A**). The amount of adhesive wear will depend on a number of factors including the load, the environment, the sliding velocity and the material properties of the friction bodies (Atkinson, 1975; Brown et al., 1976).

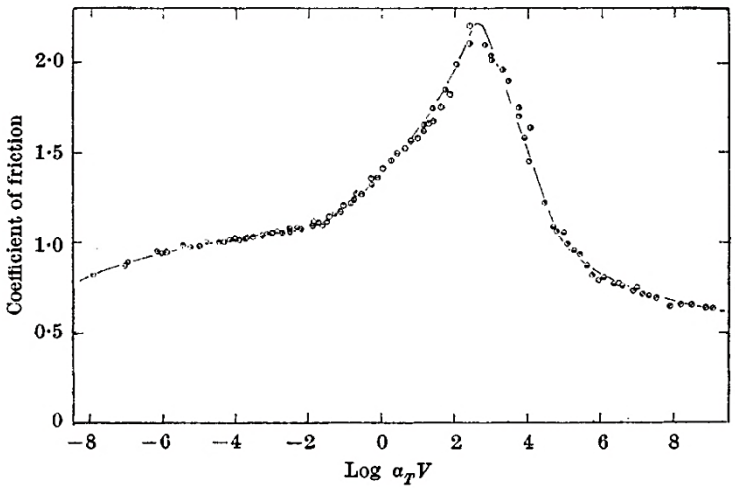

Figure 2.16: Friction master curve for the coefficient of friction of an acrylonite-butadiene gum vulcanizate (versus sliding velocity; a_T, shift factor) sliding on silicon carbide abrasive, dusted with magnesium oxide powder (to exclude adhesion) with a reference temperature of 20 °C (from Grosch, 1963).

Relative motion between the friction bodies can lead to mechanical interactions in the bulk of the material of the softer friction partner. These are induced e.g. by penetration of the harder into the softer friction partner or by hooking of both friction partners into one another (Czichos & Habig, 2010, McKellop, 2007). The mechanical interactions lead to elastic and plastic deformation (Atkinson, 1975; Brown et al., 1976) as well as to viscoelastic energy dissipation (Czichos & Habig, 2010; Lorenz et al., 2013a, 2013b). In abrasive wear hard irregularities of one friction partner penetrate a softer material and remove parts of the material by shear or cutting (**Figure 2.15, B**). Here the total deformation before fracture will be made up of an initial elastic component plus a viscous component for larger deformation (Atkinson, 1975; Brown et al., 1976). Since the friction force depends on the mechanical properties of the softer friction partner, F_F can be described as a function of the deformation characteristics and shows a corresponding de-

pendence on the velocity. Thus Grosch (1963) experimentally showed a relationship between the maximum of the friction force and viscoelastic energy dissipation (maximum of the loss factor) that could be used for applying temperature time superposition (**Figure 2.16**) (Grosch, 1963; Lorenz et al., 2013a).

Lubrication can greatly reduce friction, since the direct contact between the friction partners is (partially) substituted through the contact with a lubricant. For lubricated systems Stribeck curves are used which display the coefficient of friction over sliding velocity (**Figure 2.17**). In this, several regimes are crossed: At small sliding velocity, a "boundary regime" takes place, where the friction depends on the characteristics of the surfaces (Dresselhuis et al., 2007). The "mixed regime" at higher sliding velocities is characterized by a decrease in the solid body friction and an increased role of the rheology of the lubricant, which ideally manifests itself in a drop of the friction force. The "hydrodynamic regime" only depends on the rheology of the lubricant (Czichos & Habig, 2010).

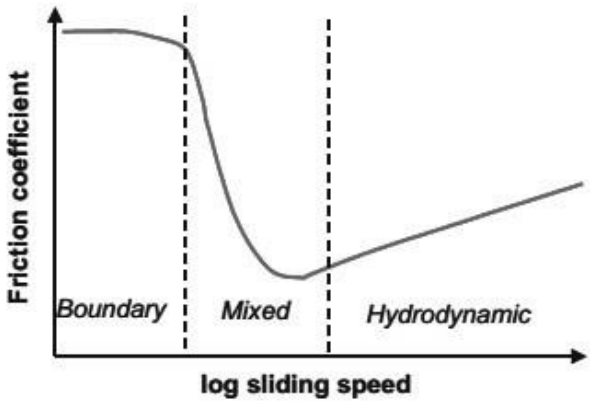

Figure 2.17: Stribeck curve with the three lubrication regimes (from Dresselhuis et al., 2007).

As described, the friction between hard and soft bodies depends on a variety of interacting parameters such as surface topography, hardness of friction partners, physicochemical surface properties, contact area, abrasive films in the interface. However individual friction mechanisms are difficult to distinguish and determine (McKellop, 2007). In summary, it is difficult to describe the friction behavior as a function of the cutting velocity. In general, the adhesion contribution to F_C should decrease at high sliding velocity. However, a strong rate-dependent deformation behavior of the food could mitigate or reverse this effect. During a cyclic cutting process wear films can build up in the course of the processing, which in turn can also influence the friction force. When cutting foods,

there are generally large differences in hardness between the friction partners. Therefore, the roughness of the blade is of great importance. This in turn affects the real contact zone, which in turn can increase F_{adh}. Additionally, foods vary greatly in their surface properties and their mechanical characteristics. Adhesive films can be formed which contribute to system lubrication or reverse, but also large plastic deformations with abrasion of particles can appear (Schneider, 2007). As foods greatly vary in their tribological properties, solutions to reduce friction in food processing (blade geometry, blade coatings) often target on specific applications and products.

2.4 Challenges in high-speed characterization

There are very few publications in which foods were tested at high velocities to draw conclusions on the cutting or processing behavior. A main reason is that it is difficult to evaluate high-speed processes on the basis of material characteristics of foods at high deformation rate, or velocity. This is because commercially available equipment for quasi-static compression or tension tests generally operates at velocities in the dimension of mm/min or a few cm/min (Chen & Opara, 2013). Leadscrew driven systems and expensive hydraulic or pneumatic systems can reach velocities of more than 1 m/s. However these devices usually are designed for the measurement of larger forces for testing polymers or metals. There is, to the best of my knowledge, no standard testing machine available on the market that allows material characterization of solid foods and the corresponding process analysis at a testing velocity > 1 m/s. Therefore, it can be an approach to build up a tailor made test station. Equipment to apply testing velocities > 1 m/s includes, for example, linear actuators, rotational systems, and pendulum or drop weight testers (Field et al., 2004; Meyers, 1994; Olwig, 2006) which provide the possibility of high-speed testing (see **Figure 2.18** for overview).

A further challenge is the selection of suitable force sensors for high-speed applications. For continuous force data capturing usually strain gauge based or piezo-electric force transducers are used (Pohlit et al., 2008). Compared to synthetic polymers or metals, foods show only small forces against deformation or cutting. This requires sensitive measuring systems, which, however, must be robust against larger force impacts at high-

er velocities. A further problem in force data capturing can be vibrations, which most likely occur in tests with dynamic or sudden impact. They arise, for example, due to an unsuitable test station design (natural resonance) or when, for example, the testing blade is excited to vibrate. These oscillations can be transmitted to the measuring system and superimpose the measured signal. For high-speed measurements, it may also be important whether the force is measured in front of the sample (at the blade) or behind the sample (at the sample support), since the sample itself can act as an attenuator. The measured force signals in front of the sample are thus more susceptible to alternations (Maurer, 2003; Shergold et al., 2006).

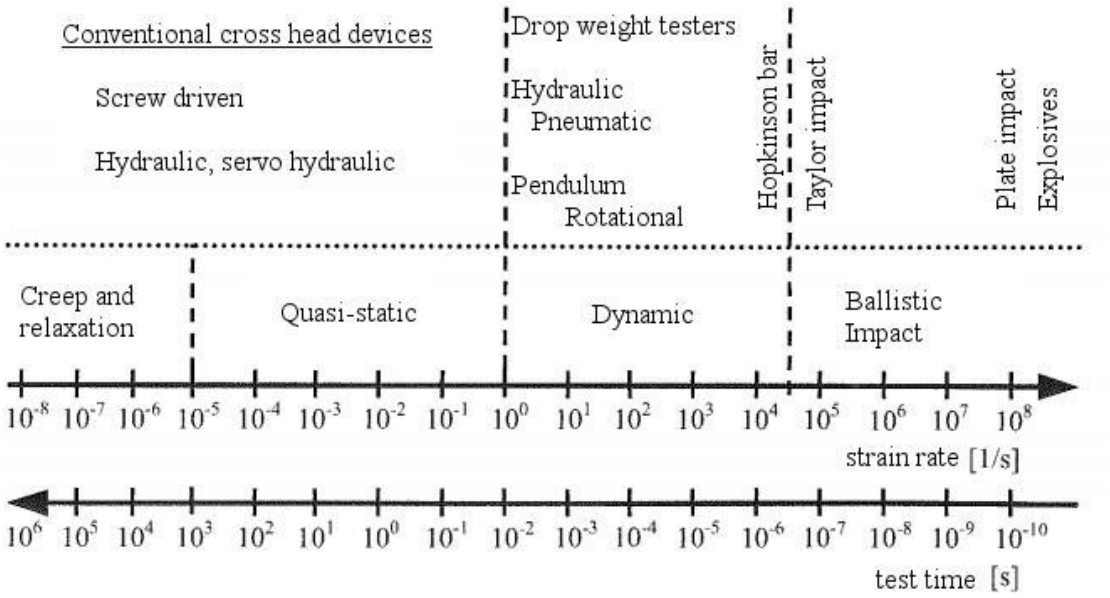

Figure 2.18: Overview of methods of material testing, classified according to strain rates or the experimental time characteristic of the type of test (modified after Olwig, 2006; Field et al., 2004; Meyers, 1994)

In general, strain gauge based force transducers are used to characterize mechanical properties in the range of typical slow and medium testing velocities, as they are common in commercially available testing devices. However, load cells for measuring small forces have low stiffness, which can lead to the transmission of vibrations especially at higher testing velocities (Stock, 2015). In comparison to piezo-electric force sensors it has also been shown that strain gauges can output false force signals with too low values at high speeds or sudden loads because of lower response times (Pohlit et al., 2008). In

general piezo-electric force transducers are well suited for dynamic measurements of small forces and with a high data rate. Their low weight and high stiffness reduce the potential for distinct natural resonance (Stock, 2015).

A demonstration of limits can be given by cutting force measurements at elevated velocity (Kretzschmar, 2013). Here the cutting forces of cheese (Gouda) and a synthetic polymer (nitrile butadiene rubber, NBR) were documented over more than 5 decades of cutting velocity (**Figure 2.19**). The low and medium cutting velocities (up to $4 \cdot 10^{-2}$ m/s) were investigated with an Instron universal testing machine and associated 100 N (cheese) or 5 kN (NBR) strain gauge force transducers. For the velocities above, a servo hydraulic system with 200 N (cheese) and 10 kN (NBR) strain gauge force transducers was used. The results show almost vibration-free cutting force profiles for the commercial measuring system (Instron) and vibrations in the force profiles of the servo hydraulic system. While these are distinct for NBR with distinct variations at $1.4 \cdot 10^{0}$ m/s (10 kN sensor with high basic stiffness), the results of cheese with the 200 N force sensor show exorbitant force deflections at $4 \cdot 10^{-1}$ m/s and $1 \cdot 10^{0}$ m/s (deflections out of scale).

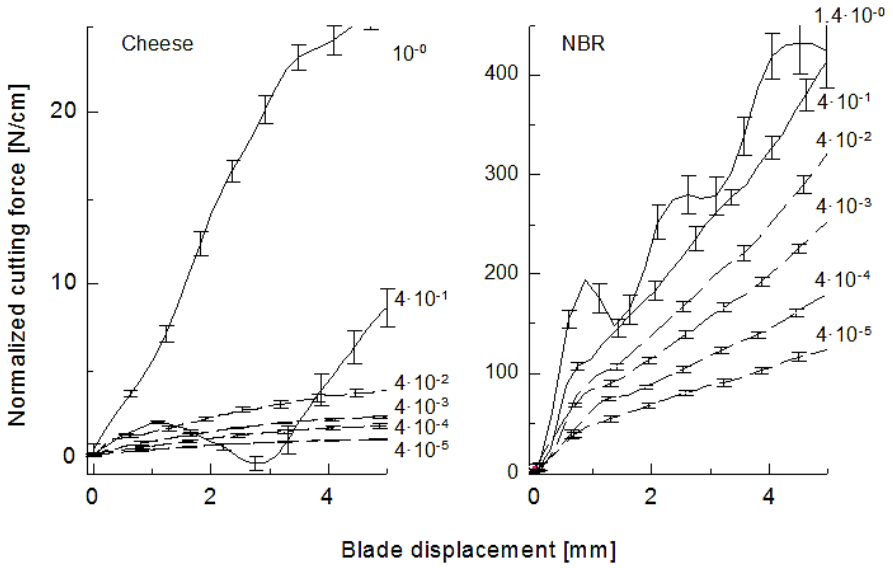

Figure 2.19: Force profiles (normalized to the cutting width) for cheese and NBR at different cutting velocities, from an Instron universal testing machine (dotted lines) and a servo hydraulic testing machine (full lines)(n = 5).

Over all, high acquisition costs, little flexibility in the applicable testing velocity, and the combination of difficult force data capturing and high engineering costs by designing

tailor-made test stations are limiting factors to build up specific test stations. Nevertheless, the literature shows some interesting approaches for high-speed measurements of foods: Dowgiallo (2005, 2015) designed a special test station by combining a servo-mechanical device with the force data acquisition system of a universal testing machine (strain gauge) to cut fibrous food materials with a velocity up to 4 m/s. King (1999) used a modified nail gun to cut lamb bone with velocities from 9 – 130 m/s using a piezo-electric force sensor to detect cutting forces for calculating the fracture energy. Brown et al. (2005) cut cheese, beef and bacon up to 0.25 m/s using a ball screw actuator and a strain gauge force measuring system. Shergold et al. (2006) used a hydraulic testing machine (until 0.8 m/s) and a gas gun (4-10 m/s) to measure the shear modulus of pig skin.

A further (but indirect) possibility to investigate the material behavior at high strain rates or high velocities is provided by the temperature time superposition, which can be explained by relaxation mechanisms or molecular transposition processes of polymers. These processes depend on temperature as well as on the time scale or strain rate (or the frequency under oscillating stress or deformation). For this reason, materials can exhibit the same relaxation behavior at different temperatures. This allows the construction of master curves by shifting deformation parameters (moduli, loss factors, compliances) along the time or frequency axis (Wrana, 2014). Hence the range of the material characterization can be expanded to very high or very low frequencies or strain rates. Strictly speaking, tts is valid only for simple polymeric systems with only one relaxation mechanism (van Gurp & Palmen, 1998). For long-chain, branched polymers, multicomponent systems or material composites with and without internal interfaces, crystalline materials and substances with phase transition within the temperature range, the tts is only restricted or not applicable (Dealy & Plazek, 2009; van Gurp & Palmen, 1998; Lakes, 2004; Nickerson et al., 2004; Wrana, 2014). As mentioned above, it is also possible to shift fracture and friction parameters along the time axis when these parameters strongly depend on the deformation behavior (Cho & Lee, 1998; Grosch, 1963; Lorenz et al., 2013a; Ludema, 1966; Pohlit et al., 2008). Precondition for tts measurements is a suitable temperature control of the samples and measuring device. A strong limitation for measurements of food is that, normally, complex multi-phase systems with different relaxation properties are present, and that these systems partly have several phase transitions (fats, water)

within the temperature ranges under investigation. The tts is well applicable when the food systems consist of larger amounts of long-chain molecules in the form of polysaccharides and proteins, e.g. gelatin or gluten (Tsiami et al., 1995), gellan (Sworn & Kasapis, 1998), pectin (da Silva et al., 1994) and carrageenan (Kasapis, 2001) but is somehow restricted for complex food systems (Ahmed, 2012; Cuq et al., 2003; Sing et al., 2006; Udyarajan et al., 2007.

3 Aims of the study

Foods are viscoelastic materials. This affects the velocity-dependent cutting behavior. In this context, effects which occur during high-speed cutting are of industrial significance and there is a need to relate general deformation, fracture and friction characteristics with cutting process parameters (**Figure 3.1**). Additionally there are no commercial solutions for test stations to directly examine the material behavior (classical material characterization) and the cutting behavior (cutting tests) of foods at high velocity. The aim of this work is to investigate the velocity-dependent cutting behavior of foods up to the high-speed range with focus on the deformation and fracture behavior.

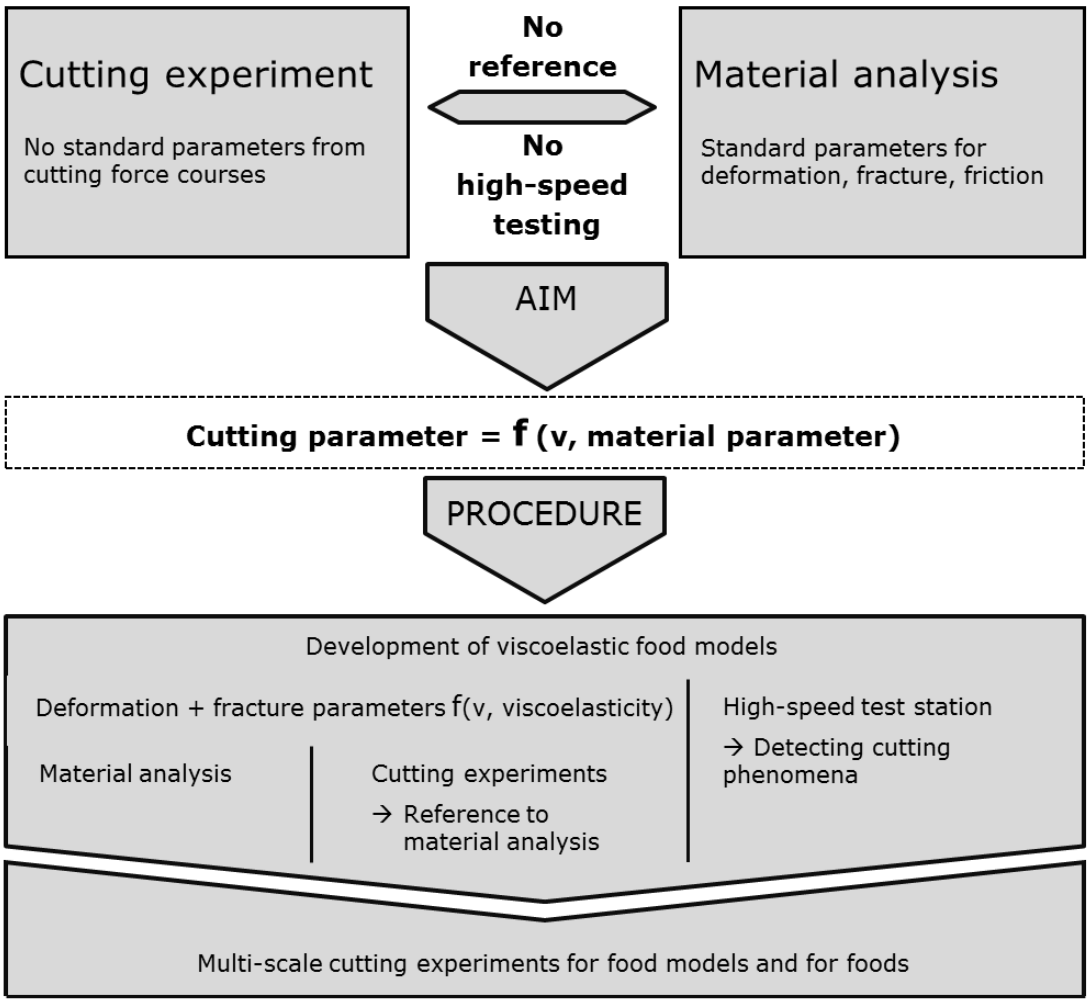

Figure 3.1: Schematic presentation of cutting process analysis and the aims and investigation approach of the study. Central aim is the development of cutting parameters related to parameters from material analysis and related to the cutting velocity *v* from small to high-speed cutting velocity (multi-scale cutting experiments).

Figure 3.1 depicts the investigation approach of the study. To generate standardized and reproducible specimen properties and to investigate the influence of viscoelasticity, elastomer based model systems will be introduced. Therefore, a synthetic material is to be used with mechanical properties similar to relevant food systems. Its viscoelastic properties should be specifically influenced by the composition of the model systems. For the purpose of deformation and fracture analysis, velocity dependent properties will be characterized with conventional testing machines in the low and medium velocity range. Deformation properties will be analysed on the basis of DMA as it provides the investigation of rate-dependency and viscoelasticity. To evaluate fracture cutting forces, it is of particular importance to investigate fracture properties depending on blade sharpness. Hence blades with different blade tip radii will be characterized by different blade sharpness parameters. Further fracture toughness will be determined by cutting experiments. In parallel, parameters from cutting force sequences that show references to the fracture and deformation behavior are to be identified at different cutting velocities. In a further analysis these cutting parameters will be related to the deformation and fracture parameters of the material characterization. Here, correlations are to be found which allow direct reference between material and cutting properties (and vice versa). For simplicity, all cutting investigations are limited to the orthogonal cutting; i. e. a straight edge blade cuts a product orthogonally to its surface without tangential motion components.

Further, cutting tests will be carried out at a tailor-made high-speed test station. In a first step the performance (including force measurement and visualization methods) of the test station will be evaluated by cutting a rate sensitive (viscoelastic) model system. On the basis of all these investigations, the overall cutting behavior of viscoelastic model systems and foodstuffs from low to high-speed (multi-scale) cutting velocities will be investigated under participation of commercial testing devices and the high-speed test station. Finally the relations between material parameters and cutting parameters for deformation and fracture will be evaluated for the food systems; and the velocity dependence of the parameters for all systems will be analysed and discussed up to the high-speed range.

4 Materials and methods

4.1 Model systems

4.1.1 Elastomers for blade sharpness evaluation

The elastomers used as synthetic cutting materials for blade sharpness evaluation were two ethylene propylene diene monomer rubbers from Karl Treske GmbH (Berlin, Germany) with different hardness (EPDMs, 50 ± 5 Shore A; EPDMh, 65 ± 5 Shore A), both provided in sheets with a thickness of 10 mm, and a nitrile butadiene rubber (NBR; obtained from a local store, producer unknown) with a sheet thickness of 6 mm and a hardness of 65 ± 5 Shore A. The complex modulus, measured in a three-point bending set-up with an RSA3 solids analyzer (Rheometric Scientific Inc., Piscataway, NJ, USA) at 10 rad/s, was 45.6 MPa for EPDMh, 28.5 MPa for EPDMs, and 32.6 MPa for NBR.

4.1.2 Elastomers as viscoelastic food models

Model systems for deformation parameter analysis were made from Elastosil® RT 745-S (Wacker Chemie AG, Munich, Germany), a two component silicone elastomer with a curing agent. Components A and B were mixed 1:1 (w/w). By adding fillers or softeners it is possible to adjust the modulus or viscoelasticity. AK1000 silicone oil (Wacker Chemie AG, Munich) was used as softener (Gundermann & Odenbach, 2014), corn starch (Schuldt et al., 2016a) or icing sugar (Boisly et al., 2016) can be used as filler. In this study only the filler corn starch, purchased in a local super market, was used (see **Table 4.1** for sample codes and composition of the model systems). The base elastomer samples were prepared by vigorously mixing components A and B with a spatula for 5 min. After adding fillers or softeners to the mixture, they were mixed with (A+B) in the same way. After mixing was completed, the sample was degassed in a vacuum chamber at 10^4 Pa for 5 min. Then the mixture was filled into PTFE molds (**Figure 4.1**). The elastomer was finally polymerized at 103 °C for 2.5 h in a convection oven.

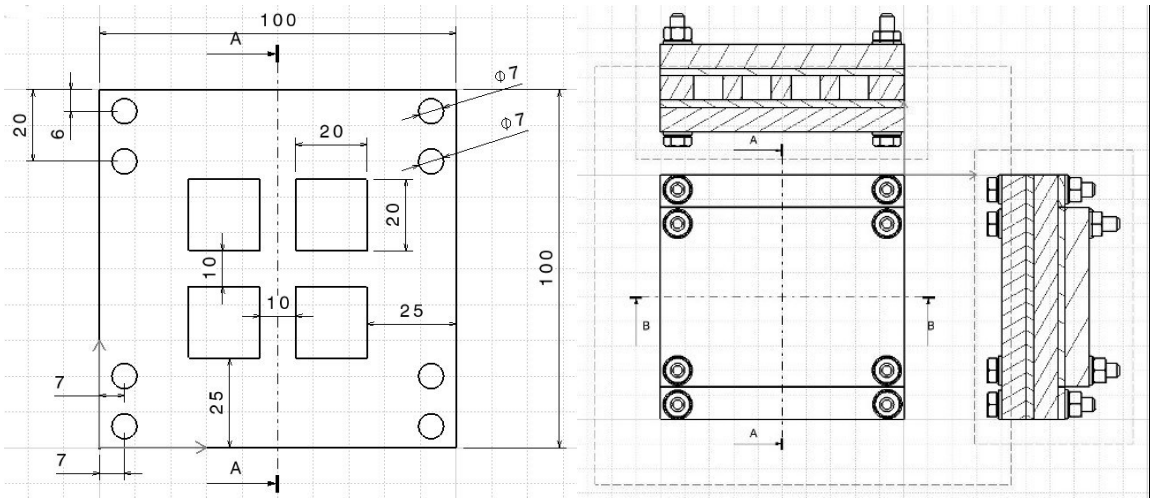

Figure 4.1: PTFE mold (left; here for rectangular samples), pressed between aluminum sheets (right; fixed with screws); dimensions in mm.

Table 4.1: Sample codes and composition of the model materials

Sample	Fraction [% w/w]		
	Base elastomer	Filler	Softener
Reference	100	-	-
f17	83	17	-
f20	80	20	-
F31	69	31	-
f35	65	35	-
f40	60	40	-
f45	55	45	-
f20s20	60	20	20
f35s20	45	35	20

4.2 Foods

To represent the wide variety of foods that are cut in industrial scale, the following items from the respective categories were selected: (a) foods consisting of a polymeric protein matrix with different disperse fillers: Bergkäse, a hard cheese variety with a casein matrix and dispersed milk fat globules; Leberkäse, a semi-solid aqueous actin/myosin ma-

trix with emulsified animal fat; and Salami, an air-dried sausage from grounded fat, muscle tissue, and spices. (b) plant tissues, with potato and carrot being presented in this study. (c) Toffee and bubble gum, representing cut and wrap sugar confectionary. Toffee is a soft candy with a continuous phase of a super-saturated sugar solution and a disperse phase, consisting of milk solids, and oil droplets (**Table 4.2**).

Table 4.2: Toffee ingredients

Ingredient	Fraction (% w/w)
Glucose	43.5
Sweetened condensed milk	41.5
Palm oil	9.9
Sugar	4.5
Lecithin	0.3
Salt	0.3

A colorant- and aroma-free model bubble gum was used in this study. There is no detailed information on the exact composition of the product. A chewing gum is a disperse system that typically consists of 20-30 % water insoluble gum base and an aqueous fraction containing sugars or other sweeteners, softeners (e.g. glycerin) and aroma. A gum base itself is typically composed of elastomers, resins, fats, waxes, emulsifiers, fillers and antioxidants (Konar et al., 2016).

All foods were obtained in local retail stores except the toffee which was manufactured in the Candy Lab of Chocotech GmbH (Wernigerode, Germany) and the bubble gum which was provided by an industrial supplier.

4.3 Cutting blades

For the cutting parameter detection (**chapter 5.1**) cutting blades made from a martensitic steel alloy (WS 1.2379, X152CrMoV12; compliant with AISI D2 and EN ISO 4957), hardened to 63 HRC and mechanically polished, were obtained from ASTOR Schneidwerkzeuge GmbH (Storkow, Germany). This blade material is regularly used in high-speed slicing applications. Blades with a different wedge angle (20°, 30°, or 40°; see **Figure 4.2**), and with a different tip radius dependent on the wear state were used in the experiments. The virgin blade with a 20° wedge angle is referred as reference blade because it

refers to typical edge geometry for food slicing knives (Marquardt, 2011). One pair of 20° blades was electrically polished by the manufacturer to enhance sharpness. To achieve different blade tip geometries, pairs of the 20° blades were worn in seasand (SiO_2) or corundum (Al_2O_3) at different rotational frequencies (25/min or 100/min) for 240 min each by applying the horizontal abrasion procedure described in Schuldt et al. (2013). Samples were cut at the middle of the blade (see **Figure 4.2**). The tip radius of these blades was determined by an optical method from blade imprints (Schuldt et al., 2013). **Table 4.3** gives an overview on the used blades and their tip geometry.

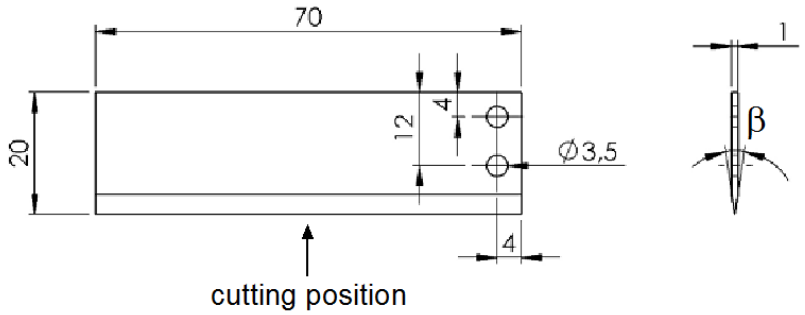

Figure 4.2: Cutting blade with dimensions (in mm) and wedge angle β; arrow indicates the cutting position of the blade.

Table 4.3: Blade characteristics

State*	Wedge angle (°)	Blade tip radius*** (µm)
Virgin (reference)	20	13.6^{a} ± 4.1
Virgin	30	18.2^{b} ± 3.2
Virgin	40	26.8^{c} ± 4.4
Abraded (SiO_2, 25)	20	17.1^{b} ± 1.2
Abraded (SiO_2, 100)	20	20.2^{b} ± 1.7
Abraded (Al_2O_3, 25)	20	33.4^{d} ± 1.3
Abraded (Al_2O_3, 100)	20	61.9^{e} ± 1.6
Virgin, e-pol**	20	12.0^{a} ± 2.1

* abrasion medium, rotational speed (rpm) during 240 min abrasion.
** Electro-polished.
*** Threefold determination per blade, 2 blades each. Values with different superscripts differ significantly.

To achieve satisfying data point resolution at high cutting velocities high data rates have to be realized by using an appropriate force measuring system. For coupling a blade

to this system a special blade geometry (**Figure 4.3**) had to be designed for the high-speed test station. This blade geometry was used for all multi-scale cutting velocity experiments (**chapter 5.2** and **chapter 5.3**).

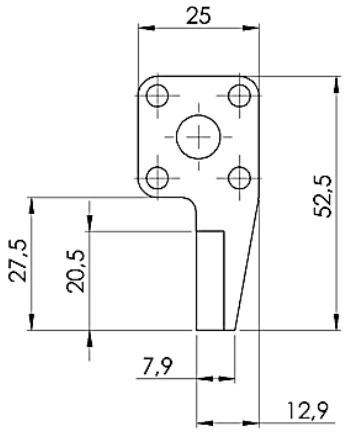

Figure 4.3: Geometry of the blade for multi-scale cutting velocity experiments; 1 mm thick, 20.5 mm of cutting edge, and 10° cutting wedge angle (dimensions in mm).

4.4 Dynamic mechanical analysis

An RSA3 Solids Analyzer (Rheometric Scientific Inc., Piscataway, N.J., U.S.A.) was used to perform dynamic mechanical experiments in compression. The cylindrical samples were placed on the lower plate of the parallel plate device. After application of a sufficient static force, frequency sweeps were performed from ω = 1 – 100 rad/s at a strain of 0.5 % (linear viscoelastic region). Complex modulus E^*, storage modulus E' and loss modulus E'' were recorded as a function of ω, as was the loss factor $\tan \delta = E''/E'$. Cylindrical samples were used for the food (except toffee and bubble gum) and the model systems (foods: height, 10 mm and diameter, 13 mm; model systems: height, 10 mm and *d*, 12 mm). All model systems were analysed at room temperature. All food samples (except toffee and bubble gum) were adjusted to 15 °C in an IPP55 environmental chamber (Memmert GmbH + Co. KG, Schwabach, Germany).

Viscoelastic properties of the bubble gum and the toffee were analysed in oscillatory shear. Cylindrical samples (diameter, 52 mm; height, 3 mm) were placed on the lower surface of a parallel plate geometry of a Physica MCR 300 rheometer (Anton Paar Germany GmbH, Ostfildern, Germany). After application of a sufficient normal force, frequency sweeps were performed in four-fold at a deformation of 0.3 % (this is within the linear

viscoelastic region) and with an angular frequency of ω = 1 – 500 rad/s at 20 °C, 30 °C or 40 °C. Temperature was controlled by a Peltier device.

All DMA tests were performed in fourfold. *E** (or *G** in case of shear experiments) was then fitted against ω using the power-law function:

$$E^* = k \cdot \omega^n \qquad \text{Eq. 4.1}$$

where *k* and *n* reflect the frequency dependence of *E** (or *G**). The corresponding slope *n* can be derived by

$$n = {}^{\partial\, log E^*}/_{\partial\, log\omega} \qquad \text{Eq. 4.2}$$

4.5 Cutting experiments

4.5.1 Test station and procedures for low and intermediate cutting velocity

A 5564 universal testing machine (UTM; Instron Ltd., High Wycombe, UK) is able to realize crosshead speeds up to 2500 mm/min or $4.17 \cdot 10^{-2}$ m/s. In the experiments it was used for cutting velocities up to 1000 mm/min ($1.17 \cdot 10^{-2}$ m/s). For all experiments a plane sample support rig was mounted on a strain gauge force transducer attached to the bottom frame of the UTM, and the cutting blade was mounted on the crosshead of the instrument. An example of a typical testing setup is given in **Figure 4.4**. After placing the samples in the rig the blade was lowered until contact with the sample was achieved, and the displacement reading of the instrument was set to zero. The cross-head was then lifted for 20 mm, and the vertical cutting procedure (without blade inclination) was started.

For the determination of the cutting parameters cuboid samples of the model systems (base area, 20 mm x 20 mm; height, 10 mm) were cut at room temperature and in fourfold determination.

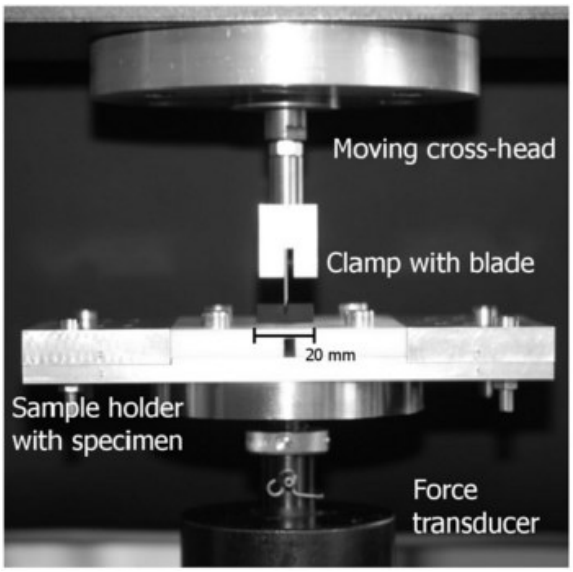

Figure 4.4: Side view of a cutting experiment from Schuldt et al. (2013).

4.5.2 Test station for high-speed cutting

The described high-speed test station (HSTS) was developed in collaboration with the chair of Processing Machines and Processing Technology (TU Dresden). The basic operation principle is the combination of rotational and linear motion (**Figure 4.5**). The sample is placed in an appropriate recess of a sample support skid mounted on a linear ball screw actuator. The sample skid is driven towards the cutting blade which is mounted on a rotor, and which moves along the perimeter of the rotor with the given circumferential velocity. By synchronizing the movement of the linear actuator and the rotor system, the sample is perpendicularly cut (almost no blade inclination) with a pre-set cutting velocity. During cutting, the blade separates the sample by moving through a gap in the skid (width, approximately 5 mm). To capture force as a function of time, the blade is mounted on a piezo-electric force transducer (Type 9027C, Kistler Holding AG, Winterthur, Switzerland) with appropriate data processing (data collection rate, up to 60 kHz). Visual documentation of the cutting process is achieved by a CR3000x2 high-speed camera system (Optronis GmbH, Kehl, Germany). A sketch of the mechanical part of the entire test station is shown in **Figure 4.6**.

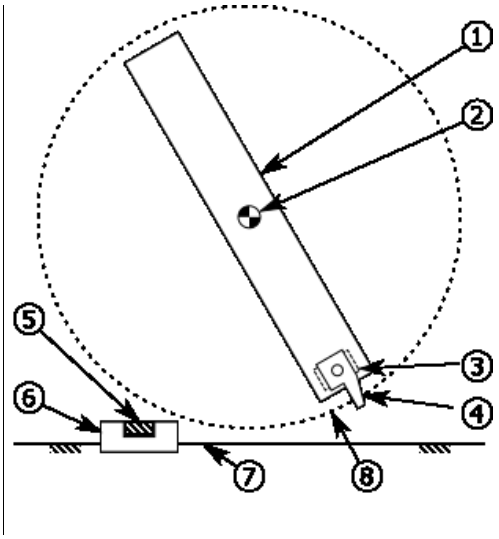

Figure 4.5: Operating principle of the high-speed test station with a rotor (1), the rotational axis (2), a blade (4) mounted on the force transducer (3), the sample (5) in the sample support skid (6), the linear axle (7) and the rotational lane with a radius of 0.5 m (8).

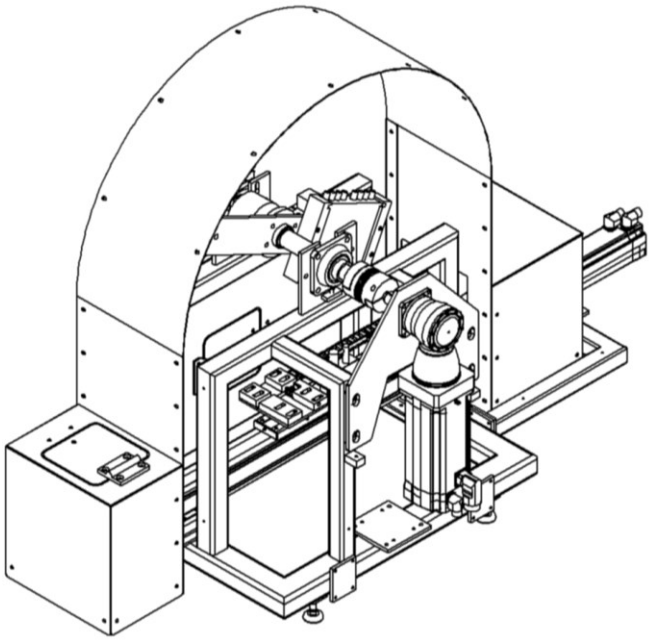

Figure 4.6: Outline of the high-speed test station.

4.5.3 Test setup for blade sharpness index determination

The elastomer sheets were clamped between two L-shaped aluminum profiles (**Figure 4.7**) where they were fixed with screws by applying a torque of 1.0 ± 0.1 Nm (7440 ESD torque wrench by Wera Werk, Wuppertal, Germany). Emery paper was placed at the inner faces of the L-profiles to avoid slippage between the metal and the samples. This specimen fixture was mounted onto a 1000 N force transducer that was placed on the

bottom frame of the UTM. The cutting blade was attached to a two-armed steel frame (see **Figure 4.7**) that was fixed to the moving crosshead of the testing machine.

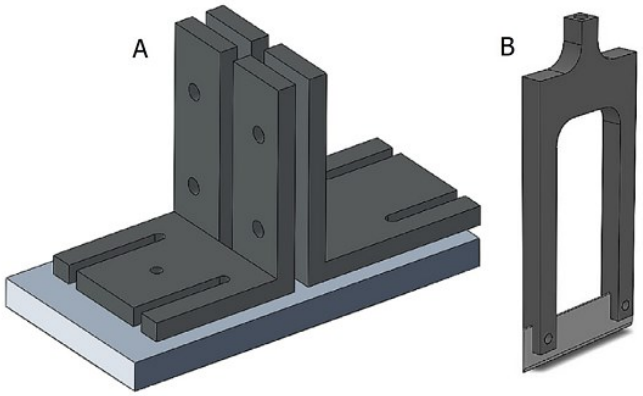

Figure 4.7: Clamping profiles for fixing the elastomer specimens (A), the blade clamp with a blade (B).

4.5.4 Cutting procedure for multi-scale cutting experiments

The multi-scale orthogonal cutting experiments were performed over 6 magnitudes of cutting velocity. This was 10^{-4}, 10^{-3} or 10^{-2} m/s for the UTM, and 10^{-2}, 10^{-1}, 10^{0} or 10^{1} m/s for the HSTS. The tests were performed with different data collection rates; at 10 m/s, this rate was limited to 6 data points per mm blade displacement. **Table 4.4** gives detailed information about the testing conditions at the respective test stations.

Table 4.4: Cutting test conditions for multi-scale velocity experiments

Cutting velocity (m/s)	Test station*	Data collection rate (kHz)	(data points/mm)
10^{-4}	UTM	0.01	100
10^{-3}	UTM	0.1	100
10^{-2}	UTM	0.5	50
10^{-2}	HSTS	1	100
10^{-1}	HSTS	60	600
10^{0}	HSTS	60	60
10^{1}	HSTS	60	6

* UTM universal testing machine, HSTS high-speed test station

For the experiments with multi-scale cutting velocity a specific sample support rig and blade support was made for the UTM to achieve similar geometrical conditions compared to the high-speed cutting test setup (**Figure 4.8**).

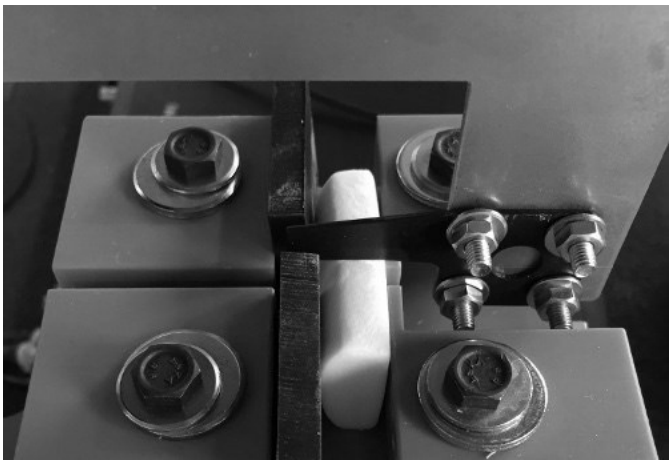

Figure 4.8: Sample support rig with a bubble gum sample (white) and blade (black) support of the universal testing machine for multi-scale cutting velocity experiments.

For the cutting experiments the samples used had a rectangular cross sectional area and were 10 x 20 mm² for the model systems, and 15 x 20 mm² for all foods except bubble gum (12 x 23 mm²) and toffee (15 x 15 mm²). The samples of toffee and bubble gum were manually cut out of a string with a nearly rectangular cross-sectional area. Cutting width was 10 mm, 12 mm (bubble gum) or 15 mm (other foods); hence the length of the cut (blade displacement until geometrical end of the sample) was 20 mm, 23 mm (bubble gum) or 15 mm (toffee), respectively (**Figure 4.9**).

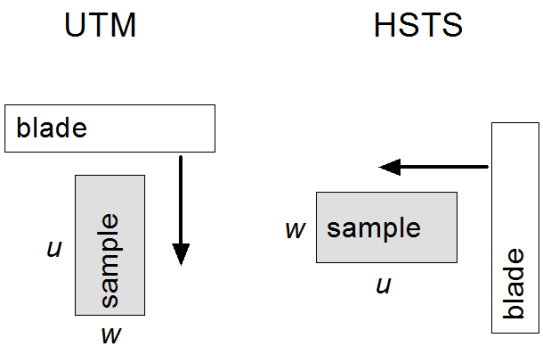

Figure 4.9: Geometrical cutting conditions for the universal testing machine (UTM) and the high-speed testing machine (HSTM) with the cutting width *w* and the length of the cut *u*. The arrows indicate the moving direction of the blade.

Cutting experiments were performed in fourfold for the model systems, fivefold for toffee and bubble gum, and sixfold for the other foods. All model systems were cut at room temperature; the sugar confectionaries were equilibrated to a cutting temperature of 20 (only bubble gum), 30 or 40 °C and the other foods to a cutting temperature of 15 °C in an IPP55 environmental chamber (Memmert GmbH & Co. KG, Schwabach, Germany).

4.5.5 Parameters from cutting force courses

Cutting force F_C was continuously recorded as a function of blade displacement l (for data rate see **Table 4.4**). Cutting stiffness d [N/mm] that was used for further evaluation refers to the first F_C/l derivative:

$$d = {}^{\partial F_C}/_{\partial l} \quad . \qquad \text{Eq. 4.3}$$

It was calculated from adjacent data points of the F/l course.

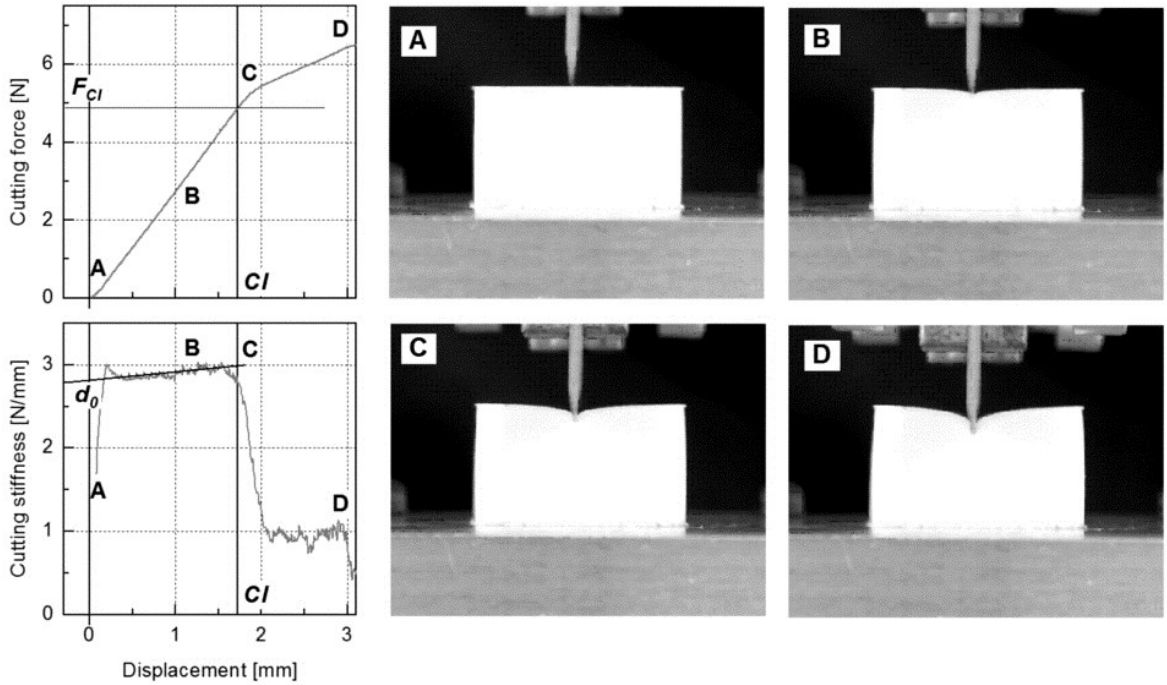

Figure 4.10: Cutting force and cutting stiffness vs. blade displacement in cutting experiments. *CI*, cut initiation; F_{CI}, force at cut initiation, d_0, initial stiffness. A, 0 mm; B, 1.0 mm; C, 1.7 mm; D, 3.0 mm blade displacement.

Figure 4.10 exemplary shows F_C and d as a function of blade displacement for an Elastosil model system f35, and the corresponding pictures of a cutting sequence starting with zero displacement (A in **Figure 4.10**). F_C initially rises linearly because of a dominant elastic, reversible deformation induced by the action of the blade (B in **Figure 4.10**). According to **Eq. 4.3**, this results in a plateau of constant d. A sudden decrease of cutting stiffness is associated with irreversible plastic changes in the material (Schuldt et al., 2013). The displacement where d starts to drop corresponds to macroscopic fracture of the sample matrix (C in **Figure 4.10**). This displacement at which the cut is initiated and the corresponding load, were defined as cut initiation *CI* [mm], and as force at cut initiation F_{CI} [N], respectively. The drop of cutting stiffness takes place before the changes in F_C become visible and therefore show that d is more sensitive for displaying cutting effects (see C in both graphs in **Figure 4.10**). Cutting stiffness before *CI* is reached is only related to deformation phenomena in the sample, and can be taken as a measure for the initial stiffness d_0 of the system. d_0 can be obtained by extrapolating the linear fit of the stiffness plateau (usually between 0.2 and 1.4 mm displacement for the model systems) towards zero displacement (see **Figure 4.10**). After cut initiation, fracture and friction between both blade sides and the sample additionally affect cutting forces (D in **Figure 4.10**). From here, it is no longer useful to interpret cutting stiffness as a material parameter.

In Schuldt et al. (2016a) the deformational pre-crack cutting properties were analysed with the parameter d_0. In later experiments it appeared that this stiffness plateau procedure is limited to systems with high cut initiation depths with a distinct plateau (as it is the case for the model systems) and is not applicable for many food systems such as cheese, toffee, bubble gum, and some vegetables. Another method to achieve a deformational cutting parameter is the analysis of the slope of cutting force s_0 [N/mm] over a series of adjacent data points in the region where F_C increases linearly (B in **Figure 4.10**); this appeared to be the more robust procedure to obtain the deformation cutting parameter. It is advantageous if small cut initiation depths (and a minor plateau) are present. **Figure 4.11** shows for two cutting velocities that the two parameters, d_0 and s_0, give nearly identical values.

To allow the comparison of cutting forces irrespective of sample dimension, F_C was normalized to a cut width of 10 mm. For the sake of clarity, this normalized cutting force

F_N is further expressed in force units [N]. $F_{N,CI}$ [N] refers to F_N at *CI*. The force/displacement curves were analysed to obtain the deformational pre-crack cutting parameter s_0 [N/mm], which corresponds to the slope of F_N *vs.* l in the deformation phase, and which was determined by linear regression of the initial linear part of the normalized cutting force.

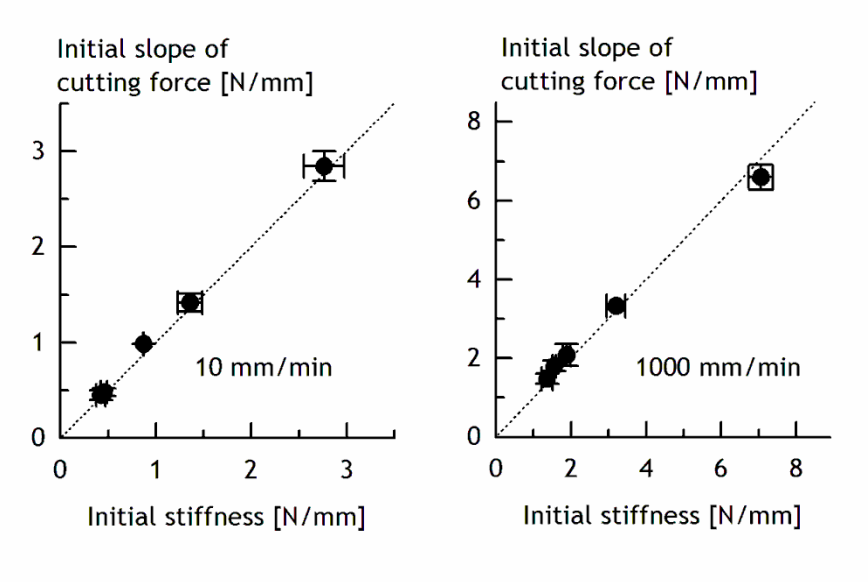

Figure 4.11: Comparison of initial slope of cutting force and initial stiffness for different Elastosil model systems and two cutting velocities. Dotted lines: f(x) = 1*x

These initial F_N *vs.* l slopes were then related to *v* using power-law by

$$s_0 = a \cdot v^b \qquad \text{Eq. 4.4}$$

where the constant *a* and the exponent *b* reflect the cutting velocity dependence of s_0.

4.5.6 Fracture toughness determination and blade sharpness index

The blade sharpness index *BSI* [-] is a dimensionless, objective parameter for sharpness evaluation which was introduced by McCarthy et al. (2007). The determination of the *BSI* is performed by fixing sheets of the testing materials between two anti-buckle clamps (**Figure 4.7**). The testing material is cut between the clamps, and all parameters needed for *BSI* calculation including fracture toughness can be achieved by choosing an appropriate experimental setup.

The *BSI* relates the energy W_{CI} [Nm] necessary to initiate a cut to the product of cut initiation depth *CI* [m], cutting width *w* [m] and fracture toughness *J* [J/m²] of the testing material

$$BSI = {W_{CI}}/{(CI \cdot w \cdot J)} \qquad \text{Eq. 4.5}$$

where *BSI* = 0 indicates a blade with ideal sharpness, and an increase in *BSI* can be interpreted as decreasing sharpness. McCarthy et al. (2007) concluded that the *BSI* is independent of the cutting material and of the cutting velocity, and that it is only influenced by the geometrical properties of the blade. In a subsequent study, McCarthy et al. (2010) used a finite element model and showed by simulation that an increase of blade tip radius and wedge angle significantly increases the *BSI*.

For the calculation of the *BSI* (**Eq. 4.5**) of the individual blades, it was necessary to perform two different cutting tests with each elastomer. The first cutting test was to determine *CI*, $F_{N,CI}$ and W_{CI}. The elastomers were cut in the middle of the sample through a 10 mm slot in the L-profiles (see **Figure 4.7**). For that purpose, the crosshead of the testing machine was lowered manually until contact between the blade and the specimen was achieved. After setting the displacement reading to zero, the crosshead was raised for 20 mm. Blade displacement was limited to 5 mm (this was deep enough to initiate a cut in each material with any blade), cutting velocity *v* was 10 mm/min or 1000 mm/min, and the F/l data collection rate was 1000 or 300 data points/mm, respectively. Cutting stiffness was then plotted against displacement (**Figure 4.12**). In contrast to McCarthy et al. (2007), the stiffness courses for virgin and blunted blades showed qualitative conformity, probably because of using thicker testing materials. The initial cutting stiffness plateau reflects the elastic deformation of the specimen in front of the blade, and *CI* was graphically determined as that displacement at which *d* starts to decrease drastically (see also **chapter 4.5.5**). This was cross-checked by progressively moving a blade into the specimen in 0.1 mm increments and intermittent analysis of the rubber surface. Subsequently, $W_{CI} = \int F \cdot d\ l$ was calculated from the force/displacement data between zero displacement and *CI*.

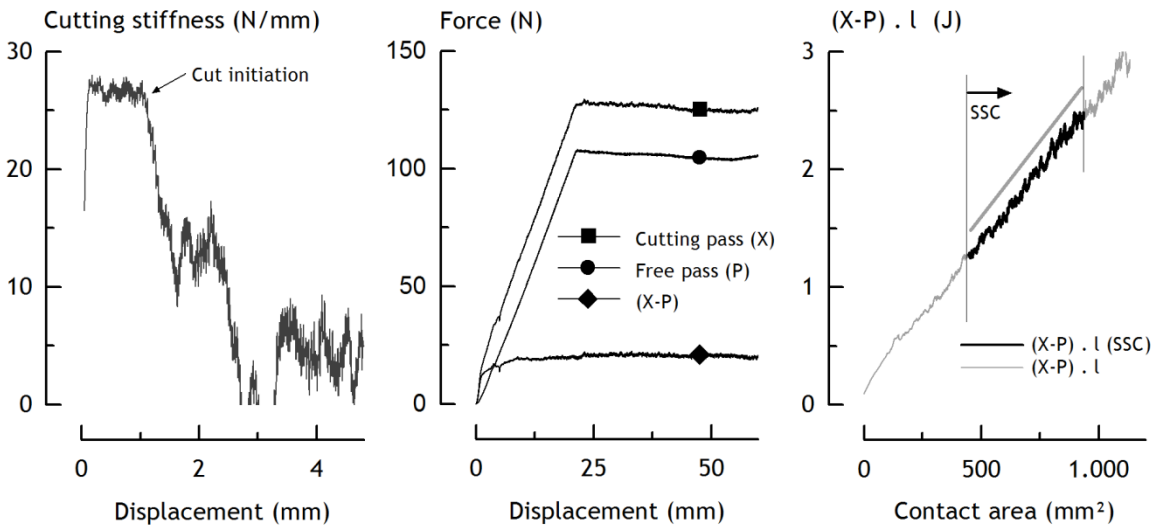

Figure 4.12: Determination of cut initiation depth (left), friction and cutting forces as a function of displacement (middle), and determination of fracture toughness (right) in the steady state cutting (SSC) region.

In the second cutting test, fracture toughness of the elastomers was determined according to McCarthy et al. (2007) by using virgin blades with 20° wedge angle. The elastomers were cut to a depth of 60 mm at v = 10 mm/min or v = 1000 mm/min (data collection rate: 120 data points/mm). The plot of F *vs.* l gives the cutting pass X (see **Figure 4.12**). The blade was then set again to its initial position, and the cutting procedure was repeated by another move of the blade through the same specimen (free pass P) to record friction force. The residual force (X-P) is consequently related to fracture of the specimen. It can be clearly seen that the forces reach an equilibrium state at about 20 mm displacement where steady state cutting (*SSC*) begins. Subsequently, the product (X-P) · l is plotted against contact area (m²) between blade and elastomer (see **Figure 4.12**). Fracture toughness can finally be obtained from the slope of the plot in the SSC region (i.e., at 25 –50 mm displacement).

The elastomers (EPDNs/h 10 mm thick; NBR 6 mm thick) were manually cut into 40 x 95 mm² sheets with a scalpel. For the two reference blades, all individual measurements were performed at 10 mm/min and 1000 mm/min and for the three elastomers in fourfold determination. Experiments with the other blades (see **Table 4.3**) were also performed in fourfold determination but only at v = 10 mm/min and only for EPDMs. All measurements were performed at room temperature.

5 Results and discussion

5.1 Developing methods for cutting parameter detection

The determination of fracture, deformation and cutting parameters of foods often provides distinct deviations because of the natural variance or heterogeneous material properties of the products (see for example Alvarez et al., 2000; Rohm et al., 1997; Schuldt et al., 2016b; Taylor et al., 2011; Vandenberghe et al., 2014). By use of elastomers as model systems these limitations can be minimized for better accuracy of the measured parameters. In **chapter 5.1.1** the development of viscoelastic polymers as model systems that reflect the cutting properties of foods will be introduced.

The scope of **chapter 5.1.2** is to identify parameters from cutting force courses of food model systems that characterize the deformation resistance of the materials in vicinity of the blade tip. These parameters will be referred to deformation behavior of the materials characterized by dynamic mechanical analysis at small deformation. Finally rate-dependence of the deformation parameters will be pointed out.

In **chapter 5.1.3** general fracture parameters will be referred to parameters from cutting force courses in dependence to cutting velocity. For foods the literature proposes different methods for characterizing fracture toughness or the energy that is necessary to break material cohesion and create new surfaces as e. g. wedge fracture tests (Vincent et al., 1991) or edge-notched tension or bending tests (Gamonpilas et al., 2009; Kamyab et al., 1998; Skamniotis et al., 2016; Taylor et al., 2011). The different methods can vary for example in mode of fracture (Vincent et al., 1991) or direction of deformation (Luyten et al., 1992); determination of fracture toughness of foods itself “is complex because of a high degree of rate dependence and non-linearity” (Kamyab et al., 1998). That may be reasons why different methods for characterizing fracture properties of foods can give substantial variations (Gamonpilas et al., 2009; Kamyab et al., 1998; Luyten et al., 1992). For fracture parameter determination it therefore seems reasonable to choose a method with equal deformation and fracture conditions as the cutting application to that this parameter should be referred to. Indeed the literature provides certain methods for frac-

ture toughness determination out of cutting experiments with different setups as orthogonal cutting with a rake (Skamniotis et al., 2016) or with straight edge blades (Cho & Lee, 1998; McCarthy et al., 2007) as well as wire cutting (Kamyab et al., 1998).

5.1.1 Development of food model systems

Several attempts have been made to make use of elastomers for the simulation of various bio-based materials. For the instrumental quantification of chewing forces, Kohyama et al. (2004) used silicone rubber as food model to overcome issues of poor reproducibility that was observed with real foods. Other authors used silicone rubber to simulate cutting properties of biological tissues such as skin (McCarthy et al., 2007), or to simulate the rate dependent development of shear moduli of soft solids in medical applications (Shergold et al., 2006).

A general requirement of model systems is that they represent the relevant attributes of the original system. That implies that the main properties of the originals are identified (Stachowiak, 1973). As important criteria for food model systems for cutting the following attributes can be defined:

- qualitatively similar cutting force courses in a similar force scope,
- similar values for cut initiation and force at cut initiation,
- similar viscoelastic and mechanical properties.

Additionally it should be possible to adjust the material characteristics by proper selection of composition to study effects concerning viscoelasticity.

Many sliceable foods such as cheese or sausages comprise a bio-polymeric network structure containing solid, semi-solid and liquid fillers (Barden et al., 2015; Bruno & Moresi, 2004; Jaros et al., 2001). As reference foods for slicing operations one can therefor choose Gouda cheese and Leberkäse. Both systems show a linear increase of cutting force at the beginning of cutting procedure which means that cutting stiffness is constant (**Figure 5.1**). For Gouda this plateau is very narrow and more like a maximum. If the blade advances in the cutting substrate cutting stiffness drops significantly when the cut is initiated (Schuldt et al., 2013). In the case of young Gouda cheese this happens early at approximately 0.2 mm. Compared to that Leberkäse is deformed elastically in front of the

cutting edge over a larger blade displacement scale. Consequently a cutting stiffness plateau is formed until approximately 2 mm. At higher blade displacement cutting stiffness weakens and marks a cut initiation at 2.8 mm. After cut initiation the force course progressively increases for Gouda which indicates a substantial contribution of friction to the overall cutting force. For Leberkäse friction has a minor role because of no further force increase after cut initiation. In comparison to standard elastomers (see Schuldt et al., 2013) both food systems show low maximum normalized cutting forces between 1 N and 2 N.

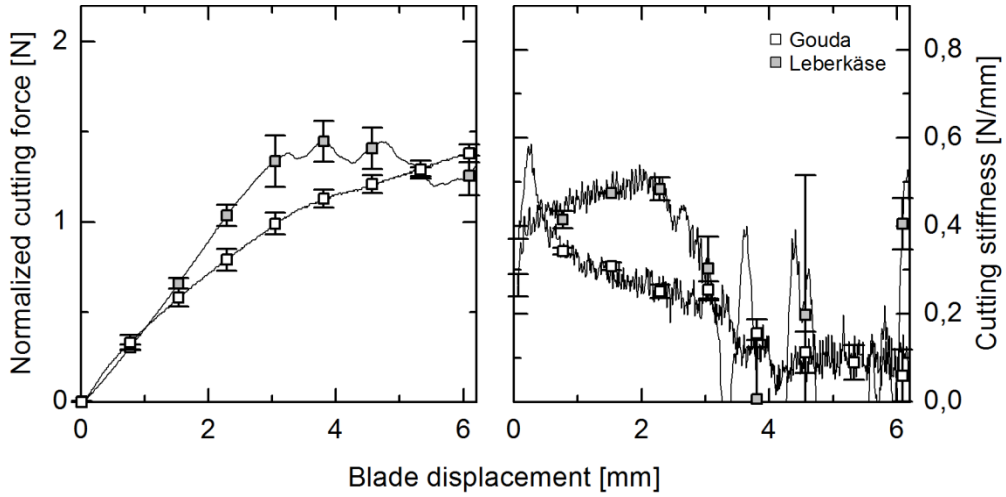

Figure 5.1: Normalized cutting force and cutting stiffness of Gouda and Leberkäse at a cutting velocity of 10 mm/min. Only selected datapoints are displayed as sample identifiers. Cutting stiffness is referred to normalized cutting force.

Elastomers also consist of a polymer-matrix in that liquid or solid fillers can be dispersed. These can influence the mechanical properties as tensile strength, hardness or viscoelasticity (Zhang et al., 2011). Moreover elastomers can be supplied in big quantity from one batch and comprise other advantages concerning geometry and handling (e.g., negligible temperature dependency). The silicone based elastomer Elastosil was used to evaluate its potential as food model. By adding fillers or softeners it is possible to adjust the modulus or viscoelasticity.

Figure 5.2 depicts cutting force and cutting stiffness vs. blade displacement of different Elastosil model systems (for sample codes see **Table 4.1**). They showed a high quantitative and qualitative equivalence to food systems containing bio-polymeric matrices (**Figure 5.1**). Maximum normalized cutting forces were in the range of 2.5 to 7.5 N

which is in the same magnitude as the selected foods. The addition of a filler resulted in an increase of F_C and, hence, higher stiffness before cut initiation. Incorporating a softener in the matrix had the opposite effect, namely a decrease of F_C and d. After cut initiation, friction forces that are proportional to the contact area appeared, and led to a further increase of F_C when blade displacement increased.

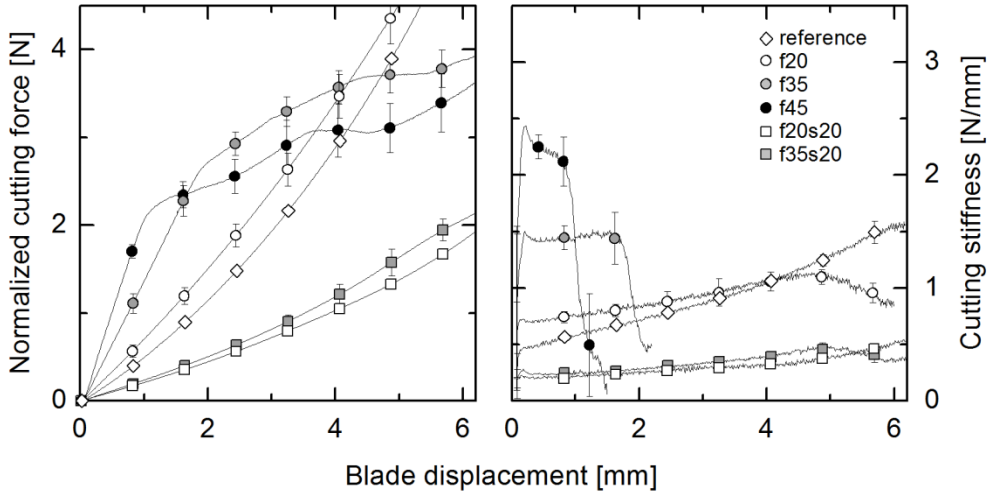

Figure 5.2: Cutting force and cutting stiffness of different model systems at a cutting velocity of 10 mm/min. Only selected data points are displayed as sample identifiers. For sample code, see **Table 4.1**. Cutting stiffness is referred to normalized cutting force.

Model systems without (reference) or with a low amount of filler (sample f20), and those with softener (f20s20, f35s20) showed a distinctive softness. These systems did not exhibit a stiffness plateau with constant values but a continuous or even progressive rise of d before cut initiation. In these cases samples get compressed, and the rigid probe support influences the development of cutting force with ongoing blade displacement. Consequently, in these cases, the cutting stiffness can no longer be considered as only being sample dependent, and interpretation of the data has to be done with care. Nevertheless, $F_{N,CI}$ reflects the force that is needed to provoke a macroscopic fracture of the sample matrix and can therefore be interpreted independently from the development of d.

Table 5.1 depicts selected model systems and shows that the addition of fillers led to a progressive reduction of CI and $F_{N,CI}$. These systems were less compliant, and a lower force was needed to induce macroscopic fracture at the surface. A probable cause for the latter is the alteration of the network because of a reduced strength of binding forces

between matrix and filler particles. The addition of a softener increased compliance and, hence, cut initiation depth (see also Zhang et al., 2011). For f35s20 and f20s20, there was an increase in *CI* and a decrease in $F_{N,CI}$ compared to the systems without softener but equal amounts of filler, indicating a further alteration of the network. f20s20 did not show a cut initiation within 8 mm of blade displacement. Over all the systems with high amounts of filler show *CI* values that are well in the range of the food examples, especially Leberkäse. In comparison Gouda has very low *CI* with high standard deviation. This underlines the need of a model system to examine cutting properties.

Table 5.1: Cutting parameters of selected food and Elastosil model systems at 10 mm/min cutting velocity (for sample codes see **Table 4.1**).

Sample	Cut initiation [mm]	Normalized force at cut initiation [N]	Initial slope of cutting force [N/mm]
Gouda	0.2 ± 0.1	0.08 ± 0.01	0.57 ± 0.07
Leberkäse	2.8 ± 0.2	1.28 ± 0.17	0.45 ± 0.02
Reference[a]	6.1 ± 0.2	5.62 ± 0.20	0.49 ± 0.01
f20	5.0 ± 0.1	4.51 ± 0.22	0.71 ± 0.05
f35	1.5 ± 0.2	2.16 ± 0.35	1.42 ± 0.08
f45	0.8 ± 0.1	1.70 ± 0.20	2.24 ± 0.06
f20s20	-	-	0.23 ± 0.03
f35s20	5.2 ± 0.0	1.73 ± 0.10	0.24 ± 0.02

[a] model system (Elastosil) without filler

The initial slope of cutting force s_0 is unaffected by stiffening effects due to the sample support rig. The addition of filler and softener showed distinctive effects on the development of the cutting force. Systems containing the filler showed a high, and systems containing the softener showed lower cutting forces at the beginning of the measurements. Hence, the addition of the filler increased s_0, whereas the addition of the softener reduced s_0 (**Table 5.1**). It should also be mentioned that the reducing effect caused by the softener was stronger than was the increasing effect caused by the filler (see f20s20 and f35s20 *vs*. f20 and f35, respectively).

In general foods have viscoelastic properties and, compared to technical materials as wood, metals or plastics, the hardness is low. **Table 5.2** gives an overview of complex modulus and loss factor for selected foods. Most of the systems exhibit dominantly elastic

properties at the given frequency (loss factor < 1), except toffee with dominant viscous contribution. The complex moduli are in the range from 0.44 to 5.60 MPa.

Table 5.2: Mechanical properties[a] of selected food systems at 15 °C

Sample	*E** at 10 rad/s [MPa]	*tan δ* at 10 rad/s [-]
Bergkäse	3.17 ± 0.10	0.277 ± 0.002
Gouda[b]	0.50 ± 0.03	0.314 ± 0.007
Leberkäse	0.44 ± 0.01	0.170 ± 0.014
Salami	3.32 ± 0.39	0.240 ± 0.014
potato	5.60 ± 1.21	0.157 ± 0.014
toffee[c]	0.87 ± 0.05	1.500 ± 0.044
bubble gum[c]	2.55 ± 0.15	0.346 ± 0.021

[a] *E**, complex modulus from dynamic mechanical analysis; *tan δ*, loss factor
[b] data at room temperature; [c] data at 30 °C, *G** from shear modus

Table 5.3: Mechanical properties[a] of the model systems (for sample codes see **Table 4.1**).

Sample	*E** at 10 rad/s [MPa]	*tan δ* at 10 rad/s [-]
Reference	0.30 ± 0.02	0.241 ± 0.007
20	0.69 ± 0.03	0.318 ± 0.002
f35	1.40 ± 0.06	0.378 ± 0.003
f45	2.74 ± 0.13	0.411 ± 0.020
f20s20	0.80 ± 0.01	0.441 ± 0.001
f35s20	0.41 ± 0.02	0.564 ± 0.017

[a] *E**, complex modulus; *tan δ*, loss factor

Table 5.3 depicts mechanical properties of selected Elastosil model systems.

The addition of corn starch as filler led to a successive and significant increase of *E** for the sample with 45 % (w/w) filler (f45), and also to a significant increase of the loss factor *tan δ*. The increase of *E** is the result of the inclusion of a considerable amount of rigid particles in the gel network matrix (Bokobza, 2009; Jampen, 2001). The reference and the filled polymers exhibited a loss factor < 1, which corresponds to predominantly elastic properties. An increase of *tan δ* means that viscous contributions become more important in the system. The fact that the incorporation of the filler resulted in an

increase of *tan δ* points on an alteration of the network because of poor interactions between the filler and the polymer matrix (Chen & Dickinson, 1999). The addition of silicone oil as softener reduced *E** and increased *tan δ* which agrees with Zhang et al. (2011) who documented a decrease of hardness, crosslinking density, and an increase of *tan δ* and of the fracture strain when silicone oil was added to silicone rubber. The addition of the softener elevated *tan δ* to a higher extent than in mixtures without softener that contained a similar amount of filler. This indicates a further alteration of the network structure. Depending on composition the complex moduli are in the range of 0.3 to approximately 3 MPa and loss factors are between 0.24 and 0.56. This demonstrates that the DMA properties of a broad selection of foods (see **Table 5.2**) are matched by the model systems.

From these results it can be concluded that, compared to polymeric food systems the use of Elastosil silicone rubber with varying filler and softener content provides model systems with similar cutting force courses and similar cutting parameters. By proper selection of system ingredients it is possible to adjust the viscoelastic and mechanical properties which lie in the scope of a broad selection of foods. Over all the model systems fulfill the above-named attributes as a food model system for cutting applications.

5.1.2 Deformation cutting parameter

For all model systems, the complex modulus showed power law dependence on angular frequency (**Figure 5.3**). From **Eq. 4.2** it is possible to derive the corresponding slopes n_i (Bruno & Moresi, 2004) (**Table 5.4**). The lowest value refers to the reference, and the addition of filler and softener leads to an increase of *n*, indicating higher rate dependence. This comes from more pronounced viscous contribution properties that are reflected by *tan δ* (**Table 5.2**). According to Booij and Thoone (1982), there is an approximate relation between *δ* [rad] and *n*:

$$\delta = {}^{\pi}/_{2} \cdot n \qquad \text{Eq. 5.1}$$

In case of gel systems with *tan δ* < 1, this relation applies at higher angular frequency and can be used where **Eq. 4.1** is valid (Bruno & Moresi, 2004; Friedrich and Heymann, 1988). The fact that *δ* measured in the experiments and *δ* from **Eq. 5.1** is highly intercorrelated with a correlation coefficient close to 1 therefore means that the frequency dependence of the samples highly depends on their viscoelastic properties: the more important the viscous contribution of the system, the higher is *n*. Consequently, a system showing a higher *n* and *δ* can be expected to be more sensitive to different loading rates or cutting velocities than a system with a lower *n* and *δ*.

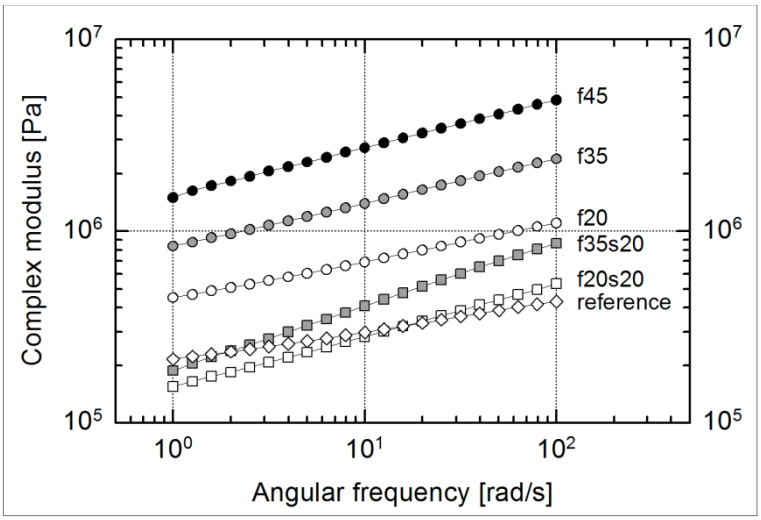

Figure 5.3: Frequency dependence of Elastosil model systems with different fillers. For sample code see **Table 4.1**.

Table 5.4: Mechanical properties[a] of the model systems derived from DMA (for sample codes see **Table 4.1**)

Sample	*n* [-]	0.5 π · *n* [-]
Reference	0.153 ± 0.002	0.240 ± 0.004
20	0.197 ± 0.001	0.309 ± 0.002
f35	0.230 ± 0.004	0.361 ± 0.006
f45	0.252 ± 0.010	0.396 ± 0.015
f20s20	0.268 ± 0.002	0.421 ± 0.003
f35s20	0.334 ± 0.003	0.524 ± 0.004

[a] n, logarithmic slope of E* *vs*. angular frequency; 0.5 π · n, phase shift calculated by **Eq. 5.1**

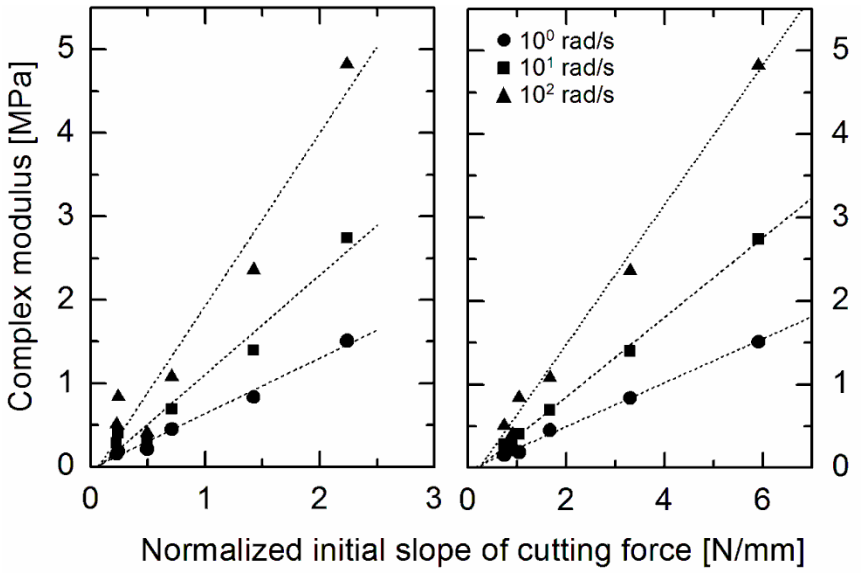

Figure 5.4: Complex modulus measured at 1, 10 and 100 rad/s (identifiers, see insert) as a function of the normalized initial slope of cutting force s_0 derived from cutting experiments at 10 mm/min (left) and 1000 mm/min cutting velocity (right). Each data point at a distinct s_0 represents one model system.

The comparisons of s_0 from cutting experiments at different cutting velocity with E^* from DMA at different angular frequency showed significant correlations that were independent of the model systems ($r \geq 0.97$) (**Figure 5.4**). E^* is defined as the ratio of the stress to strain amplitude at low deformation, and stress is calculated from the oscillating force amplitude that is related to the cross-section of the sample. On the other hand, the initial slope of cutting force is derived from the force generated through a one-dimensional deformation exerted by a cutting blade. In both cases, force appears to be proportional to deformation so that Hooke's law is valid. **Figure 5.4** also shows that E^* and d_0 can be regarded as equivalent material parameters, which indicates that the rate dependence in both methods is similar. In other experiments (results not shown) it was observed that cutting force and cutting energy of nitrile butadiene rubber was power law related to cutting velocity in the range from approx. 10^0 – 10^5 mm/min. Consequently, the relationship between individual $s_{0,i}$ and individual cutting velocities v_i can be established similar to **Eq. 4.1**:

$$m_i = {log\Delta s_{0,i}}\Big/{log\Delta v_i} \qquad \text{Eq. 5.2}$$

This m_i ratio reflects to which extent cutting stiffness and pre-crack forces increase when cutting velocity is increased by one magnitude (**Figure 5.5**). As was observed for *tan δ* and *n*, the addition of filler and/or softener led to an increase of m_i, which was highest for the system f35s20. This means that the pre-crack forces show a higher increase with increasing cutting velocity when viscous contributions in the systems are more important.

In **Figure 5.5**, m_i from **Eq. 5.2** is also plotted against the phase shift obtained from DMA experiments at 10 rad/s, and δ calculated from the E^*/ω slope (**Eq. 5.1**). The linear relationship ($r > 0.97$) between the cutting velocity dependence of s_0 (i.e., m_i), and the phase shift extracted from DMA experiments by two different procedures demonstrate that the viscoelastic properties of a system have a significant impact on the pre-crack cutting force. Therefore, it appears reasonable to predict pre-crack cutting forces at high cutting velocity when DMA parameters and cutting force values at moderate cutting velocity have been already measured. This assumption, however, only holds if no fundamental change in the mechanical properties takes place at very high cutting velocity (which might be the case for viscoelastic solids; Mulliken and Boyce, 2006; Shergold et al., 2006) and will be analysed in **section 5.3.3**.

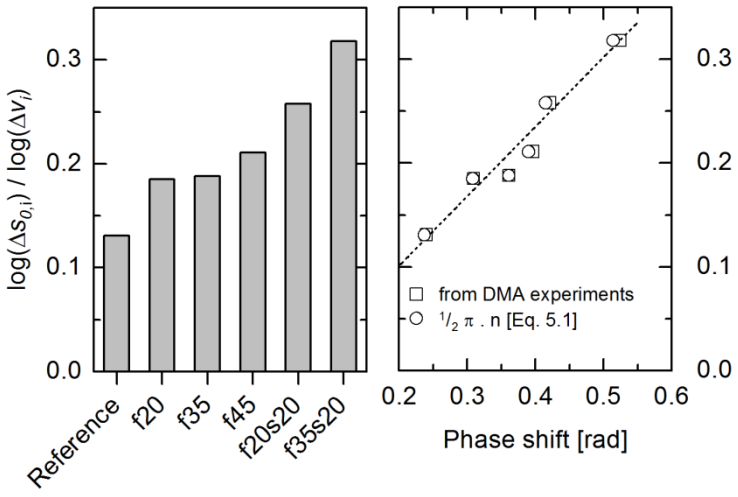

Figure 5.5: log(Δs_0) / log(Δv) for the different model systems. Power law dependence of the initial cutting stiffness $s_{0,i}$ on cutting velocity v_i of different model systems (left, for sample code, see **Table 4.1**), and power law dependence of $s_{0,i}$ on v_i as function of the phase shift from dynamic mechanical analysis (DMA, right).

In summary, silicone rubbers with fillers can be considered as useful model systems for food with tailor-made viscoelastic properties, and as suitable for linking mechanical

properties at small deformation to cutting behavior: the initial slope of force from cutting experiments appears as useful material parameter to conclude on the complex modulus from small deformation testing, and vice versa. s_0 measured at different cutting velocity reflects the rate dependence during cutting processes, and can be related to viscoelastic material parameters such as the loss factor *tan δ* or *n* obtained by DMA. The more viscous (or the higher *tan δ*) a cutting material is, the more it is sensitive to velocity changes induced by angular frequency in small deformation experiments, but also to different cutting velocities. Small deformation testing is therefore very useful to predict cutting properties of different materials before cut initiation. Consequently, the modification of viscoelastic and deformation properties of particular foods, or the modification of the cutting process may be a sufficient tool to optimize high-speed cutting applications.

5.1.3 Fracture cutting parameter

When cutting with a blade or wire into a sample the measured fracture energy is highly correlated to the blade tip radius (Goh et al., 2005; Kamyab et al., 1998). For fracture toughness determination from blade cutting tests it therefore is essential to characterize the cutting tool geometry, i. e. the sharpness of the blade. Therefore the sharpness of blades will be characterized by different parameters (including the *BSI*) and fracture toughness of the elastomeric model systems will be determined after McCarthy et al. (2007). Then this fracture toughness will be linked to parameters from cutting experiments that refer to the fracture of the cutting substrates.

In a previous study, Schuldt et al. (2013) showed that the blade tip radius is a measure for the geometrical characterization of blades, and that it can be taken as appropriate measure to quantify the abrasion of blades that leads to sharpness reduction. **Figure 5.6** depicts the relationship between *CI* and blade tip radius for EPDMs that was cut at v = 10 mm/min. *CI* was, independent of blade surface finishing, almost identical for the 20° blades. An increase in the blade tip radius that comes from different wedge angles resulted in an increase of *CI*, as did the increase in the blade tip radius that comes from abrasion of the 20° blades (r = 0.94, p < 0.05). The dependency of $F_{N,CI}$ on blade tip radius follows the same pattern: again, effects of blade surface finishing (insignificant effect on

blade tip radius; see **Table 4.3**) are negligible whereas the increase in blade tip radius caused by changes in blade geometry or induced by abrasion result in a significant (r = 0.97) increase of this measure.

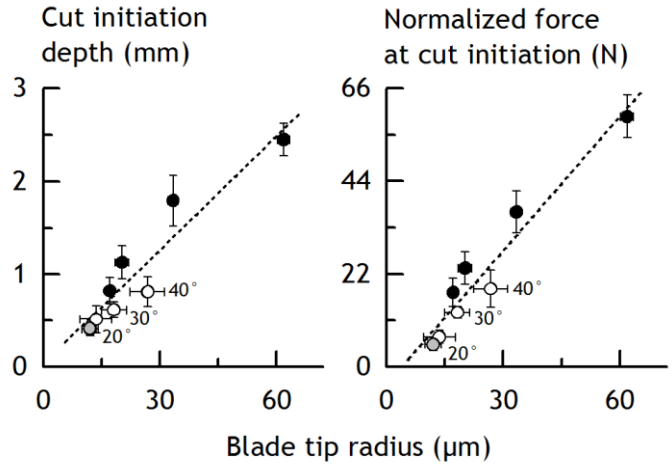

Figure 5.6: Cut initiation depth and normalized force at cut initiation as a function of blade tip radius for elastomer EPDMs cut with different blades at 10 mm/min. White symbols, virgin blades with different wedge angle (indicated in figure). Black symbols, 20° blades with different degree of abrasion (see **Table 4.3**). Grey symbol, 20° electro-polished blade. Data are arithmetic means ± standard deviation of (n=8) determinations (two blades per geometry, quadruplicate testing).

The fact that both *CI* and $F_{N,CI}$ depend linearly on the blade tip radius implies that, for a particular material, both parameters might be taken as an indicator for blade sharpness. The respective correlation coefficient between *CI* and $F_{N,CI}$ is significant (r = 0.99).

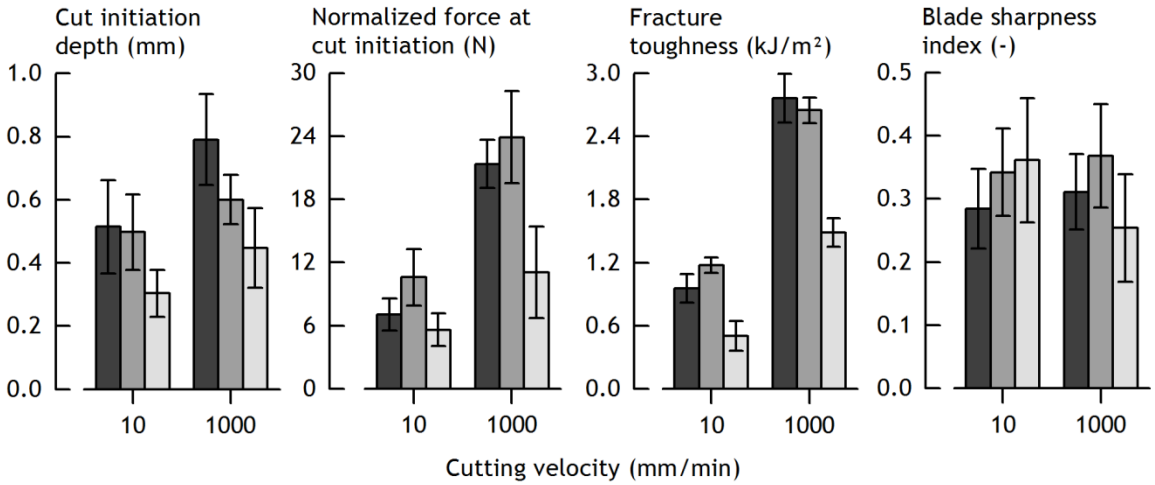

Figure 5.7: Cut initiation depth, normalized force at cut initiation, fracture toughness and blade sharpness index as a function of cutting velocity for EPDMs (dark grey), EPDMh (grey) and NBR (light grey) for the reference blade (20°, virgin). Data are arithmetic means ± standard deviation of (n=8) determinations (two blades per geometry, quadruplicate testing). Different letters in a block indicate significant ($p < 0.05$) differences.

For 20° virgin blades, **Figure 5.7** summarizes the influence of cutting velocity and cutting material on *CI*, $F_{N,CI}$, *J* and *BSI*. As already shown in **chapter 5.1.1**, cut initiation depth is higher for the softer material, especially at v = 1000 mm/min. Despite a similar Shore A hardness, NBR exhibited a significantly lower *CI* than EPDMh. Similar trends are evident for the force at cut initiation, meaning that a lower force is necessary to initiate a crack in the NBR material.

McCarthy et al. (2007) also tested velocity effects during cutting of polyurethane and did not observe a rate dependence for cutting force, *CI* and, hence, $F_{N,CI}$. This is in contrast to the results in this study: an increase of cutting velocity resulted in a significant increase of *CI* for EPDMs and NBR, and in a significant increase of $F_{N,CI}$ in case of all materials. A rate dependency of fracture strain and fracture stress in compression or tensile testing was observed by, e.g., Fatt & Ouyang (2007) and van Vliet et al. (1993). In contrast to the results obtained with different blades but one particular cutting material and velocity (see **Figure 5.6**), the correlation coefficient between *CI* and $F_{N,CI}$ is remarkably lower but still significant (r = 0.80) when different materials and different cutting velocities are considered. A higher cutting velocity leads to a higher cutting force (results not shown) which corresponds to a typical rate-dependent behavior for rubber (see for example Boisly et al., 2016 or Yang et al., 2000). Fracture toughness, a parameter that is necessary to calculate the blade sharpness index (**Eq. 4.5**), was in a range that was specified for other polymer materials (McCarthy et al., 2007; Shergold & Fleck, 2004), and depended significantly on cutting velocity. This is typical for rate-dependent solids (Landis et al., 2000) and has also been observed for viscoelastic food materials such as cheese or starch gels (Gamonpilas et al., 2009; Kamyab et al., 1998). Whereas *J* is independent of material hardness and similar for EPDMs and EPDMh, NBR showed significantly lower values at both cutting velocities.

Finally, the blade sharpness indices for the reference blades, obtained after cutting the different materials at two different cutting velocities, are also depicted in **Figure 5.7**. Generally, *BSI* of the industrial blade geometries used in this study ranged from 0.25 – 0.35, which is by a factor of 1.5 – 2.0 higher than the *BSI* that was calculated by McCarthy et al. (2007) for scalpels and commercial razor blades, but in the range of the *BSI* of blunted scalpel blades. It is also evident from the results in this study that, at least for the

tested conditions, neither material properties nor cutting velocity show a significant influence on the blade sharpness index (see also McCarthy et al., 2007).

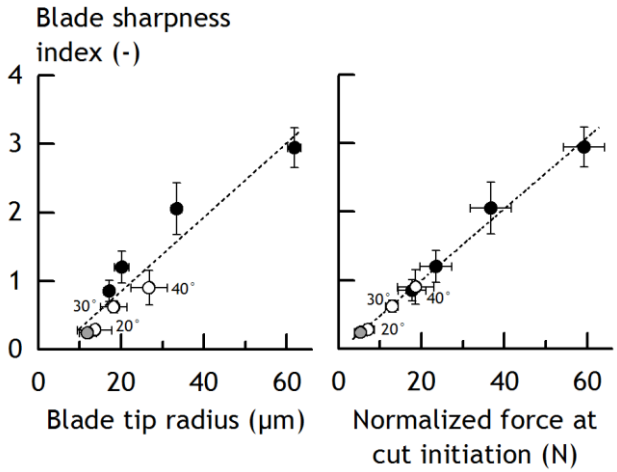

Figure 5.8: Blade sharpness index as a function of blade tip radius, or normalized force at cut initiation. Data are from cutting of EPDMs at 10 mm/min. White symbols, virgin blades with different wedge angle (indicated in figure). Black symbols, 20° blades with different degree of abrasion (see **Table 4.3**). Grey symbol, 20° electro-polished blade. Data are arithmetic means ± standard deviation of (n=8) determinations (two blades per geometry, quadruplicate testing).

Figure 5.8 shows that the blade sharpness index, determined by using blades with different wedge angle or differently abraded 20° blades, depends linearly and significantly on blade tip radius (r = 0.95), and even more on $F_{N,CI}$ (r = 0.99). The general trends are similar as observed for *CI* versus blade tip radius (see **Figure 5.6**). In the case of virgin blades with increasing wedge angle, the *BSI* increase is not disproportionate but follows the fabrication-induced tip radius increase. Hence an increase in the wedge angle at constant blade tip radius does not lead to an increase of *BSI*. These experimental data are contradictory to simulation results of McCarthy et al. (2010) who calculated a higher *BSI* for larger wedge angles at similar blade tip radii. The higher r of the linear relationship between *BSI* and $F_{N,CI}$ also supports Schuldt et al. (2013) who argued that a mechanical blade analysis is much more sensitive for the detection of wear than the optical approach.

If $F_{N,CI}$ can be taken as a measure for the sharpness of a blade then it should be possible to derive a relation between this cutting force parameter and the resistance of materials against fracture when cutting the materials with sharp blades. From **Figure 5.7** one can suppose that $F_{N,CI}$ and fracture toughness are correlating. Covering all materials at

three different cutting velocities with sharp blades the correlation between $F_{N,CI}$ and J is significant (p = 0.001) (**Figure 5.9**). Taking into account that $F_{N,CI}$ is related to fracture stress σ_f contributing elastic and viscous energy, $F_{N,CI}$ can be taken as a measure that correlates with fracture toughness especially if the energy contribution of the system is dominantly elastic.

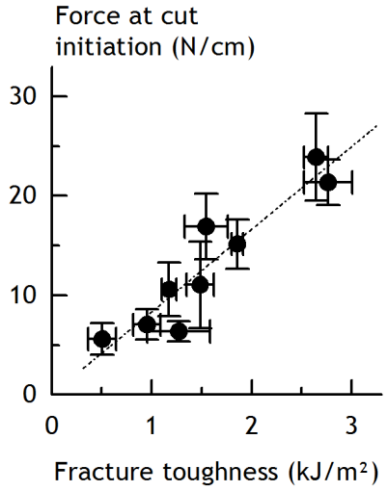

Figure 5.9: Force at cut initiation versus fracture toughness for EPDMs, EPDMh and NBR at 10 mm/min, 100 mm/min and 1000 mm/min of (n=8) determinations (two blades per data point, quadruplicate testing) with regression line (r = 0.93, n = 9).

Unlike to NBR and EPDM the fracture toughness determination of the Elastosil model systems according to McCarthy et al. (2007) showed irregularities because of different material characteristics. In contrast to the manufactured elastomers the Elastosil systems are less stiff, reflected by a lower complex modulus of one magnitude (compare **Table 5.3** and the DMA data in **chapter 4.1.1**). Hence the mounting of the samples between the L-profiles with screws led to compliance and relaxation of the material so that no constant pre-tension could be applied. To overcome this issue spring clamps were used to apply a lower constant force to the L-profiles. Nevertheless measurements showed some controversy effects as the force of the free pass (second run in the pre-cut material) was very close to or even higher than the force of the cutting pass (first cut in the material) which is not explainable by means of fracture mechanics (McCarthy et al., 2007). Interestingly this effect was more pronounced at higher cutting velocities. It was supposed that the reduced surface pressure by the spring clamps in combination with the soft materials led to slip out of the mounted material into the cutting slot as the material

was cut the first time. Hence more material had to be displaced by the blade in the second run with the effect that the measured forces were falsely raised.

It can be concluded that the blade sharpness index is suitable for characterizing the sharpness of blades for food processing. It is independent of the cutting velocity and, in contrast to McCarthy et al. (2010), independent of the wedge angle. Normalized to geometrical and fracture properties of the specimen substrate, *BSI* only depends on the blade tip radius itself. *CI* and especially $F_{N,CI}$ provide measures of sharpness equivalent to the *BSI* once a particular specimen substrate and a single velocity are used. In case a simple and fast sharpness characterization for a specific cutting application is needed, *CI* and $F_{N,CI}$ can however be advantageous.

Independent of cutting substrate and cutting velocity fracture toughness showed a significant correlation to sharpness parameter $F_{N,CI}$ that can simply be determined from cutting force courses. Fracture toughness could not be determined for the soft Elastosil model systems by the method proposed by McCarthy et al. (2007). Hence for further investigations the parameter $F_{N,CI}$ will be taken as indicator of fracture resistance of the cutting material. It should not be used as a quantitative measure to compare different systems with distinct viscoelastic variation. Moreover *CI* gives additional information about the amount of deformation until fracture in the sample is provoked by the blade.

5.2 High-speed cutting on the example of bubble gum

5.2.1 Cutting forces over 6 decades of cutting velocity

Figure 5.10 shows the progress of force during cutting of a model bubble gum, covering 6 magnitudes of cutting velocity that were applied using the universal testing machine (10^{-4}, 10^{-3} and 10^{-2} m/s), or the high-speed test station (10^{-2}, 10^{-1}, 10^{0} and 10^{1} m/s). Qualitatively, all cutting force profiles exhibited a similar shape, and the cutting forces recorded at 10^{-2} m/s with both the UTM and the HSTS show a sufficient agreement. Some slight deviations of the cutting force profiles at the beginning of the cutting process may be attributed to the dynamic response characteristics of the force transducer systems (a strain gauge transducer in the UTM, a piezo transducer in the HSTS) (Pohlit et al., 2008).

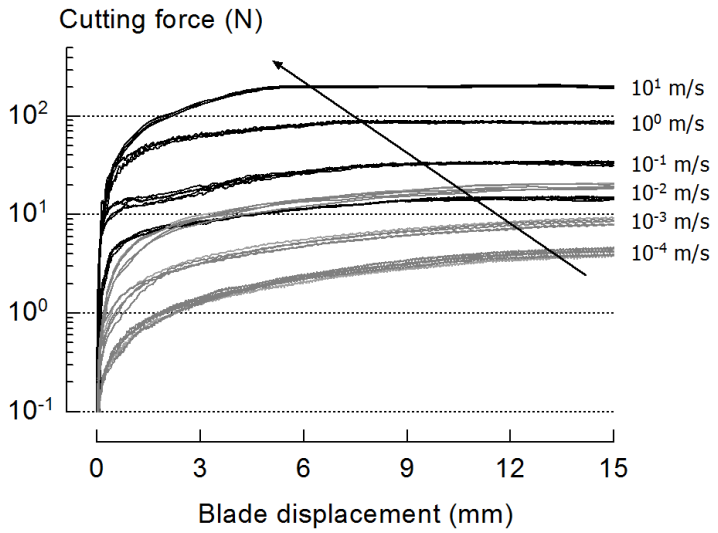

Figure 5.10: Cutting force vs. blade displacement (n = 5) for bubble gum (30 °C) cut at six different velocities with two testing machines. Grey lines, universal testing machine. Black lines, high-speed test station. The arrow indicates that the onset of the steady-state cutting plateau moves to lower displacement at higher cutting velocity.

From a quantitative point of view, the cutting force increases continuously with increasing cutting velocity. For low velocities, such a behavior was also observed in earlier cutting experiments performed on a viscoelastic food model on elastomer basis (Boisly et al., 2016; Schuldt et al., 2016a). Cutting forces generally arise from the resistance of a material against deformation, and from fracture and friction effects in the time course where the cutting blade is driven through the product. The increase in cutting force with increasing cutting velocity can be attributed to the rate-dependent behavior of viscoelastic materials at small (see **chapter 5.1.2**) and large deformation (Boisly et al., 2016). Tensile tests until rupture also indicated that fracture resistance is higher at higher velocity (Schmidt et al., 2018). The friction at the interface between cutting blade and product is determined by the complex interplay of adhesion phenomena, surface deformation, and changes in contact area (see, for example, Lovell & Deng, 1999). The evaluation of the contribution of friction to overall cutting force in dependence to cutting velocity is therefore not trivial, and out of the scope of this study.

In pure viscous materials, all deformation energy is dissipated and no fracture occurs (Luyten et al., 1991). The viscous response of the gum is clearly visible in the cutting force profiles at low cutting velocity (i.e., 10^{-4} – 10^{-2} m/s) where the initial cutting force increase is less pronounced (see **Figure 5.10**). These gentle slopes suggest that the mate-

rial is squeezed and deformed when the blade initially cuts into the sample. In addition to a more pronounced initial cutting force increase, the onset of the cutting force plateau is reached at a lower blade displacement when cutting velocity is increased. This plateau indicates steady-state conditions where the contributions of deformation, fracture and friction to the cutting force are in equilibrium and do not further change (McCarthy et al., 2007).

5.2.2 Viscoelastic effects introduced by cutting velocity and temperature

Figure 5.11 shows a series of movie stills taken during cutting of bubble gum with the HSTS device at 1 or 10 m/s. At 30 °C sample temperature, the more viscous nature of the material at 1 m/s is evident (**Figure 5.11**, left): the image reflects a significant deformation of the gum at the onset of the cut where the blade has already separated the gum

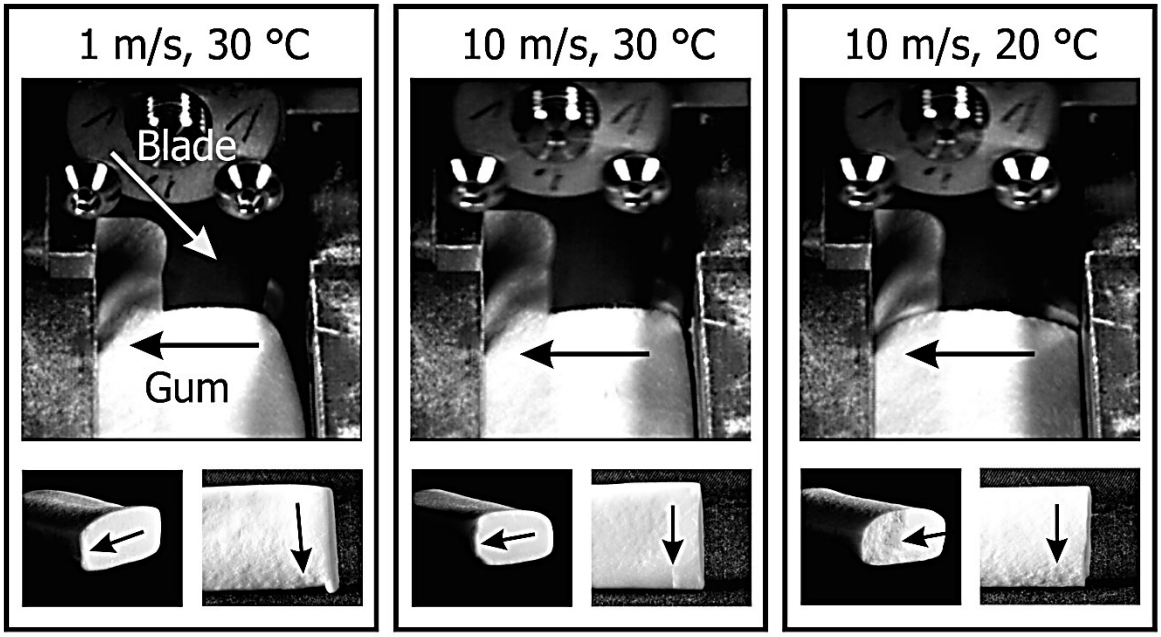

Figure 5.11: Movie stills from videos taken during cutting at the respective conditions (upper images), and representative photographs of the cutting surfaces taken from different directions. Arrows indicate direction of cutting.

(behind the blade). This type of deformation is responsible for the plastic distortion of the cutting surface, especially at the front and the back of the sample (bottom photographs in **Figure 5.11**, left), which contributes to the low quality of the cutting surface. The effect of increasing cutting velocity to 10 m/s is that the overall sample deformation introduced by

the blade is significantly decreased (see movie still, middle of **Figure 5.11**, right side of the sample behind the blade), and the corresponding cutting surface shows almost no plastic, irreversible deformation, meaning that the quality of the cutting surface is significantly improved.

A general property of many polymeric materials is that their small and large deformation behavior, as well as fracture and friction properties can be explained by temperature time superposition (Cho & Lee, 1998; Lorenz et al., 2013a; Pohlit et al., 2008) which has been applied to polymeric food systems by e.g. Sing et al. (2006). Cho & Lee (1998) described the tts principle as "*… the time and the temperature are equivalent … that data at one temperature can be superimposed upon data at another temperature by shifting the curves along the time axis*". This means that decreasing sample temperature at a given deformation rate is equivalent to an increase of deformation rate at constant sample temperature. Indeed, cutting tests performed at a velocity of 10 m/s and at 20 °C showed some interesting effects. In contrast to cutting at the same velocity at 30 °C, no deformation of the material through the cutting blade was observed (**Figure 5.11**, right). From the movie still of the cutting sequence it can be seen that an anticipatory crack is emanating in front of the cutting edge of the blade which is a typical characteristic of brittle fracture with unstable crack growth (Bryan & Ahuja, 1993; Farahmand, 2001). This phenomenon can be attributed to fracture mechanics which differs for ductile and brittle fracture: whereas ductile fracture is characterized by sufficient plastic deformation before cracking, the latter proceeds without plastic deformation (Bryan & Ahuja, 1993; Gdoutos, 2005) and is elastic in nature (Farahmand, 2001; van Vliet, 1996). Materials that show plastic or ductile behavior at low deformation rate may behave elastic or brittle when stressed at a sufficiently high deformation rate (Loncin & Merson, 1979), or at low temperature (which is denoted as tough-to-brittle transition; Langer et al., 2001). Hence, brittle fracture appears if the time scale is too short for viscous energy dissipation and if the deformational energy overcomes the amount of fracture energy (van Vliet et al., 1993). This "excessive" energy is then suddenly converted into an anticipatory crack and into acoustic energy that could be observed as an acoustic shock in the test field. This is in line with observations from the DMA experiments, also showing that the reaction of the bub-

ble gum towards deformation tends to be more elastic when decreasing sample temperature and/or when increasing angular frequency.

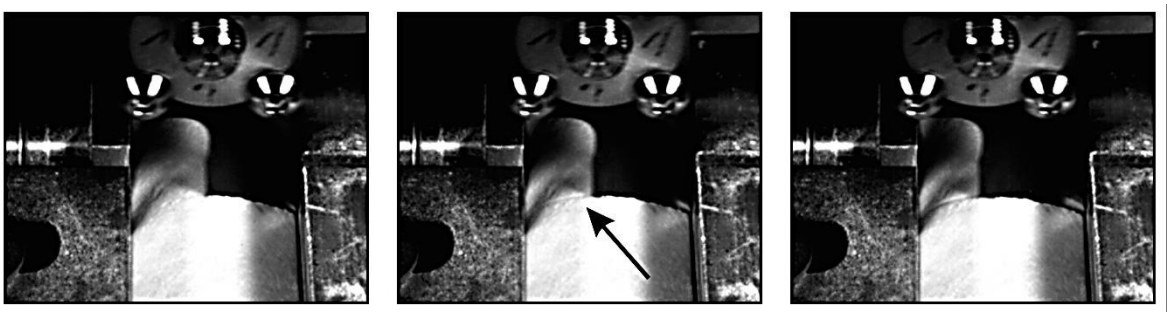

Figure 5.12: Three consecutive movie stills from a cut performed at 10 m/s, sample temperature: 20 °C. Time interval between neighboring pictures is 0.1 ms, corresponding to a 1 mm travelling distance of the blade. The arrow points to the sudden crack that appears in the stressed material.

As can be seen from consecutive images of the cutting sequence recorded at 10^4 fps (**Figure 5.12**), this crack suddenly appears from one picture to another (i.e., within 0.1 ms). Assuming that, at fracture initiation, the distance from the blade tip to the end of the sample is 10 mm implies a crack speed of at least 100 m/s which is in the range of that of polymeric systems (Dear, 1996). Crack propagation can be regarded as a stochastic process that is related to the inner structure of the material, and to initial defects such as cracks, voids or inclusions (Bryan & Ahuja, 1993; Farahmand, 2001; Gdoutos, 2005). This means that brittle fracture does not occur directed and predictable but is a somehow random phenomenon that can even lead to crack branching (Bobaru & Zhang, 2015) and product splintering. Depending on the product, both effects may lead to a low cutting quality.

Crack path instability because of brittle fracture can lead to a rough cutting surface (Bobaru & Zhang, 2015) which was also observed in our experiments (**Figure 5.11**, right, bottom). By analysing the cutting surface of the sample, the initiation of brittle fracture in the sample can therefore be estimated.

All effects shown in **Figure 5.11** are further illustrated by the high-speed videos (**Video 5.1**: 1 m/s, 30 °C; **Video 5.2**: 10 m/s, 30 °C; **Video 5.3**: 10 m/s, 20 °C)[1].

[1] See permalink http://dx.doi.org/10.25532/OPARA-5; for further information see **List of videos**

5.2.3 Quantitative cutting force analysis at different conditions

Apart from the qualitative viscoelastic effects observed at varying cutting velocity and temperature, it is also the development of the cutting force F_C that is significantly affected by the applied condition. Cutting the bubble gum at 1 m/s resulted in a continuously increasing F_C that, from approx. 7 mm blade displacement onwards, became constant once steady-state cutting was achieved (**Figure 5.13**, left); F_C remained constant even after the sample was completely separated (blade displacement > 23 mm). This can

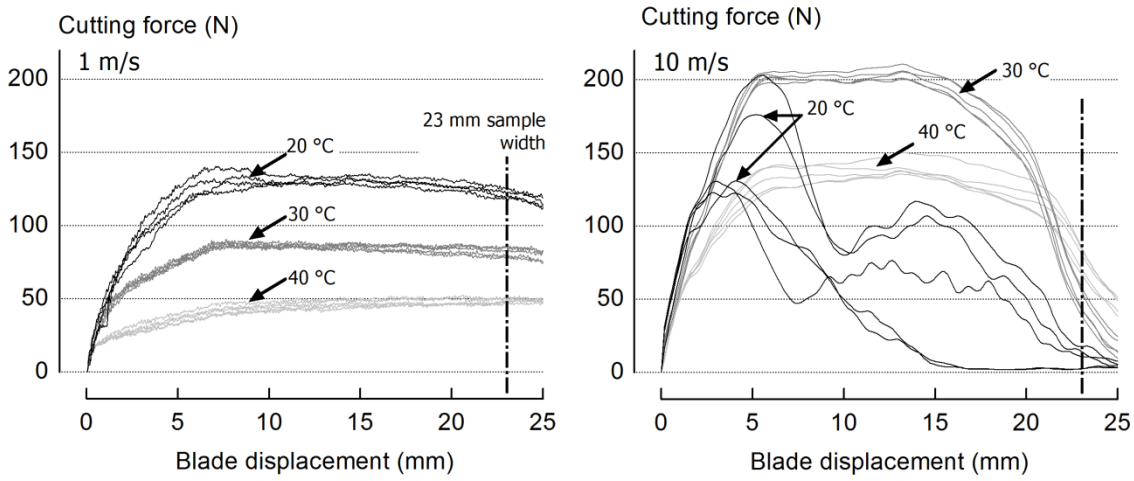

Figure 5.13: Cutting force vs. blade displacement of bubble gum (n = 5) cut at different velocity and temperature.

be attributed to a distortion of the sample in the cutting gap because of sample deformation in front and at the back of the blade. Increasing sample temperature led to a decrease of the cutting force, which is associated to lower sample stiffness. When cutting samples at 30 °C and 40 °C but at 10 m/s, the maximum F_C was by a factor of approx. 2.5 higher (**Figure 5.13**, left). Steady-state cutting was reached at 5 mm blade displacement, indicating that the deformation at the onset of the cut is lower. F_C is, however, significantly reduced before the end of the sample is reached. This can be attributed to the reduction of friction and fracture forces through anticipatory sample separation because of a partly brittle behavior that could not be identified from the video data (see **Figure 5.11**, middle). Cutting at 10 m/s and 20 °C showed a highly brittle reaction of the gum, identified by the steep F_C increase and an F_C maximum in the first quarter of the sample. The subsequent decline of the force because of increasing brittle fracture was also reported

for example for polypropylene at different temperature and velocity (Dijkstra et al., 2002; Olwig, 2006). Multiple determinations showed a large variation that can be attributed to the random nature of brittle cracks (Bobaru & Zhang, 2015). The fact that, after passing its maximum, F_C did not always decrease to zero can be primarily attributed to persisting friction forces at the blade when the product fractures only partially. Interestingly, the maximum F_C at 20 °C and 10 m/s is on average lower than at 30 °C and the same velocity, and also not higher than at 20 °C and 1 m/s. This can be attributed to a decrease of fracture toughness with brittle fracture (Langer et al., 2001) as well as to the reduction of energy dissipation because of a reduced plastic deformation (Gdoutos, 2005).

5.2.4 Qualitative relation between DMA and cutting behavior

Now the question arises whether the deformation behavior of the chewing gum observed in rheological experiments can be linked to the behavior observed during cutting. **Figure 5.14** shows the dependency of the mechanical properties of the bubble gum on temperature and on deformation speed (angular frequency). The complex modulus G^* as a measure of sample stiffness increased with increasing angular frequency ω (or shorter time scale), and it was higher when sample temperature was lower. In the latter case, the ω dependency was less pronounced, pointing on lower viscous contributions (Schuldt et al., 2016b). This is also evident from the dissipation factor $tan\ \delta$, the ratio of viscous to elastic contributions. Viscous contributions to material stiffness were lowest at 20 °C and maximum ω and highest at 40 °C and 1 rad/s. Whereas tan δ apparently approaches an equilibrium at high ω it constantly increases with decreasing angular frequency. The DMA data show a remarkable shift in the mechanical properties of bubble gum between 40 °C and 20 °C which is in accordance with Martinetti et al. (2014) who characterized the mechanical properties of post-chewed bubble gum at different temperature.

The DMA results are in line with observations from the cutting experiments, also showing that cutting forces increase with increasing cutting velocity (shorter time scale) and decreasing sample temperature and that viscous effects occurred at lower cutting velocity. In addition the reaction of the bubble gum towards cutting tends to be more

elastic when decreasing sample temperature and/or when increasing cutting velocity which is in line with *tan δ* dependence on angular frequency.

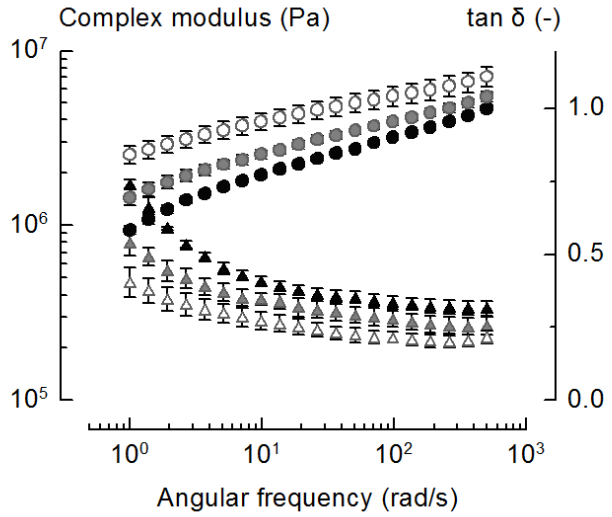

Figure 5.14: Frequency dependence of the complex modulus E* (circles) and the loss factor *tan δ* (triangles) of bubble gum at 40 °C (black), 30 °C (grey) and 20 °C (white). Each data point is arithmetic mean ± standard deviations of 4 replicate measurements.

5.3 Multi-scale cutting behavior of viscoelastic materials

After the detection of the cutting parameters in **chapter 5.1** and the evaluation of the HSTS in **chapter 5.2**, the following chapter will bring together the two experimental approaches. For this purpose, the object of investigation is extended from model systems to food systems. In a first step, the mechanical properties of the investigated materials will be determined with DMA and their multi-scale cutting properties will be investigated. Finally, an analysis of the cutting parameters with regard to deformation and fracture properties is carried out.

5.3.1 Deformation properties from dynamic mechanical analysis

Over two magnitudes of ω, the food models are characterized by power law behavior of *E**, and dominant elastic contributions that are almost independent of angular frequency (**Figure 5.15**). The frequency dependency of the food models is similar to that of the category (a) and (b) foods, which however exhibit more dominant elastic contributions (*tan δ* is lower). In contrast toffee is a system of strong frequency dependence

which is similar to the behavior of other sugar confectionary such as bubble gum (see **Figure 5.14**). The behavior of toffee is predominantly viscous at 1 rad/s (*tan δ* ≈ 2), shows the *G*"/*G*' crossover at approximately 50 rad/s and is predominantly elastic at 500 rad/s (*tan δ* ≈ 0.3). Consequently, the slope of *G* vs.* ω decreases from low to high frequency (Booij and Thoone, 1982). From the sigmoid shape of the *tan δ vs.* ω function it may be assumed that the loss factor approaches an equilibrium value at both small and high frequency.

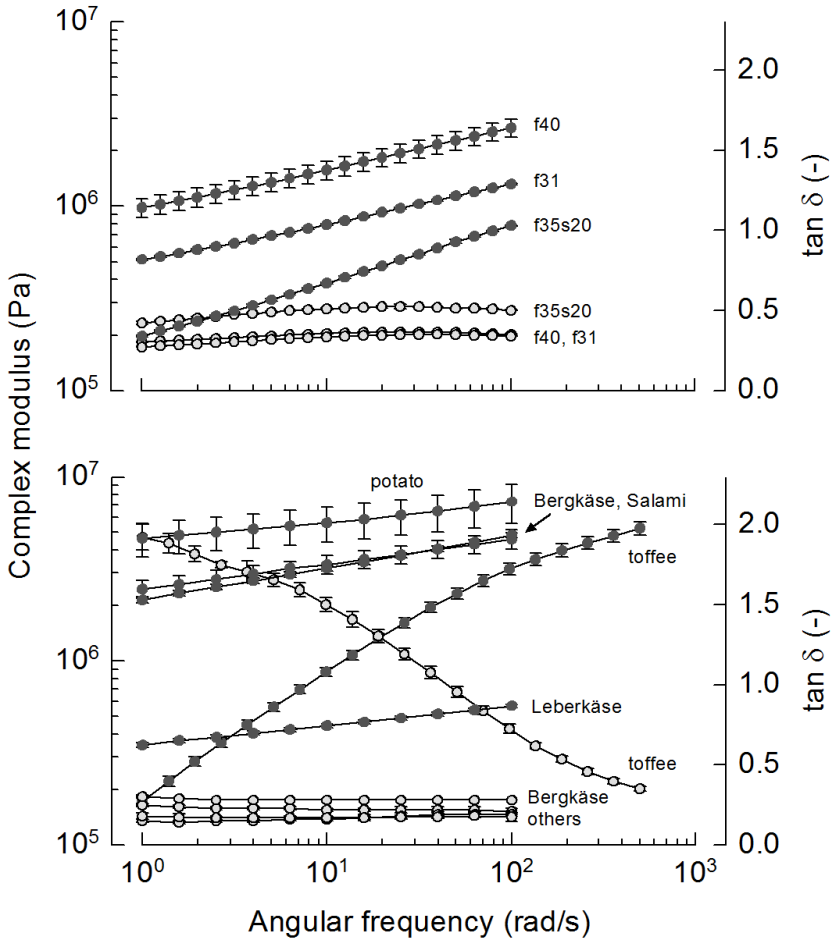

Figure 5.15: Dynamic mechanical analysis of model samples and foods. Dark symbols, complex modulus; light symbols, tan δ. For sample code see **Table 4.1**.

5.3.2 Cutting forces and cutting properties at multi-scale cutting velocity

Figure 5.16 shows the force profiles of different systems obtained during cutting at $v = 10^{-3}$, 10^{-1} and 10^{1} m/s. f35s20 and the other food models (data not shown) exhibited a behavior qualitatively similar to that of the foods having a polymeric matrix, namely Bergkäse with a very low between-specimen variation, and the processed meat products.

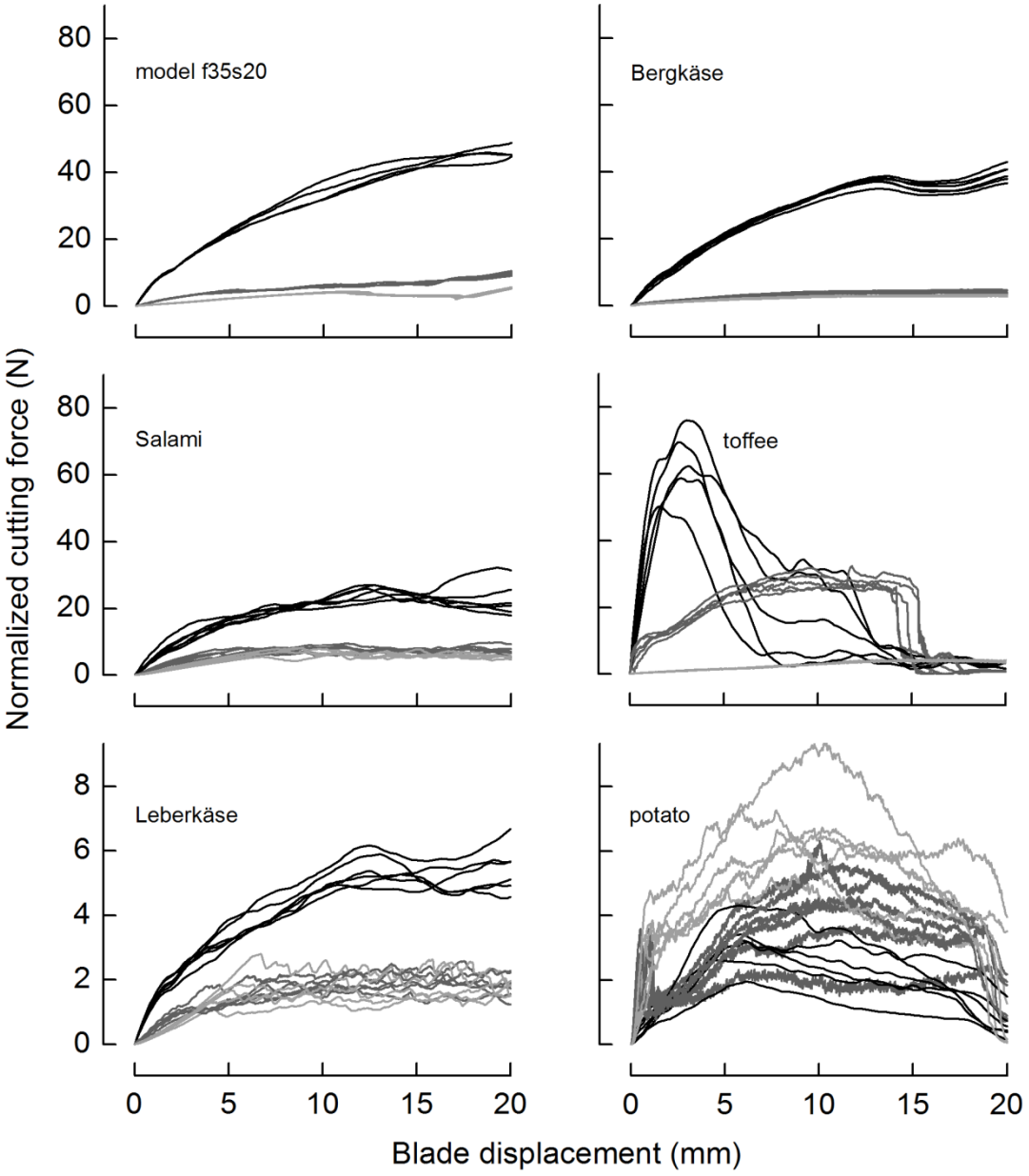

Figure 5.16: Force profiles of one food model and foods, obtained by applying different cutting velocities. Cutting force is normalized to 10 mm cut width. Light grey, 10^{-3} m/s (Instron); dark grey, 10^{-1} m/s (high-speed device); black, 10^{1} m/s (high-speed device).

As the cutting force represents the sum of the contributions of deformation, fracture and friction, and as the stiffness of the hard cheese is one magnitude above that of model f35s20 (see DMA results), friction and/or fracture forces of the cheese are obviously smaller than that of the filled elastomer. Both systems show a distinct contribution of friction because of the nearly linear increase of F_N with l, caused by a proportional increase of the contact area between blade and product until the entire blade is penetrated into the material (at around 10 mm blade displacement). Hence, the similar level of F_N can therefore be attributed to the low fracture toughness of cheese, compared to elastomeric systems (see also Schuldt et al., 2016b). In contrast to Bergkäse, the meat products show an attenuated F_N increase in the separation phase (3), visible from approximately 3 mm blade displacement onwards. This indicates a reduced contribution of friction, probably because of the lubrication of the blade by the dispersed fat or water. The much lower cutting forces of Leberkäse are a result of the lower material stiffness (see **Figure 5.15**). Salami and Leberkäse exhibited higher between-specimen variations of F_N at every cutting velocity, presumably caused by a more heterogeneous microstructure. In all systems, F_N increased pronouncedly with increasing velocity (Boisly et al., 2016; Brown et al., 2005), but almost no effects on the cutting profiles were observed; this points on ductile fracture behavior (see **chapter 5.2**).

The increase of F_N with v is also evident for toffee. Especially for intermediate cutting velocity, the cutting forces were much higher than for all other systems. Because material stiffness (see **Figure 5.15**) is of the same magnitude and because of the non-prominent friction forces (see **Figure 5.16**; no linear increase of F_N until full blade penetration at 10 mm blade displacement), these result from the higher fracture resistance of the material (see also **chapter 5.3.4**). At low v, the F_N profile points on a significant plastic sample deformation (see also **chapter 5.2**). At 10 m/s there is a remarkable variation of cutting forces and, compared to v, the cutting force maximum is at a displacement where the dimensional end of the sample (u = 15 mm) is by far not reached. Both effects can be associated with brittle fracture (Bobaru & Zhang, 2015; Olwig, 2006) (see also **chapter 5.2.3**) which becomes evident from the video data of toffee, cut at 10 m/s (**Video 5.4**)[2]. Similar to bubble gum, toffee showed a strong dependence on the temperature, with

[2] See permalink http://dx.doi.org/10.25532/OPARA-5; for further information see **List of videos**

lower temperatures favoring brittle behavior (results not shown). A detailed discussion of the temperature dependence of toffee with respect to tts can be found in Schmidt et al. (2018).

Potato showed relatively high cutting forces at low *v* which may be attributed to its high stiffness (see **Figure 5.15**). Interestingly there was no F_N increase with increasing *v* even though DMA suggested increasing deformation forces at a shorter time scale. This was also reported for potato and carrots by Dowgiallo et al. (2005), and may be attributed to brittle fracture that goes in line with decreasing deformation forces and decreasing fracture toughness (Aderinola et al., 2014; Langer et al., 2001). Vincent et al. (1993) described vegetables as a "*supercomposite …* " that is "*arranged in a series of morphological hierarchies*" containing fibrous components (e.g., cell wall structures) and non-fibrous parenchyma, the latter fracturing in a brittle manner. Alvarez et al. (2000) analysed fracture behavior of fruits and vegetables and also proposed brittle failure of the cells. From these explanations one can derive that cellular plant tissues show partly brittle fracture characteristics. For every cutting velocity, the remarkable between-specimen variation is apparently linked to this brittle behavior and/or to the variability of the material itself (see also Schuldt et al., 2016b). The behavior of carrots, which reveals more directional internal structures, was comparable (data not shown).

To analyse cutting behavior in more detail, the maximum normalized cutting forces $F_{N,max}$ and the corresponding blade displacement $l_{FN,max}$ were plotted against cutting velocity (**Figure 5.17**). For all model systems and the cheese, a power-law increase of $F_{N,max}$ with *v* is evident. Leberkäse and Salami also show a distinct increase of $F_{N,max}$ but only for $v > 0.1$ m/s. This can be attributed to the heterogeneous structure, as both systems contain a significant amount of macroscopic filler that resists transection. At low *v*, these fillers are squeezed rather than dissected so that cutting forces for separating the material may be superimposed. At higher velocity the filler particles are separated because of internal stiffening, and the contribution of deformation forces (see **Figure 5.15**) to F_N is more pronounced. This is supported by rough cutting surfaces of salami (**Figure 5.18**) and the residues that remained at the cutting edge of the blade when cutting with a velocity of up to 1 m/s (see the rough cutting path in the material and the blade edge after cutting

at 10^{-1} m/s (**Video 5.5**)[3] and the smooth cutting surface (**Figure 5.18**) and cutting path in the material when cutting with 10 m/s (**Video 5.6**)[3]. In all these cases, blade displacement at $F_{N,max}$ is almost constant and close to the dimensional end of the sample, indicating that the general fracture behavior is not affected by *v* (see **Figure 5.17** and **chapter 5.2**).

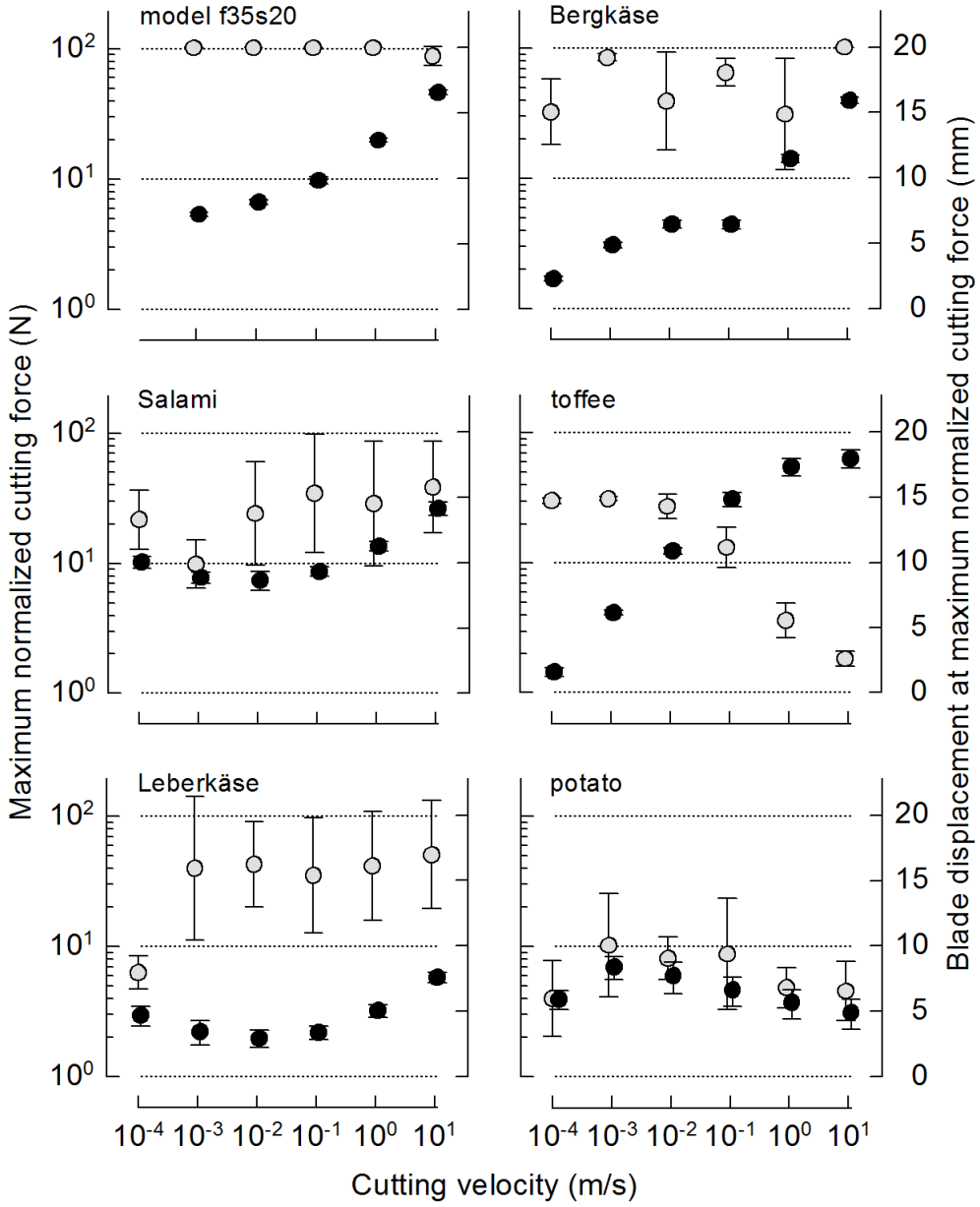

Figure 5.17: Cutting velocity dependence of maximum normalized cutting force (black), and blade displacement at this force (grey) of different foods. Length of the cut of the samples is 20 mm (except for toffee, 15 mm). For the sake of clarity, markers are slightly shifted along the x-axis.

[3] See permalink http://dx.doi.org/10.25532/OPARA-5; for further information see **List of videos**

In case of toffee, $F_{N,max}$ increased exponentially with cutting velocity at small and intermediate *v.* The attenuated increase at higher velocity reflects a progressively brittle behavior (as was discussed for bubble gum in **chapter 5.2**), and is in line with the frequency dependence of the complex modulus (see **Figure 5.15)**. In addition, $l_{FN,max}$ illustrates the brittle material reaction. At low *v*, it is deformed and squeezed during the entire passage of the blade, and $F_{N,max}$ is reached at the end of the sample. Because of the anticipatory brittle fracture of the material, $l_{FN,max}$ is progressively decreasing from $v = 10^{-1}$ m/s onwards and reached values lower than 5 mm blade displacement at *v* = 10 m/s (Dijkstra et al., 2002; Olwig, 2006) (see also **chapter 5.2.3**).

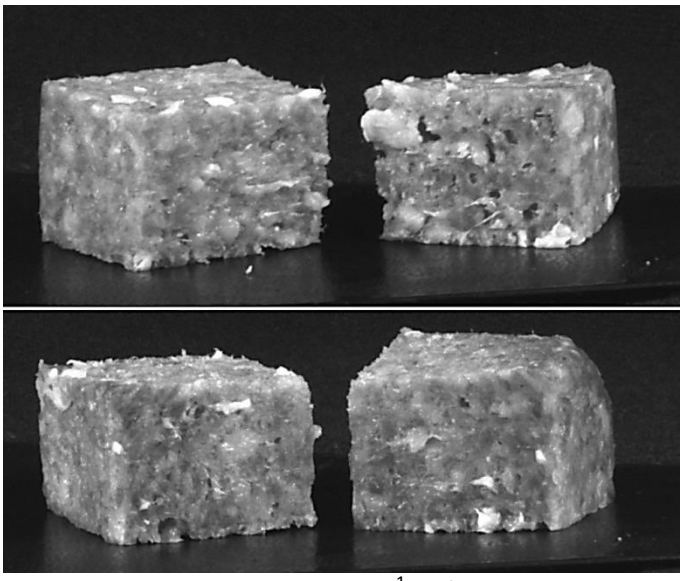

Figure 5.18: Surfaces of Salami after cutting at 10^{-1} m/s (rough, upper picture) or at 10 m/s (smooth, lower picture).

$F_{N,max}$ of potato (see **Figure 5.17**) and carrot (data not shown) are only slightly affected by *v*, and $l_{FN,max}$ alternates distinctly but is in general located in the first half of the sample, which does not disprove the thesis of brittle cutting. The fact that, for potato and carrot, Dowgiallo (2005) reported a decreasing maximum cutting force over nearly two magnitudes may be attributed to technical differences regarding force measurement. Pohlit et al. (2008) compared the results of force capturing with a strain gauge and a piezo-electric force sensor at a velocity up to 10^{0} m/s; they concluded that the piezo transducer gave higher force responses from 10^{-1} m/s upwards and supposed the strain gauge to give erroneous results because of slower response times.

In summary a broad variety of foods has been cut at several magnitudes of cutting velocity up to 10^1 m/s. It could be shown that the polymeric model systems and the foods on polymeric basis showed similar cutting behavior. The results do not indicate brittle fracture behavior at the highest velocities. Even though plant tissues show similar material characteristics from DMA measurements they reveal fundamental differences in cutting behavior which is most likely attributable to their inherent composite structures that includes partly brittle fracture behavior. For all other systems the DMA characteristics basically coincide with the cutting velocity dependence of the cutting forces. It was shown that the highly rate dependent deformation behavior of the investigated confectionaries significantly influenced the cutting behavior, as a transition from ductile to brittle fracture at high cutting velocities was determined. The strong dependence on temperature and time scale reflects the challenges in processing these materials. Analysing $F_{N,max}$ and blade displacement at $F_{N,max}$ can provide additional information on the nature of fracture mechanism.

5.3.3 Deformation parameters at multi-scale cutting velocity

The cutting parameter s_0 was used to characterize the deformation properties of the foods and the model systems. **Figure 5.4** shows that E^* and s_0 of the different Elastosil model systems correlate linearly ($r \geq 0.97$). This strong dependency does not exist when considering foodstuffs and model systems together (**Table 5.5**). Even though there is a general tendency of increasing moduli with increasing s_0, the correlation is not always significant.

Figure 5.19 shows an example of the dependence of E^* over s_0 with a regression line over values of the food and the model systems (solid line) and a regression line only over the values of the model systems (broken line). Except for Leberkäse, the data points of the foods are clearly above the regression line of the model systems. The reasons why E^*/s_0 of foods und food models do not clearly correlate may be attributed to the detection of the cutting parameter s_0 and differences of the structures and fracture properties of the specific materials. At the beginning of the cutting sequence the cutting force increase of the foods could have been attenuated according to creeping and plastic defor-

mation in front of the blade tip (salami), cell damage (i.e. fracture; potato) or a very early *CI* (cheese). This may have led to smaller s_0-values that are not in line with the s_0-trend of the food models. In contrast Leberkäse shows a good agreement with the model systems. A pronounced stiffness plateau (see **Figure 5.1**) and a high cut initiation depth indicate a distinct elastic deformation before cut initiation which is similar to the model systems.

Table 5.5: Correlation coefficients from linear regression of complex-modulus versus normalized initial cutting force slope at different cutting velocities and angular frequencies for f31, f40, f35s20 (for sample code see **Table 4.1**), Bergkäse, Leberkäse, potato and Salami.

	Regression coefficients [-]		
Angular frequency →	1 rad/s	10 rad/s	100 rad/s
Cutting velocity ↓			
10^{-3} m/s	0.83*	0.80*	0.78*
10^{-2} m/s	0.63	0.62	0.62
10^{-1} m/s	0.60	0.62	0.62

* significant correlation (p = 0.05)

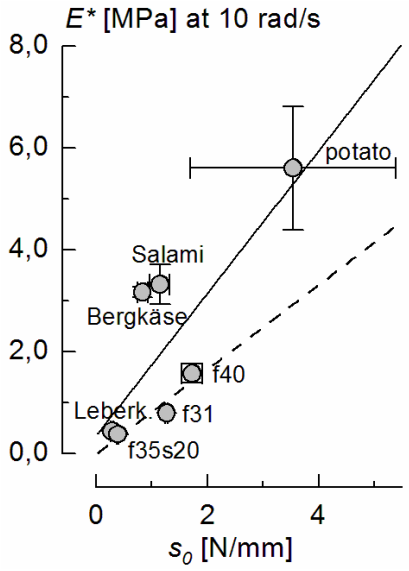

Figure 5.19: Complex modulus *E** at 10 rad/s versus normalized initial slope s_0 at 10^{-3} m/s cutting velocity for foods and model systems (n = 4); solid line, regression line of all data points; broken line, regression line of only the model systems.

Chapter 5.1.2 discussed how viscoelastic contributions affect the pre-crack properties of food models and showed that there is a close linear relation between particular parameters obtained from DMA measurements. These were, in particular, the slope *n*

that related E^* to ω (**Eq. 4.1**) and the phase shift δ (here in rad, taken as average value from the frequency sweeps), supposed to be related to this slope via the approximate relation from Booij and Thoone (1982) (as transformation from **Eq. 5.1**):

$$n = {}^{2\delta}/_{\pi} \qquad \text{Eq. 5.3}$$

This equation holds for materials that follow **Eq. 4.1** (Bruno and Moresi, 2004; Friedrich and Heymann, 1988) and implies that, the higher the viscous contribution of a system, the higher is the frequency dependence of the complex modulus. **Figure 5.20** shows that **Eq. 5.3** is valid for both, the model systems and the analysed foods, giving values of *n* that are nearly identical to those obtained from the frequency sweeps (see **Eq. 4.2**).

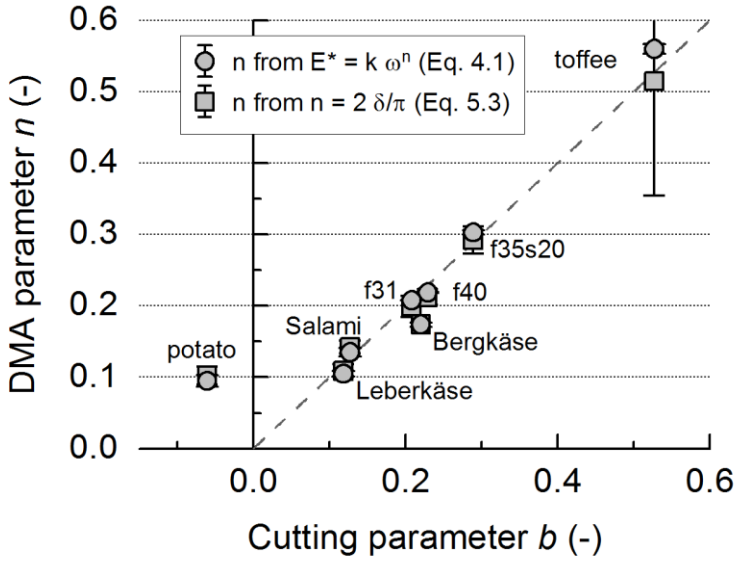

Figure 5.20: Comparison of velocity and time related measures from dynamic mechanical analysis and multi-scale cutting experiments. Broken line: f(x) = 1**b*.

b, the cutting velocity dependence of s_0, was calculated from cutting experiments by applying **Eq. 4.4**. Except for potato (r = 0.35), all regression coefficients were $r \geq 0.96$, indicating a significant interaction between s_0 and v. By considering all samples, **Figure 5.20** shows that the two power law exponents from the DMA experiments are linearly related to *b* that relates cutting force to cutting velocity (**Eq. 4.4**). This linear relation however is not applicable to potato as no increase of the initial F_N slopes with increasing v was detected. In contrast to the other systems, toffee shows a rather high standard deviation for *n* calculated by **Eq. 5.3** which results from the distinct shift of viscoelastic properties

versus angular frequency (see **Figure 5.15**; coefficient of variance of nearly 30 % for δ); these results should therefore be considered with caution.

The dotted line in **Figure 5.20** has a slope of 1, therefore showing that *n* from DMA experiments and *b* are equivalent. It clearly demonstrates the validity of

$$b \cong n = {2\delta}/{\pi} \qquad \text{Eq. 5.4}$$

from low to high-speed cutting velocity for the model systems and the non-composite foods of category (a) and (c). The system with the highest deviation from the dotted line (approx. 20%) is Bergkäse, presumably because of a small cut initiation depth and a low fracture toughness (see Schuldt et al., 2016b) that might affect the interrelationship from **Eq. 5.4**.

In practice, the velocity dependence of cutting forces as expressed in **Eq. 5.4** is important for e.g. dimensioning gear drives for industrial cutting or processing machines, or for modeling cutting forces at different *v*. Starting point for predicting material behavior could be a model approach with as few parameters as possible. It would further be advantageous to use results that can be obtained by using conventional testing machines. From these considerations a model approach derived from **Eq. 4.4** is proposed:

$$s_{0,M} = a_M \cdot v^n \qquad \text{Eq. 5.5}$$

with $s_{0,M}$ being the modeled initial F_N *vs.* l slope that depends on *v*, and the exponent *n* as the slope from **Eq. 4.1** obtained by DMA material characterization. The model constant a_M is calculated by transposing **Eq. 5.5**:

$$a_M = {s_{0@10^{-3}\,m/s}}/{(10^{-3}\,m/s)^n} \qquad \text{Eq. 5.6}$$

With $s_{0@10^{-3}\,m/s}$ determined in a cutting experiment performed at $v = 10^{-3}$ m/s (= 60 mm/min), a common velocity for food characterization that is covered by commercial testing machines (Chen & Opara, 2013). Consequently, the model constant a_M can be obtained by determining two parameters, namely *n* and $s_{0@10^{-3}\,m/s}$. With the two parameters *n* and a_M , $s_{0,M}$ can be calculated for any cutting velocity.

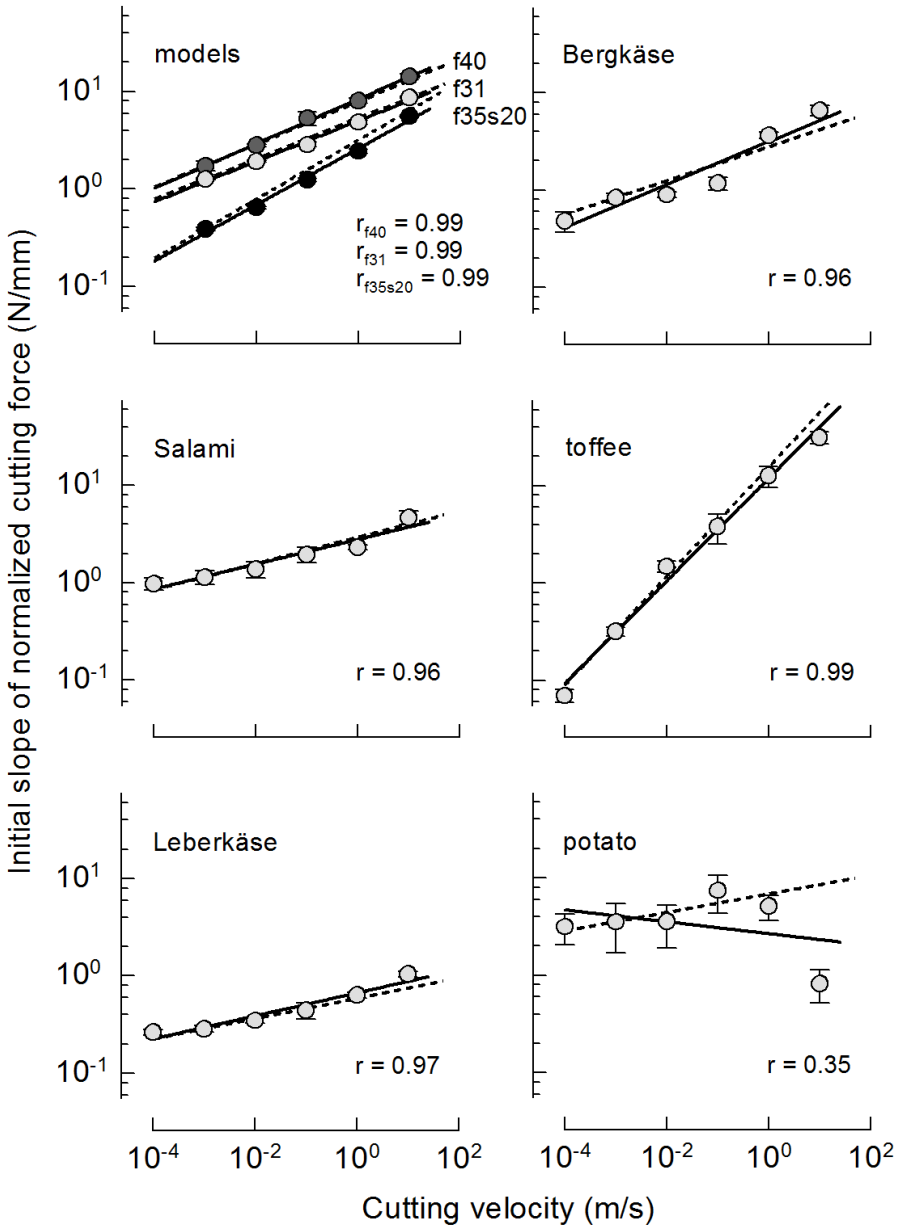

Figure 5.21: Experimental s_0 values as a function of cutting velocity (markers). Solid lines and regression coefficients are from power law fits according to **Eq. 4.4**. The dotted line indicates the results of the model approach **Eq. 5.5**.

Figure 5.21 shows the individual s_0 slopes *vs*. cutting velocity for the different materials, the corresponding power law regression functions (**Eq. 4.4**) and the model functions obtained by applying **Eq. 5.5**. The regression functions show sufficient agreement for all materials except for potato, and the respective correlation coefficients are significant ($p < 0.01$). It is evident that the synthetic elastomeric materials show high conformity at any cutting velocity, therefore giving the best power law fits, and indicating that they can

be considered as food models with almost ideal properties. The foods however show some deviations from power law which may come from their natural variability (Rohm et al., 1997; Schuldt et al., 2016b; Vandenberge et al., 2014). In case of the cellular plant materials, the measured s_0 does neither increase nor decrease with increasing v so that regression and model cannot be considered as appropriately expressing material behavior. Nevertheless, the model approach for potato apparently fits the increase of s_0 until 10^{-1} m/s. In case of toffee, both regression through **Eq. 4.4** and modeling through **Eq. 5.5** seem sufficiently linked to the experimental data. However, the increase of s_0 is not constant but apparently attenuated for $v > 10^{-1}$ m/s, which is also in accordance with the response to DMA (see **Figure 5.15**).

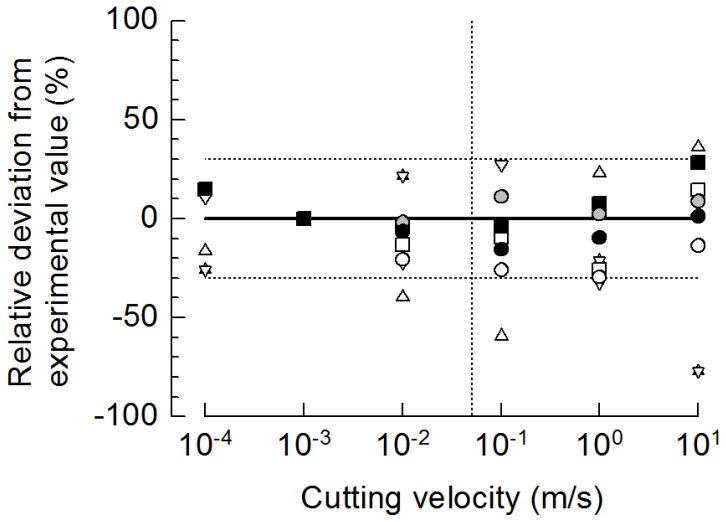

Figure 5.22: Relative deviation of the model values from the experimental data (at 0 % the model equals the experimental value). Circles, food models (white, f35s20; grey, f40; black, f31); squares, meat products (white, Salami; black, Leberkäse); upright triangle, Bergkäse; inverted triangle, potato; diamond, toffee.

Figure 5.22 depicts the relative deviations of the calculated values $s_{0,M}$ based on **Eq. 5.5** from the experimental data s_0, calculated from $(s_0 - s_{0,M})/s_0$. For nearly all systems, the model values deviate by less than 30 % which can be considered as an appropriate forecast of experimental data. Three systems show substantial deviations from the 30 % line, that is Bergkäse, toffee and potato (the latter with more than 900 % deviation at 10 m/s; out of range in **Figure 5.22**). The model for the cheese is unsatisfactory, mainly

because experimental data somewhat deviate from power law behavior. This probably reflects a limitation of the slope determination method because Bergkäse has small cut initiation depths so that s_0 has to be obtained from a lower number of cutting force data points. The model for toffee shows a distinct overestimation at higher velocity, especially at 10 m/s, which comes from the attenuation of the s_0 increase.

It can be concluded that the cutting parameter s_0 reflects the initial stiffness of the cutting material and can therefore be related to the complex modulus from DMA. Presumably because of differences in morphology and structure the correlation between s_0 and E^* is not significant for the food systems. The velocity dependence of s_0 can be expressed by the parameter b from **Eq. 4.4**. and the relation between the pre-crack cutting parameter b and the DMA parameters n and δ is valid from low to high cutting velocity and can be expressed by **Eq. 5.4** for all investigated systems except for cellular or fibrous plant tissues. The application of a simple model approach as given by **Eq. 5.5** can be a useful engineering tool to estimate initial cutting forces, mostly for materials that reveal constant viscoelastic properties. For systems with increasing elastic contributions at higher velocity the experimental values can be overestimated as this appeared in the case of toffee. For plant tissues the model does not fit.

5.3.4 Fracture parameters at multi-scale cutting velocity

In **chapter 5.1.3** $F_{N,CI}$ from cutting force courses was depicted as fracture measure for the cutting process. Additionally *CI* shows which amount of deformation is needed until fracture in the sample is provoked. *CI* and normalized cutting force at cut initiation $F_{N,CI}$ for foods and the food model f35s20 (as example for the other model systems) from 10^{-4} m/s (10^{-3} m/s for f35s20) to 10^{0} m/s cutting velocity are depicted in **Figure 5.23**. For 10 m/s cut initiation could not be derived because of cutting force smoothing and limited number of data points. Two trends can be reported for *CI*: either a clear decrease (model systems, Salami, Leberkäse) or a trend to stay constant (Bergkäse, carrot, potato, toffee; see also **Figure 5.24**) with increasing v. It is known that fracture strains from compression or tensile experiments of polymeric food systems can increase, fall or stay constant with higher rate (van Vliet et al., 1993; van Vliet & Walstra, 1995). The decrease of fracture

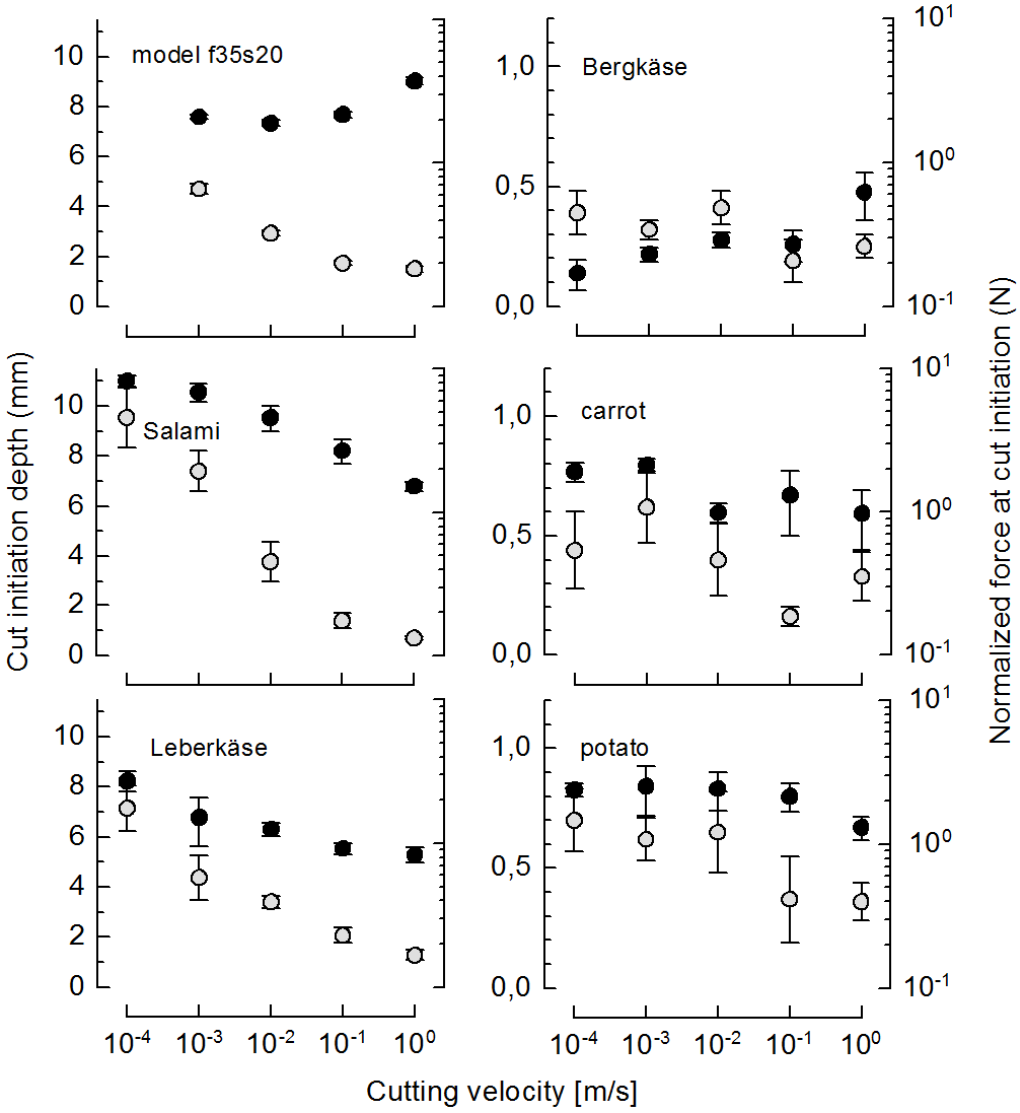

Figure 5.23: Cutting velocity dependence of cut initiation depth (grey) and normalized force at this blade displacement (black) of different systems.

strain with increasing velocity can be associated to the viscoelastic effect that less energy is dissipated by viscous flow and relaxation so that energy transport to the crack tip is enhanced (van Vliet et al.,1993; van Vliet & Walstra, 1995). Consequently the material has to be deformed less to reach an amount of energy to induce fracture. For vegetables it is known that fracture strains tend to decrease with increasing strain rate which is associated to a limited fluid release (stress relaxation) through the cell walls with higher deformation speed. Hence higher stress buildup in the cell causes fracture at lower extensions (Ormerod et al., 2004; Zdunek & Umeda, 2006). Even though fracture strains of polymeric systems containing fillers often increase with increasing velocity (Boisly et al., 2016; Rohm & Lederer, 1992, van Vliet & Walstra, 1995) and although it was the case for the elasto-

mers in this study used for fracture toughness determination (**Figure 5.7**), it was not the case for *CI* of the model systems. Moreover fracture strain from tensile experiments of an Elastosil model system containing iced sugar as filler was also increasing when applying higher deformation speeds (Boisly et al., 2016). Cutting means that a blade is pressed in a material which will partly be compressed in front of the blade tip. If the sample is compressed against the sample support (as it is the case in these experiments and in industrial practice), stiffness increases with increasing blade displacement (Schuldt et al., 2013). This stiffening will further increase with higher cutting velocity (see **Figure 5.4** and **Figure 5.21**). Consequently the force for fracture initiation tends to be reached at lower blade displacements. In case of EPDM and NBR (**Figure 5.7**) measurement setup (see **chapter 4.5.3**) prevented material stiffening against a sample support and may have led to increasing *CI* with increasing cutting velocity. This could be associated to inner friction between the structural elements of the composite which can lead to inefficient energy transport to the crack tip (van Vliet et al., 1993).

For the force at cut initiation three categories of velocity dependence can be derived (**Figure 5.23**). (1) For most systems $F_{N,CI}$ increases with increasing cutting velocities (model systems, Bergkäse, toffee (see **Figure 5.24**)). (2) For vegetables it stays constant or slightly decreases at high velocities and (3) for Leberkäse and Salami, $F_{N,CI}$ progressively decreases with increasing cutting velocities.

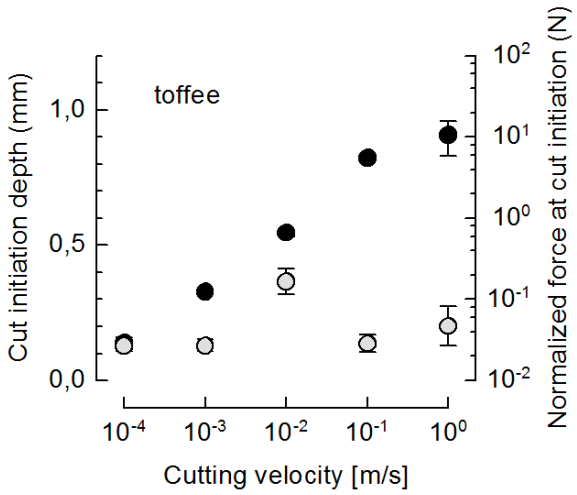

Figure 5.24: Cutting velocity dependence of cut initiation depth (grey) and normalized force at this blade displacement (black) of toffee (30 °C).

The increase of fracture toughness or stress at fracture of viscoelastic systems with higher rate is often reported in the literature (see for example Gamonpilas et al., 2009; Luyten & van Vliet, 1995; van Vliet et al., 1993; Forte et al., 2015; McCulloch, 2008). After van Vliet et al. (1993) this can be explained macroscopically by an increasing dissipation of energy at higher velocity because of friction between the structural elements of the composite systems. This can lead to an increase of σ_f after constant values at lower deformation rates, as it is also the case of $F_{N,CI}$ for the model systems. Controversially toffee shows a sharp increase of $F_{N,CI}$ even at small velocities. This is in accordance to σ_f from tension and compression experiments of McCulloch (2008) with toffee at small velocities. At 1 m/s increase of $F_{N,CI}$ seems to attenuate which possibly indicates ongoing brittle fracture with decrease of fracture toughness (Aderinola et al., 2014; Langer et al., 2001). On small-scale the increase of bond strength (van Vliet et al., 1993) or the increase of defect or void growth (Luyten & van Vliet, 1995; Tang, 2008) can be associated to an increase of fracture toughness which contributes to the overall force response of $F_{N,CI}$. Similar to the $F_{N,CI}$ of the model systems several authors reported on an increase of fracture toughness at higher velocities after primal constancy at lower velocities i.e. for gelatin (Forte et al., 2015) and starch gels (Luyten et al., 1992). In model simulations Tang et al. (2008) showed that this dependency can be associated to the interference of viscoelastic dissipation at small and void growth in front of the crack tip at higher velocities (**Figure 2.10**).

Vegetables showed nearly constant values or a slight decrease of $F_{N,CI}$ with cutting velocity increase as it was also the case for fracture stress of potato (Canet et al., 2007; Scanlon & Long, 1995). This can be associated to brittle failure of the cells of the plant materials (Alvarez et al., 2000; Vincent et al., 1993) which can be linked to rate-independent fracture toughness (Langer et al., 2001).

Leberkäse and Salami show a distinct decrease of $F_{N,CI}$ with increasing cutting velocity. For fracture stress (Luyten & van Vliet, 1995; van Vliet et al., 1993; van Vliet & Walstra, 1995) and fracture toughness (Tang et al., 2008) this is the case if viscoelastic dissipation is dominating overall energy composition (W''_{visc} in **Eq. 2.11**). Because the dissipation is inhibited with shorter time scales the fracture parameters decrease with ongoing velocity. As Leberkäse and Salami show high *CI* values at the lower cutting velocities the material in front of the blade tip is extensively deformed before fracture (see also discussion in

chapter 5.3.2). After van Vliet et al. (1993) at higher deformations friction between the components of composite systems is enhanced. Especially Salami with its heterogeneous composition shows a distinct structural deformation (**Figure 5.18**) at lower cutting velocities. This leads to inter-particle friction (W''_{frict} in **Eq. 2.12**) which can also result in an increase of overall force response (van Vliet et al., 1993) at low cutting velocities.

In summary fracture properties have been analysed with *CI* and $F_{N,CI}$. For the chosen test setup *CI* decreased with increasing cutting velocity because of increased tension buildup. Depending on the materials and energy dissipation mechanism with higher *v*, $F_{N,CI}$ increased, decreased or stayed constant. Over all using the fracture parameter $F_{N,CI}$ from the initial cutting force data includes limitations because the derivation from the initial cutting force data at 10^1 m/s was not possible. Ideally it would be advantageous to use an alternative fracture parameter that reflects the fracture behavior during cutting and could easily be derived at high velocities. However $F_{N,CI}$ seems a suitable tool for fracture characterization. Generally it can be concluded that increasing the cutting velocity leads to minimization of *CI* and hence lower product deformation which is attributed to enhanced cutting quality (Schneider et al., 2010). After Atkins et al. (2004) and Dowgiallo (2005) minimizing of cutting forces leads to optimization of cutting quality. Especially polymeric foods with heterogeneous structures (Leberkäse and Salami) show a substantial improvement of cut initiation and a substantial reduction of force for cut initiation. This enhancement of cutting quality with increasing cutting velocity is in line with the findings in **chapter 5.3.2** (**Figure 5.18**).

5.3.5 Conclusions on the friction forces

As the total cutting force (represented by $F_{N,max}$) summarizes deformation (represented by s_0), fracture (represented by $F_{N,CI}$) and friction forces (**Eq. 2.6**), it should be possible to derive information about the velocity dependence of the friction component from the velocity dependence of $F_{N,max}$, s_0 and $F_{N,CI}$. **Figure 5.25** compares the slopes of the power law functions of $F_{N,max}$, s_0 and $F_{N,CI}$ from $v = 10^{-4}$ (10^{-3} for the model systems) to $v = 10^0$ m/s. As $F_{N,max}$ represents the velocity dependence of the total cutting force, higher values of s_0 mean that the contribution of the deformation force to total force is increas-

ing with higher cutting velocity. Since the values compared are not suitable for accurate, quantitative energy analyses, only tendencies on qualitative basis can be derived.

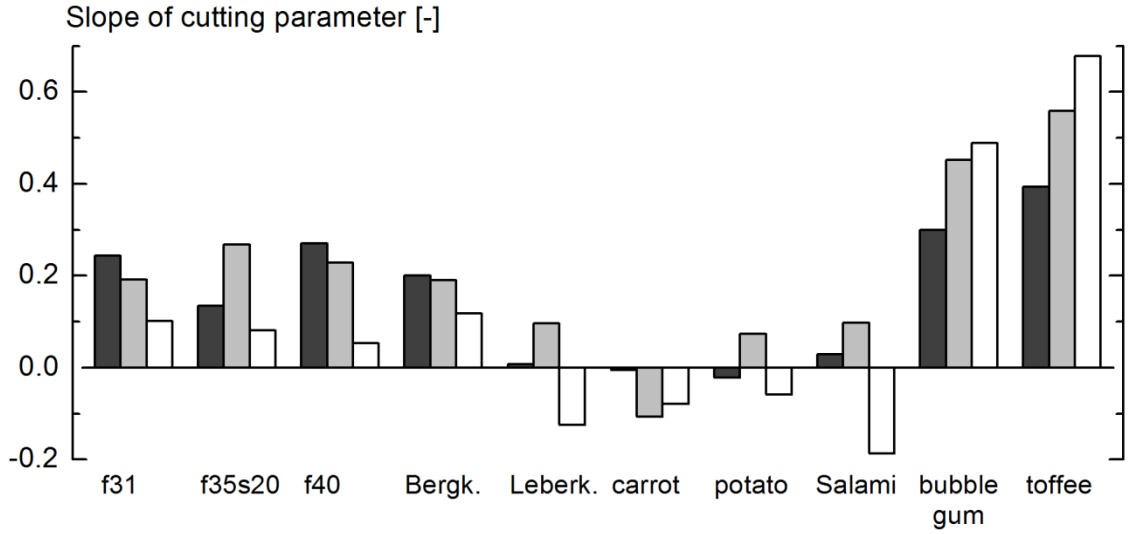

Figure 5.25: Cutting velocity dependence of the cutting parameters normalized maximum cutting force (dark grey), initial slope of the normalized cutting force (light grey) and normalized force at cut initiation (white) for different model systems (for sample code see **Table 4.1**) and foods.

From **Figure 5.25** it can be stated that for some systems (f31, f40, Bergkäse, carrot) the ratio of fracture force to the total cutting force is decreasing with increasing *v*. To equilibrate the "energy balance" it can be concluded that in these systems friction forces gain importance at higher velocities. Since friction forces stem from adhesion forces and viscoelastic deformation forces (**Eq. 2.14**), and adhesion forces decrease at high sliding velocities (Grosch, 1963; Moore & Geyer, 1972), the velocity-induced increase in friction forces should follow the frequency response of the complex moduli (**Figure 5.15**). For other systems (f35s20, Leberkäse, Salami, potato) velocity trends of fracture and deformation parameters have contrary tendencies and therefore could equilibrate each other. No conclusion on the friction force is possible in these cases. For toffee and bubble gum velocity dependence of deformation and fracture both tends to gain importance compared to velocity dependence of $F_{N,max}$. In this case friction contribution may decrease with increasing cutting velocity. This appears to be conclusive because both confectionaries showed increased adhesion to the blades at low velocities. This adhesion decreased with increasing cutting velocity. Assuming that the adhesion forces make up a large part of the friction force, it is understandable that the ratio of the friction force to the total cutting force decreases.

6 Conclusions and outlook

Foods are heterogeneous material systems: from the morphological viewpoint, cellular, fibrous, crystalline and amorphous structures can be present. Their viscoelastic properties can vary from dominantly viscous to dominantly elastic and have a decisive influence on velocity-dependent processing operations such as cutting. This can lead to process-disturbing effects, especially at high cutting velocity. To correctly classify the deformation, fracture and friction processes during cutting and to understand the cutting behavior of the foods, it is of importance to reveal relationships between the mechanical behavior and cutting force parameters. Since the natural variability of food can be disadvantageous in experimental process analysis, the use of model systems with reproducible mechanical properties is an interesting advancement.

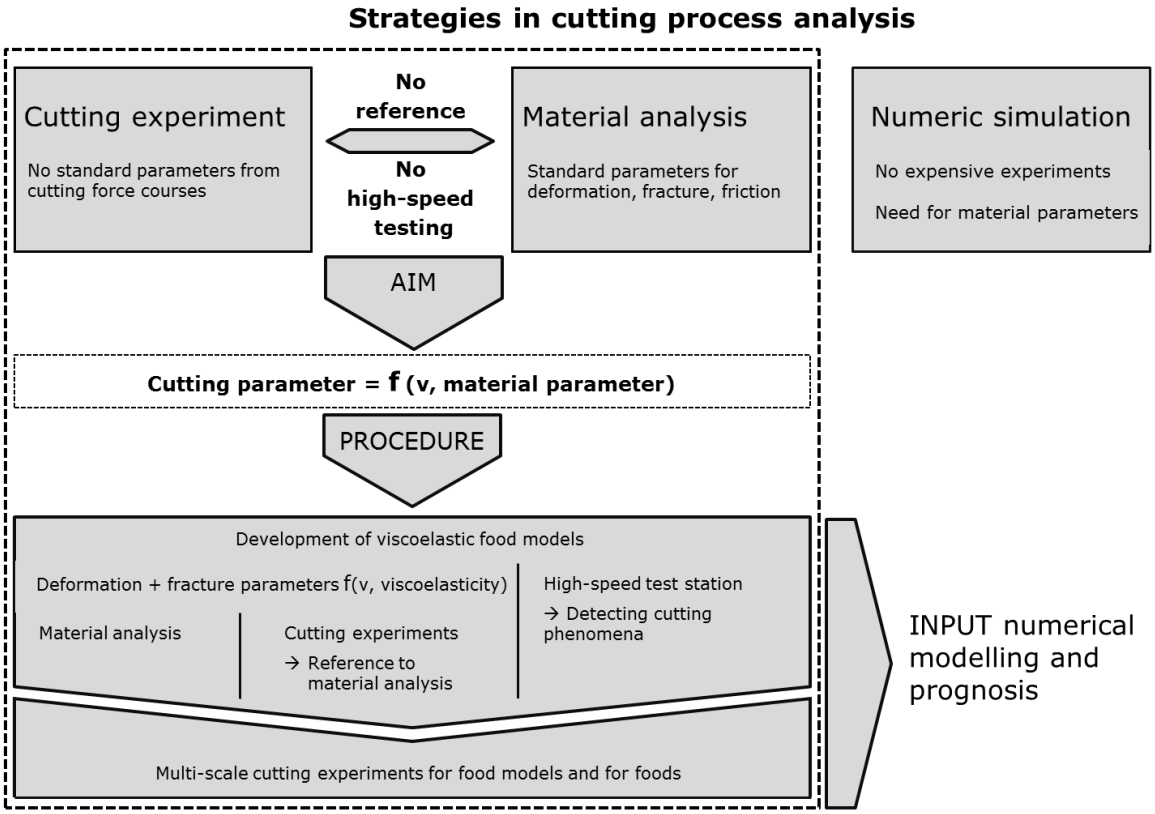

Figure 6.1: Strategies in cutting process analysis: cutting experiments, material analyses and numeric simulations. The broken line specifies the investigation approach of this study.

Investigation approach of this work was to use a test station for phenomenological and energetic high-speed cutting experiments. Simultaneously, correlations between

deformation and fracture parameters from material analysis as well as parameters from cutting force sequences in the low-speed range were to be determined using proper viscoelastic model systems. Furthermore, the suitability of the detected parameters for real food systems as well as the high-speed range had to be assessed (**Figure 6.1**).

By using the developed high-speed test station and a commercial universal testing device it was possible to analyse the cutting behavior over 6 magnitudes of cutting velocity. Capturing force data allows to detect and to distinguish materials on the basis of their viscoelastic behavior. This could be shown using bubble gum as an appropriate model system to reflect viscoelastic phenomena: at low cutting velocity, the cutting process is dominated by viscous effects that are continuously replaced by elastic effects (brittle fracture) as cutting velocity increases. Decreasing the temperature of the bubble gum led to similar effects as increasing cutting velocity. In line with cutting force data, video analysis of the cutting process and material characterization allow a holistic description of the cutting process and the cutting behavior of materials at high velocity.

A broad variety of foods had been cut at several magnitudes of cutting velocity up to 10 m/s. It could be shown that the polymeric model systems and the foods on polymeric basis showed similar cutting behavior. The results did not indicate brittle fracture at the highest velocities. Even though cellular plant materials show similar material characteristics from DMA they revealed fundamental differences in cutting behavior which was most likely attributed to their cellular structures that provoke partly brittle fracture behavior. For all other systems the DMA characteristics basically coincided with the cutting velocity dependence of the cutting forces. Analysing $F_{N,max}$ and blade displacement at $F_{N,max}$ can provide additional information on the nature of fracture mechanism. Generally it can be concluded that increasing the cutting velocity led to minimization of *CI* and hence lower product deformation which is, next to minimizing of cutting forces, attributed to enhanced cutting quality. Especially polymeric foods with heterogeneous structures (Leberkäse and Salami) showed a substantial decrease of *CI* and a substantial reduction of F_{CI}. For confectionaries cutting velocity had a very strong effect on cutting behavior as these are very sensitive to temperature and velocity; like that fundamental changes of fracture mechanism from ductile to brittle fracture could be detected. The products seem to have a cutting velocity range with optimum cutting quality (see **Figure 5.11**). Beyond

and above this range, extensive plastic product deformation (below) or extensive product splintering (above) lead to unacceptable product quality. This optimum velocity range can significantly be influenced by the temperature. This clearly reflects the sensibility of confectionaries to temperature variations during processing.

Elastosil silicone rubbers can be considered as useful model systems for food which viscoelastic properties can be adjusted by a proper selection of filler and softener. The silicone rubbers provided similar cutting force courses and similar cutting parameters compared to polymeric food systems and were generally suitable for linking mechanical properties at small and large deformation to cutting behavior.

An important parameter deviated from the cutting force is the cutting stiffness. From this, *CI* and $F_{N,CI}$ can be derived. The cutting stiffness before cut initiation is equivalent with the initial cutting force increase s_0 which is a useful material parameter to conclude on the complex modulus from small deformation testing, and vice versa. s_0 of the model systems measured at different cutting velocity reflects the rate dependence of the cutting process (by parameter *b* from from **Eq. 4.4**), and could be related to viscoelastic material parameters such as the loss factor *tan δ* or *n* obtained by DMA. The more viscous (or the higher *tan δ*) the model material was, the more it was sensitive to velocity changes induced by angular frequency in small deformation experiments, but also to different cutting velocities. In further experiments with the high-speed test station these basic findings could also be transferred to different food systems. In general the relation between the cutting velocity reflecting parameter *b* and the DMA parameters *n* and *δ* was valid from low to high-speed range and could be expressed by **Eq. 5.4** except for cellular or fibrous plant tissues. Over all DMA was very useful to predict pre-crack cutting properties of different materials. Furthermore the application of a simple model approach that was given by **Eq. 5.5** showed to be a useful engineering tool to estimate initial cutting forces, mostly for materials that reveal constant viscoelastic properties. For systems with increasing elastic contributions at higher velocity (brittle fracture) the experimental values had been overestimated as this appeared in the case of toffee. For fibrous plant tissues the model did not fit.

Independent of cutting substrate (in case of the elastomers analysed in **chapter 5.1.3**) and cutting velocity, fracture toughness showed a significant correlation to sharp-

ness parameter $F_{N,CI}$, that can simply be determined from cutting force courses. This parameter was taken as indicator of fracture resistance of the cutting material. *CI* additionally gives information about the amount of deformation until fracture in the sample is provoked by the blade. For the chosen test setup *CI* decreased with increasing cutting velocity because of increased tension buildup. Depending on the materials and energy dissipation mechanism with higher v, $F_{N,CI}$ increased, decreased or stayed constant. The internal structures of the composite materials had a distinct influence on this velocity dependence. A single consideration of viscoelasticity did not allow a general derivation to the rate-dependence of cutting fracture resistance. As a result, the fracture properties must be determined for each material system and for the relevant velocity range. For most systems the contribution of fracture force to overall cutting force seems to attenuate with increasing v. From that it may be assumed that, for some systems, friction can play an important role at high cutting velocities. Over all using the fracture parameter $F_{N,CI}$ from the initial cutting force data included limitations because the derivation from the initial cutting force data at 10 m/s was not possible.

The starting point for further research should therefore be the detection of a fracture parameter, e.g. from wire cutting tests, that allows the direct determination of fracture toughness. On this basis, the influence of viscoelastic dissipation and pure work of separation could separately be detected and evaluated. For a holistic description of the cutting process it is important to investigate friction phenomena. Here, the development of suitable methods for describing friction during cutting at multi-scale cutting velocity should be the future focus. Ideally it would be advantageous to use fracture and friction parameters that could easily be derived at high cutting velocities. A solution could be the tts which, in addition to mechanical properties at small deformation, can also represent fracture and friction properties for large velocity ranges. Over all the description of the cutting behavior by means of cutting force parameters forms the foundations for the phenomenological understanding of cutting processes; on the other hand, it can be used as basis for energetic cutting process descriptions in numerical modeling approaches (**Figure 6.1**), which is, next to cutting experiments and material characterization, the third pillar of cutting process analysis.

Bibliography

Abadyan, M., Kouchakzadeh, M.A., Bagheri, R., 2012. Fracture toughness of a hybrid rubber modified epoxy. II. Effect of Loading Rate. J. Appl. Polym. Sci. 125, 2476–2483.

Aderinola, O., O., Kah, P., Martikainen, J., 2013. Efficient welding technologies tpplicable to HSS arctic offshore structures. In: Proc. of the 23rd International Offshore and Polar Engineering, Anchorage, Alaska, USA, ISBN 978-1-880653-99–9, pp. 257–264.

Ahmed, J., 2012. Applicability of time–temperature superposition principle: Dynamic rheology of mung bean starch blended with sodium chloride and sucrose – Part 2. J. Food Eng. 109, 329–335.

Alvarez, M. D., Saunders, D. E. J., Vincent, J. F. V., Jeronimidis. G., 2000. An engineering method to evaluate the crisp texture of fruit and vegetables. J. Texture Stud. 31, 457–473.

Alwis, K., G., N., C., Burgoyne, C., J., 2006. Time-temperature superposition to determine the stress-rupture of aramid fibres. Appl. Compos. Mater. 13, 249–264.

Atkins, A. G., Xu, X., Jeronimidis, G., 2004. Cutting, by 'pressing and slicing,' of thin floppy slices of materials illustrated by experiments on cheddar cheese and salami. J. Mater. Sci. 39, 2761–2766.

Atkins, T., 2009. Food and food-cutting devices and wire cutting. In: T. Atkins (Ed.), The Science and Engineering of Cutting. Elsevier, Amsterdam, NL, pp. 283–306.

Atkinson, J. R., 1975. Mechanical properties and wear behaviour of plastics in relation to their use in prostheses. Br. Polym. J. 7, 93–107.

Barden, L.M., Osborne, J. A., McMahon, D. J., Foegeding, E. A., 2015. Investigating the filled gel model in Cheddar cheese through use of Sephadex beads. J. Dairy Sci. 98, 1502–1516.

Bobaru, F., Zhang, G., 2015. Why do cracks branch? A peridynamic investigation of dynamic brittle fracture. Int. J. Fract. 196, 59–98.

Bokobza, L., 2009. New developments in rubber reinforcement. Kautsch. Gummi Kunstst. 62, 23–27.

Boisly, M., Schuldt, S., Kästner, M., Schneider, Y., Rohm, H., 2016. Experimental characterisation and numerical modelling of cutting processes in viscoelastic solids. J. Food Eng. 191, 1–9.

Booij, H.C., Thoone, G.P.J.M., 1982. Generalization of Kramers-Kronig transforms and some approximations of relations between viscoelastic quantities. Rheol. Acta 21, 15–24.

Brown, K.J., Atkinson, J.R., Dowson, D., Wright, V., 1976. The wear of ultrahigh molecular weight polyethylene and a preliminary study of its relation to the in vivo behaviour of replacement hip joints. Wear 40, 255–264.

Brown, T., James, S.J., Purnell, G.L., 2005. Cutting forces in foods: experimental measurements. J. Food Eng. 70, 165–170.

Bruno, M., Moresi, M., 2004. Viscoelastic properties of Bologna sausages by dynamic methods. J. Food Eng. 63, 291–298.

Bryan, H.H., Ahuja, K.K., 1993. Review of crack propagation under unsteady loading. AIAA J. 31, 1077–1089.

Canet, W., Alvarez, M.D., Gil, M.J., 2007. Fracture behaviour of potato samples (cv. Desiree) under uniaxial compression. J. Food Eng. 82, 427–435.

Cessna, L.C., 1974. Dilatometric studies of polymers undergoing high and low rate tensile deformation. Polym. Eng. Sci. 14, 696–701.

Chen J., Dickinson E., 1999. Effect of surface character of filler particles on rheology of heat-set whey protein emulsion gels. Colloids Surf. B 12, 373–381.

Chen L., Opara U.L., 2013. Approaches to analysis and modeling texture in fresh and processed foods – A review. J. Food Eng. 119, 497–507.

Cho, K., Lee, D., 1998. Viscoelastic effects in cutting of elastomers by a sharp object. J. Polym. Sci. Pol. Phys. 36, 1283–1291.

Cuq, B., Goncalves, F., Mas, J.F., Vareille, L., Abecassis, J., 2003. Effects of moisture content and temperature of spaghetti on their mechanical properties. J. Food Eng. 59, 51–60.

Czichos, H., Habig, K.-H., 2010. Tribologie Handbuch. Vieweg und Teubner, Wiesbaden, DE.

Dealy, J., Plazek, D., 2009. Time-temperature superposition - a users guide. Rheol. Bull. 78, 16–32.

Dear, J.P., 1996. Comparison of fast fracture properties of thermoplastics. Polym. Eng. Sci. 36, 1210–1216.

Dijkstra, P.T.S., van Dijk, D.J., Huétink, J., 2002. A microscopy study of the transition from yielding to crazing in polypropylene. Polym. Eng. Sci. 42, 152–160.

Dowgiallo, A., 2005. Cutting force of fibrous materials. J. Food Eng. 66, 57–61.

Dowgiallo, A., 2015. Personal communication.

Dresselhuis, D.M., Klok, H.J., Stuart, M.A.C., Vries, R.J. de, Aken, G.A. van, Hoog, E.H.A. de, 2007. Tribology of o/w emulsions under mouth-like conditions: determinants of friction. Food Biophys. 2, 158–171.

Farahmand, B., 2001. Linear elastic fracture mechanics (LEFM) and applications. In: Fracture mechanics of metals, composites, welds, and bolted joints : application of LEFM, EPFM, and FMDM theory. Kluwer, Boston, US, pp. 52–117.

Fatt, M.S.H., Ouyang, X., 2007. Integral-based constitutive equation for rubber at high strain rates. Int. J. Solids Struct. 44, 6491–6506.

Field, J.E., Walley, S.M., Proud, W.G., Goldrein, H.T., Siviour, C.R., 2004. Review of experimental techniques for high rate deformation and shock studies. Int. J. Impact Eng. 30, 725–775.

Forte, A.E., D'Amico, F., Charalambides, M.N., Dini, D., Williams, J.G., 2015. Modelling and experimental characterisation of the rate dependent fracture properties of gelatine gels. Food Hydrocolloid. 46, 180–190.

Friedrich, C., Heymann, L., 1988. Extension of a model for crosslinking polymer at the gel point. J. Rheol. 32, 235–241.

Gamonpilas, C., Charalambides, M.N., Williams, J.G., 2009. Determination of large deformation and fracture behaviour of starch gels from conventional and wire cutting experiments. J. Mater. Sci. 44, 4976–4986.

Gdoutos, E.E., 2005. Introduction. In: Gladwell, G.M.L. (Eds.), Fracture Mechanics: an introduction [2. ed.]. Springer, Dordrecht, NL, pp. 1–13.

Goh, S.M., Charalambides, M.N., Williams, J.G., 2005. On the mechanics of wire cutting of cheese. Eng. Fracture Mech. 72, 931–946.

Grosch, K.A., 1963. Relation between the friction and visco-elastic properties of rubber. Nature 197, 858–859.

Gundermann, T., Odenbach, S., 2014. Investigation of the motion of particles in magnetorheological elastomers by X-µCT. Smart Mater. Struct. 23, 105013.

Gurp, M. van, Palmen, J., 1998. Time-temperature superposition for polymeric blends. Rheol. Bull. 67, 5–8.

ISO 527-1: 2012 Plastics -- Determination of tensile properties - Part 1: General principles.

Jampen, S., Britt, I.J., Yada, S., Tung, M.A., 2001. Rheological properties of gellan gels containing filler particles. J. Food Sci. 66, 289–293.

Jaros, D., Petrag, J., Rohm, H., Ulberth, F., 2001. Milk fat composition affects mechanical and rheological properties of processed cheese. Appl. Rheol. 11, 19–25.

Kamyab, I., Chakrabarti, S., Williams, J.G., 1998. Cutting cheese with wire. J. Mater. Sci. 33, 2763– -2770.

Kasapis, S., 2001. The use of Arrhenius and WLF kinetics to rationalise the rubber-to-glass transition in high sugar/κ-carrageenan systems. Food Hydrocoll. 15, 239–245.

King, M.J., 1999. Knife and impact cutting of lamb bone. Meat Sci. 52. , 29–38.

Kohyama, K., Hatakeyama, E., Sasaki, T., Dan, H., Azuma, T., Karita, K., 2004. Effects of sample hardness on human chewing force: a model study using silicone rubber. Arch. Oral Biol. 49, 805–816.

Konar, N., Palabiyik, I., Toker, O.S., Sagdic, O., 2016. Chewing gum: Production, quality parameters and opportunities for delivering bioactive compounds. Trends Food Sci. Technol. 55, 29–38.

Kretzschmar, M., 2013. Experimental determination of speed-related forces during cutting of food-like model systems. Technische Universität Dresden (diploma thesis).

Lakes, R.S., 2004. Viscoelastic measurement techniques. Rev. Sci. Instrum. 75, 797–810.

Landis, C.M., Pardoen, T., Hutchinson, J.W., 2000. Crack velocity dependent toughness in rate dependent materials. Mech. Mat. 32, 663–678.

Langer, B., Seidler, S., Grellmann, W., 2001. Influence of temperature and moisture on toughness behaviour of polyamide. In: Grellmann, W., Seidler, S. (Eds.), Springer, Berlin, DE.

Lillford, P. J., 2001. Mechanism of fracture in foods. J. Texture Stud. 32, 397–417.

Loncin, M., & Merson, R. L., 1979. Mechanical operations. In: Food engineering: principles and selected applications. Academic Press, New York, US, 231–270.

Lorenz, B., Persson, B. N. J., Fortunato, G., Giustiniano, M., Baldoni, F., 2013a. Rubber friction for tire tread compound on road surfaces. J. Phys.: Condens. Matter 25, 095007.

Lorenz, B., Krick, B.A., Mulakaluri, N., Smolyakova, M., Dieluweit, S., Sawyer, W.G., Persson, B. N. J., 2013b. Adhesion: role of bulk viscoelasticity and surface roughness. J. Phys.: Condens. Matter 25, 225004.

Lovell, M.R., Deng, Z., 1999. Experimental investigation of sliding friction between hard and deformable surfaces with application to manufacturing processes. Wear 236, 117-127.

Ludema, K.C., Tabor, D., 1966. The friction and visco-elastic properties of polymeric solids. Wear 9, 329–348.

Luyten, H., 1988. The rheological and fracture properties of Gouda cheese. Wageningen Agricultural University (PhD. thesis).

Luyten, H., van Vliet, T., Walstra, P., 1991. Characterization of the consistency of Gouda cheese: Fracture properties. Neth. Milk Dairy J. 45, 55–80.

Luyten, H., van Vliet, T., Walstra, P., 1992. Comparison of various methods to evaluate fracture phenomena in food materials. J. Texture Stud. 23, 245–266.

Luyten, H., van Vliet, T., 1995. Fracture properties of starch gels and their rate dependency. J. Texture Stud. 26, 281–298.

Marquardt†, B., 2011. personal communication. www.astorblades.com.

Martinetti, L., Mannion, A.M., Voje, Jr., W.E., Xie, R., Ewoldt, R.H., 2014. A critical gel fluid with high extensibility: The rheology of chewing gum. J. Rheol. 58, 821–838.

Maurer, G., 2003. Hochgeschwindigkeitsprüfung von Kunststoffen mit Hilfe von Schnellzugversuchen. 9. Problemseminar: Deformation und Bruchverhalten von Kunststoffen. Merseburg, DE.

McCarthy, C.T., Hussey, M., Gilchrist, M.D., 2007. On the sharpness of straight edge blades in cutting soft solids: Part I – indentation experiments. Eng. Fracture Mech. 74, 2205–2224.

McCarthy, C.T., Annaidh, A.N., Gilchrist, M.D., 2010. On the sharpness of straight edge blades in cutting soft solids: Part II – Analysis of blade geometry. Eng. Fracture Mech. 77, 437–451.

McCulloch, E., 2008. Experimental and finite element modeling of ultrasonic cutting of food. University of Glasgow (PhD. thesis).

McKellop, H.A., 2007. The lexicon of polyethylene wear in artificial joints. Biomaterials 28, 5049–5057.

Meyers, M.A., 1994. Experimental techniques: methods to produce dynamic deformation. In: Dynamic behavior of materials. John Wiley & Sons, Inc., New York, US, pp. 296–322.

Metzger, T.C., 2014. The rheology handbook. Vinventz Network, Hannover, DE.

Miri, T., 2011. Viscosity and oscillatory rheology. In I. T. Norton, F. Spyropoulos, P. cox (Eds.), Practical food rheology. An interpretative approach (pp. 7–27). Wiley-Blackwell, Chichester, UK.

Moore, D. F., Geyer, W., 1972. Review of adhesion theories for Elastomers. Wear 22, 113–142.

Mulliken, A.D., Boyce, M.C., 2006. Mechanics of the rate-dependent elastic–plastic deformation of glassy polymers from low to high strain rates. Int. J. Solids Struct. 43, 1331–1356.

Nickerson, M.T., Paulson, A.T., Speers, R.A., 2004. A time–temperature rheological approach for examining food polymer gelation. Trends Food Sci. Tech. 15, 569–574.

Olwig, R., 2006. Untersuchungen zum zeit- und temperaturabhängigen Materialverhalten von Polymeren unter Scher- und Zugbelastung bei hohen Verformungsgeschwindigkeiten. Technische Universität Clausthal (PhD. thesis).

Ormerod, A.P., Ralfs, J.D., Jackson, R., Milne, J., Gidley, M.J., 2004. The influence of tissue porosity on the material properties of model plant tissues. J. Mater. Sci. 39, 529 – 538.

Pohlit, D. J., Dillard, D. A., Jacob, G. C., Starbuck, J. M., 2008. Evaluating the rate-dependent fracture toughness of an automotive adhesive. J Adhes. 84, 143–163.

Rohm, H., Lederer, H., 1992. Uniaxial compression of Swiss-type cheese at different strain rates. Int. Dairy J. 2, 331–343.

Rohm, H., Jaros, D., de Haan, M., 1997. A video-based method for determination of stress-strain relations in uniaxial compression of selected foods. J. Texture Stud. 28, 245–255.

Scanlon, M.G., Alison, E.L., 1995. Fracture strengths of potato tissue under compression and tension at two rates of loading. Food Res. Int. 28, 397–402.

Schell, T., 2005. Grundlegende Untersuchungen einer neuen Rapid Tooling Technik für die Blechumformung. Universität Erlangen-Nürnberg (PhD. thesis).

Schmidt, C., Bornmann, R., Schuldt, S., Schneider, Y., Rohm, H., 2018. Thermo-mechanical properties of Soft Candy: Application of Time-Temperature Superposition to Mimic Response at High Deformation Rates. Food Biophys. 13, 11–17.

Schneider, Y., Zahn, S., Linke, L., 2002. Qualitative process evaluation for ultrasonic cutting of food. Eng. Life Sci. 2, 153–157.

Schneider, Y., 2007. Einsatz von Ultraschall zur Modifikation lebensmitteltechnischer Grundoperationen am Beispiel des Schneidens. Technische Universität Dresden (PhD. thesis).

Schneider, Y., Zahn, S., Schindler, C., Rohm, H., 2009. Ultrasonic excitation affects friction interactions between food materials and cutting tools. Ultrasonics 49, 588–593.

Schneider, Y., Kluge, C., Weiß, U., Rohm, H., 2010. Packaging materials and equipment. In: Law, B.A., Tamime, A.Y. (Eds.), Technology of Cheesemaking. Wiley-Blackwell, Oxford, UK, pp. 413–439.

Schuldt, S., Arnold, G., Roschy, J., Schneider, Y., Rohm, H., 2013. Defined abrasion procedures for cutting blades and comparative mechanical and geometrical wear characterization. Wear 300, 38–43.

Schuldt, S., Boden, L., Schneider, Y., Rohm, H., 2016a. Pre-crack cutting properties of viscoelastic food models. J. Food Eng. 169, 272–277.

Schuldt, S., Arnold, G., Kowalewski, J., Schneider, Y., Rohm, H., 2016b. Analysis of the sharpness of blades for food cutting. J. Food Eng. 188, 13-20.

Schuldt, S., Witt, T., Schmidt, C., Schneider, Y., Nündel, T., Majschak, J-P., Rohm, H., 2018. High-speed cutting of foods: Development of a special testing device. J. Food Eng. 216, 36–41.

Shergold, O.A., Fleck, N.A., 2004. Mechanisms of deep penetration of soft solids, with application to the injection and wounding of skin. Proc. R. Soc. Lond. A 460, 3037–3058.

Shergold, O.A., Fleck, N.A., Radford, D., 2006. The uniaxial stress versus strain response of pig skin and silicone rubber at low and high strain rates. Int. J. Impact Eng. 32, 1384–1402.

Silva, L.J.A. da, 1994. Influence of temperature on the dynamic and steady-shear rheology of pectin dispersion. Carbohyd. Polym. 23, 77–87.

Singh, A.P., Lakes, R.S., Gunasekaran, S., 2006. Viscoelastic characterization of selected foods over an extended frequency range. Rheol. Acta 46, 131–142.

Skamniotis, C. G., Patel, Y., Charalambides, M. N., Elliott, M., 2016. Fracture investigation in starch-based foods. Interface Focus 6.

Stachowiak, H., 1973. Allgemeine Modelltheorie. Springer Verlag, Wien, AUT.
Steffe, J.F., 1996. Rheological Methods in Food Process Engineering. Freeman Press, East Lansing, USA.
Stock, M., 2015. personal communication. www.kistler.com.
Sworn, G., Kasapis, S., 1998. The use of Arrhenius and WLF kinetics to rationalize the mechanical spectrum in high sugar gellan systems. Carbohydr. Res. 309, 353–361.
Tang, S., Guo, T.F., Cheng, L., 2008. Rate effects on toughness in elastic nonlinear viscous solids. J. Mech. Phys. Solids. 56, 974–992.
Taylor, D., O'Mara, N., Ryan, E., Takaza, M., Simms, C., 2011. The fracture toughness of soft tissues. J. Mech. Behav. Biomed. Mater. 6, 139–147.
Tscheuschner, H.D., 2004. Grundzüge der Lebensmitteltechnik. Behr's Verlag, Hamburg, DE.
Tsiami, A., Bot, A., Agterof, W.G.M., Graveland, A., Henderson, T., 1995. Time-temperature superposition for networks formed by gluten subfractions. in: Schofield, J.D. (Ed.), Wheat Structure. Woodhead Publishing, Cambridge, UK, pp. 99–105.
Udyarajan, C.T., Horne, D.S., Lucey, J.A., 2007. Use of time–temperature superposition to study the rheological properties of cheese during heating and cooling. Int. J. Food Sci. Tech. 42, 686–698.
Vandenberghe, E.L.S., Choucharina, S., De Ketelaere, B., De Baerdemaeker, J., Claes, J., 2014. Spatial variability in fundamental material parameters of Gouda cheese. J. Food Eng. 131, 50–57.
Vincent, J. F. V., Jeronimidis, G., Khan, A. A., Luyten, H., 1991. The wedge fracture test – A new method for measurement of food texture. J. Texture Stud. 22, 45–57.
Vincent, J. F. V., 1993. Mechanical and fracture properties of fruit and vegetables. In: Dickinson, E., Walstra, P. (Eds.), Food colloids and polymers: Stability and mechanical properties. Royal Society of Chemistry, Cambridge, UK, pp. 191–203.
Vincent, J. F. V., 2012. Basic elasticity and viscoelasticity. In: Structural Biomaterials: third edition. Princeton University Press, Princeton, USA, pp. 1–28.
Vliet, T. van, Luyten, H., Walstra, P., 1991. Fracture and yielding of gels. In: Dickinson, E. (Ed.), Food polymers, gels and colloids. Royal Society of Chemistry, Cambridge, UK, pp. 392–403.
Vliet, T. van, Luyten, H., Walstra, P., 1993. Time dependent fracture behaviour of food. In: Dickinson, E., Walstra, P. (Eds.), Food colloids and polymers: Stability and mechanical properties. Royal Society of Chemistry, Cambridge, UK, pp. 174–189.
Vliet, T. van, Walstra, P., 1995. Large Deformation and fracture behaviour of gels. Faraday Discuss. 101, 359–370.
Vliet, T. van, 1996. Large deformation and fracture behavior of gels. Curr. Opin. Colloid Interface Sci. 1, 740–745.
Williams, G., 2009. New methods for measuring fracture toughness. Strain 45, 313–315.
Wrana, C., 2014. Polymerphysik : Eine physikalische Beschreibung von Elastomeren und ihren anwendungsrelevanten Eigenschaften, Springer Spektrum, Heidelberg, DE.
Yang, L.M., Shim, V.P.W., Lim, C.T., 2000. A visco-hyperelastic approach to modelling the constitutive behaviour of rubber. Int. J. Impact Eng. 24, 545–560.
Zahn, S., 2009. Ultraschallschneiden von Lebensmitteln – Optimierung durch Abstimmung der Verfahrensparameter auf die spezifischen Eigenschaften des Schnittgutes. Technische Universität Dresden (PhD. thesis).

Zdunek, A., Umeda, M., 2006. Extension and fracture of cell walls after parenchyma tissue deformation. Biosyst. Eng. 93, 269–278.
Zhang, C., Liu, L., Zhang, Z., Pal, K., Kim, J.K., 2011. Effect of Silica and Silicone Oil on the Mechanical and Thermal Properties of Silicone Rubber. J. Macromol. Sci. B 50, 1144–115.

List of figures

List of tables

List of videos

Video 5.1: product: bubble gum, temperature: 30 °C, cutting velocity: 1 m/s, time: 5 s, real time: 50 ms

Video 5.2: product: bubble gum, temperature: 30 °C, cutting velocity: 10 m/s, time: 13 s, real time: 13 ms

Video 5.3: product: bubble gum, temperature: 20 °C, cutting velocity: 10 m/s, time: 13 s, real time: 13 ms

Video 5.4: product: toffee, temperature: 30 °C, cutting velocity: 10 m/s, time: 8 s, real time: 88 ms

Video 5.5: product: Salami, temperature: 15 °C, cutting velocity: 0.1 m/s, time: 7 s, real time: 1.47 s

Video 5.6: product: Salami, temperature: 15 °C, cutting velocity: 10 m/s, time: 11 s, real time: 85 ms

The videos are available online via permalink http://dx.doi.org/10.25532/OPARA-5.

List of publications

Publications referring to the doctoral thesis

Schuldt, S., Arnold, G., Roschy, J., Schneider, Y., Rohm, H., 2013. Defined abrasion procedures for cutting blades and comparative mechanical and geometrical wear characterization. Wear 300, 38–43.

Schuldt, S., Boden, L., Schneider, Y., Rohm, H., 2016. Pre-crack cutting properties of viscoelastic food models. J. Food Eng. 169, 272–277.

Schuldt, S., Arnold, G., Kowalewski, J., Schneider, Y., Rohm, H., 2016. Analysis of the sharpness of blades for food cutting. J. Food Eng. 188, 13–20.

Boisly, M., Schuldt, S., Kästner, M., Schneider, Y., Rohm, H., 2016. Experimental characterisation and numerical modelling of cutting processes in viscoelastic solids. Journal of Food Engineering 191, 1–9.

Schuldt, S., Witt, T., Schmidt, C., Schneider, Y., Nündel, T., Majschak, J-P., Rohm, H., 2018. High-speed cutting of foods: Development of a special testing device. J. Food Eng. 216, 36–41.

Schmidt, C., Bornmann, R., Schuldt, S., Schneider, Y., Rohm, H., 2018. Thermo-mechanical properties of Soft Candy: Application of Time-Temperature Superposition to Mimic Response at High Deformation Rates. Food Biophys. 13, 11–17.

Schuldt, S., Schneider, Y., Rohm, H., 2018. High-speed cutting of foods: Cutting behavior and initial cutting forces. J. Food Eng. 230, 55–62.

Other publications

Mutungi, C., Schuldt, S., Onyango, C., Schneider, Y., Jaros, D., Rohm, H., 2011. Dynamic Moisture Sorption Characteristics of Enzyme-Resistant Recrystallized Cassava Starch. Biomacromolecules 12, 660–671.

Passauer, L., Struch, M., Schuldt, S., Appelt, J., Schneider, Y., Jaros, D., Rohm, H., 2012. Dynamic moisture sorption characteristics of xerogels from water swellable oligo(oxyethylene) lignin derivatives. ACS Applied Materials and Interfaces 4, 5852–62.

Arnold, G., Schuldt, S., Schneider, Y., Friedrichs, J., Babick, F., Werner, C., Rohm, H., 2013. The impact of lecithin on rheology, sedimentation and particle interactions in oil-based dispersions. Colloids and Surfaces A: Physicochemical and Engineering Aspects 418, 147–156.

Schuldt, S., Raak, N., Jaros, D., Rohm, H., 2014. Acid-induced formation of soy protein gels in the presence of NaCl. LWT-Food Science and Technology 57, 634–639.

Posters and presentations

Schuldt, S., Arnold, G., Kretzschmar, M., Schneider, Y., Rohm, H., 2011. Impact of DLC Coatings on Wear Properties of Cutting Blades in Food Processing. Poster, EFFoST Annual Meeting

Schuldt*, S., Kretzschmar, M., Arnold, G., Schneider, Y., Rohm, H., 2012. Methodenvergleich zur Charakterisierung von Verschleißzuständen an Schneidklingen. Presentation, 6. Kongress Lebensmitteltechnologie der GDL

Schuldt*, S., Kretzschmar, M., Faivre, L., Schneider, Y., Rohm, H., 2014. Mechanische Produkteigenschaften und Schneidverhalten bei wachsenden Beanspruchungsgeschwindigkeiten. Presentation, 7. Kongress Lebensmitteltechnologie der GDL

Schuldt*, S., Schneider, Y., Rohm, H., 2016. Parameteridentifikation zur Charakterisierung des Schneidverhaltens von Lebensmitteln. Presentation, Jahrestreffen der ProcessNet-Fachgruppe Lebensmittelverfahrentechnik 2016

Schuldt*, S., Witt, T., Schmidt, C., Schneider, Y., Rohm, H., 2016. Detektion von Hochgeschwindigkeitseffekten beim Schneiden von Lebensmittelmodellmassen. Presentation, 8. Kongress der Lebensmitteltechnologie der GDL

Schmidt*, C., Schuldt, S., Bornmann, R., Schneider, Y., Rohm, H., 2016. Thermomechanische Eigenschaften von Zuckerwarenmassen. Presentation, 8. Kongress der Lebensmitteltechnologie der GDL

*speaker